

~~CONFIDENTIAL~~

C. 2 6  
Copy  
RM L55H19

NACA RM L55H19



# RESEARCH MEMORANDUM

A SYSTEMATIC STUDY OF THE EFFECTS OF LEADING-EDGE  
CHORD-EXTENSIONS ON THE LOW-SPEED LONGITUDINAL STABILITY  
CHARACTERISTICS OF THREE 45° SWEEPBACK WINGS

By H. Neale Kelly

Langley Aeronautical Laboratory

Langley Field, Va.

CLASSIFICATION CHANGED

To UNCLASSIFIED

By authority of NACA Res Abs  
RP-119 *efficiency*  
*Aug. 16, 1957*  
G.M. 9-5-57

CLASSIFIED DOCUMENT

LANGLEY AERONAUTICAL LABORATORY  
LIBRARY, NACA

This material contains information affecting the National Defense of the United States within the meaning of the espionage laws, Title 18, U.S.C., Secs. 793 and 794, the transmission or revelation of which in any manner to an unauthorized person is prohibited by law.

NATIONAL ADVISORY COMMITTEE  
FOR AERONAUTICS

WASHINGTON

October 27, 1955

~~CONFIDENTIAL~~

## NATIONAL ADVISORY COMMITTEE FOR AERONAUTICS

## RESEARCH MEMORANDUM

A SYSTEMATIC STUDY OF THE EFFECTS OF LEADING-EDGE  
CHORD-EXTENSIONS ON THE LOW-SPEED LONGITUDINAL STABILITYCHARACTERISTICS OF THREE  $45^\circ$  SWEEPBACK WINGS

By H. Neale Kelly

## SUMMARY


A low-speed leading-edge chord-extension investigation has been conducted in the Langley 19-foot pressure tunnel. In the course of the investigation, chord-extensions of various geometric designs were tested on three  $45^\circ$  sweptback wings of aspect ratio 5 and taper ratio 0.28 incorporating different airfoil sections. The tests were made at a Reynolds number of  $4.6 \times 10^6$  and a corresponding Mach number of 0.11.

The experimental data indicated that leading-edge chord-extensions could be used to produce large reductions in the longitudinal instability of all three wings tested. For a given chord-extension, the reduction was largest on the wing with smallest leading-edge radius. On all the wings the magnitude of the reduction was dependent upon the geometry of the extension, with the chord-extension of the largest leading-edge radius and largest projection being the most effective. Further reductions in the instability were obtained on the wing of largest leading-edge radius by drooping the extension.

What appeared to be rather severe buffeting was encountered during the investigation. Audiovisual observation of the tests indicated that this buffeting was most severe for the configurations having the most effective chord-extension.

## INTRODUCTION

In recent years considerable flight and wind-tunnel research has been devoted to improving the undesirable pitching-moment characteristics of sweptback wings. Of the many devices tested in an attempt to improve



or "fix" these characteristics, partial-span leading-edge chord-extensions have proved to be one of the more promising. Early experiments (see ref. 1) indicate that the location, projection, and nose shape of the chord-extension are significant geometric factors in the design of this device. Furthermore, as noted in reference 1 and as more fully developed in the analysis of reference 2, the type of flow separation exhibited by the basic wing to which the extension is attached greatly influences the action and effectiveness of the leading-edge chord-extension.

To date, however, little or no attention other than inboard end-positioning studies has been given to the design of leading-edge chord-extensions. Moreover, the application of this device has been limited to predominately leading-edge flow-separation wings (sharp or nearly sharp airfoil) of relatively low aspect ratio (4 or less).

A low-speed investigation has, therefore, been conducted in the Langley 19-foot pressure tunnel in order to study the influence of geometric design on the effectiveness of leading-edge chord-extensions. In the course of this investigation, extensions of various chords, spanwise positions, and leading-edge radii were tested on three  $45^\circ$  sweptback wings of aspect ratio 5. The basic wings were of identical plan form, but were designed, through the use of airfoils with different leading-edge radii, to exhibit different types of flow separation.

#### SYMBOLS

$C_L$  lift coefficient,  $\frac{\text{Lift}}{qS}$

$C_m$  pitching-moment coefficient about  $\bar{c}/4$ ,  $\frac{\text{Pitching moment}}{qS\bar{c}}$

$\Delta C_m$  increment in pitching moment from line defined by slope of pitching-moment curve through  $C_L = 0$  (see sketch in fig. 5)

$C_{mC_L}$  rate of change of pitching moment with lift

$b$  wing span, ft

$c$  local streamwise chord, ft

$\bar{c}$  mean aerodynamic chord,  $\frac{2}{S} \int_0^{b/2} c^2 dy$ , ft

q	dynamic pressure, $\frac{1}{2}\rho V^2$ , lb/sq ft
S	wing area, sq ft
V	free-stream velocity, ft/sec
y	spanwise ordinate, ft
$\alpha$	angle of attack, deg
$\rho$	density, slugs/cu ft

## MODEL, TESTS, AND CORRECTIONS

## Model

Data contained in the present paper were obtained from tests of leading-edge chord-extensions on three wings of identical plan form. The wings were constructed of laminated mahogany and each had an aspect ratio of 5.0, a taper ratio of 0.29, 45° sweepback of the quarter-chord line, and 9-percent-thick airfoil sections. The wings, which will be identified by their leading-edge radii in the text, incorporated the following airfoil sections:

Airfoil section	Leading-edge radius, fraction c
NACA 0009-(3.18)3	0.0025
NACA 0009-(4.53)3	.0050
NACA 0009-63	.0089

Geometric characteristics of the leading-edge chord-extensions which were tested with the inboard end at various spanwise positions are as follows:

Basic Wing	Chord-Extension	
Leading-edge radius, fraction c	Leading-edge radius, fraction c	Projection (streamwise), fraction c
0.0025	0 .00125 .00250 .00445	0.130, 0.198 0.064, 0.130, 0.198 0.130, 0.198 0.064, 0.130, 0.198
.0050	0 .00250 .00445	0.064, 0.130, 0.198 0.064, 0.130, 0.198 0.064, 0.130, 0.198
.0089	0 .00445 .00890	0.064, 0.130, 0.198 0.064, 0.130, 0.198 0.064, 0.130, 0.198, 0.180 drooped

Additional details of the construction and geometry of the wings and chord-extensions can be found in figures 1 and 2. A photograph of the model as installed in the tunnel is presented in figure 3.

#### Tests

All tests reported herein were conducted in the Langley 19-foot pressure tunnel at a tunnel pressure of approximately 33 psia. A few of the initial tests were made at a Reynolds number of  $4.9 \times 10^6$  and a corresponding Mach number of 0.12. However, because of the violent behavior of the model, the tunnel speed was lowered for the remainder and majority of the tests to a Reynolds number of  $4.6 \times 10^6$  and a corresponding Mach number of 0.11.

#### Corrections

Jet-boundary corrections determined by the method of reference 3 have been applied to all of the data. The angle of attack has been corrected for airstream misalignment. No corrections have been applied for support tare and interference effects.

## RESULTS

Tables and figures summarizing the present test data (tables I, II, and III and figs. 4, 5, and 6) will form a basis for the discussion to follow. The lift and pitching-moment characteristics of all the configurations tested in the course of the present investigation are presented in succeeding figures. Figures 7 to 16, 17 to 25, and 26 to 36 contain the results obtained for wings with 0.0025c, 0.0050c, and 0.0089c leading-edge radii, respectively.

## DISCUSSION

In the present report, the ability of a chord-extension to linearize the pitching-moment characteristics of the configuration will serve as a basis for an assessment of the value of the extension. The maximum incremental pitching moment between a line defined by the slope through zero lift and the actual curve (see sketch, fig. 5) will serve as a measure of the linearity or nonlinearity of the pitching-moment characteristics.

## Basic Wings

The basic wings of the present investigation are part of a series of wings which have been used to study the influence of sweep, aspect ratio, airfoil section (leading-edge radius), Reynolds number, and Mach number on the formation of leading-edge vortex flow, hence the type of flow separation, and ultimately the pitching-moment characteristics of sweptback wings. Some of the initial results of the basic wing investigation are contained in reference 4. Lift and pitching-moment characteristics of the basic wings are reproduced on figure 4.

At the Reynolds number of the present tests ( $4.6 \times 10^6$ ) all three wings exhibited a mixture of leading-edge and trailing-edge flow separation of varying degrees. Flow studies and pressure-distribution measurements (unpublished) indicate that trailing-edge flow separation predominates on the wing with 0.0089c leading-edge radius while leading-edge separation predominates on the wing with 0.0025c leading-edge radius.

## Wings With Chord-Extensions

It is apparent from tables I, II, and III and figure 5 that all the chord-extension configurations tested reduced the instability of the basic wings. Nevertheless, all configurations exhibited a destabilizing break prior to maximum lift that was equivalent to or greater than a

15-percent aerodynamic-center shift. In some cases, however, the lift range over which the instability occurred was extremely small. The difficulty in eliminating the unstable break is ascribed to the relatively high aspect ratio of the present wings. In the earlier work of reference 1, where chord-extensions showed striking improvement of the moment curves, the aspect ratio was only 2.84.

In general, a chord-extension of a given leading-edge radius and projection produced more nearly linear pitching-moment characteristics when used in conjunction with the wings with smaller leading-edge radii. The actual reduction in the destabilizing pitching moment due to the addition of leading-edge chord-extensions  $\Delta C_{m_{\text{basic wing}}} - \Delta C_{m_{\text{wing} + \text{extension}}}$  on the wing with smallest leading-edge radius of the present investigation was of the same order of magnitude as that found in reference 5 on a similar wing of lower aspect ratio.

The majority of the chord-extensions tested caused a small reduction in the initial stability of the basic wings. With the exception of the extensions extending inboard of the midsemispan location (fig. 27 only) the chord-extensions did not reduce the initial stability of the basic wings by more than 4 percent. As is shown in figure 6, this reduction in the initial stability decreased rapidly as the inboard end of the extension moved outboard, and in some cases a small stabilizing contribution was evident.

Plan-form effects.-- As has been pointed out by previous investigators the spanwise location of the inboard end of leading-edge stall-control devices is of prime importance. For the wings with 0.0050c and 0.0025c leading-edge radii of the present investigation the optimum spanwise location for the inboard end of the chord-extension is near the 0.55b/2 wing station (see fig. 5 and tables I and II). The optimum position for the wing with 0.0089c leading-edge radius is less clearly defined (table III) and appears to vary from 0.575b/2 to 0.070b/2 with changes in the other geometric characteristics (leading-edge radius and percent extension) of the extensions.

Tests to determine the effects of chord-extension-end geometry were not made in the course of the present investigation. However, unpublished data from tests of a current swept wing fighter model indicate that fairing the inboard end of the leading-edge chord-extension into the contour of the basic wing completely destroys the effectiveness of the device. This loss in effectiveness is due to the dispersion and consequent weakening or destruction of the inboard end vortex upon which the action of the extension depends.

The position and geometry of the outboard end of the leading-edge chord-extensions is of small importance relative to the problem of

obtaining proper placement of the inboard end. As pointed out in reference 1 and as substantiated by figure 9, movement of the outboard end of the extension inboard from the basic wing tip results in some reduction in the effectiveness of the extension. Unpublished data, however, indicate that this loss in effectiveness can be counteracted by fairing the outboard end of the chord-extension into the wing leading edge. (In the specific case cited, full effectiveness was retained for a  $0.05b/2$  span chord-extension through the use of an outboard end fairing.)

With a single exception, the larger the projection of the leading-edge chord-extension, the more effective was the device. The single exception was the 13-percent chord-extension with 0.00445c leading-edge radius, on the wing with 0.0089c leading-edge radius (see table III), which appeared to be inferior to the 6.4-percent extension as well as the 19.8-percent extension of the same leading-edge radius. No explanation is offered for this apparent contradiction to the general trend.

Section effects.- In general, it is seen (tables I, II and III) that (independent of the basic wing to which it is attached) the chord-extensions with the larger leading-edge radii produce the most nearly linear pitching-moment characteristics. In this respect it was found that the extensions with zero leading-edge radii produced almost no beneficial effects while those with the largest leading-edge radii produced pitching-moment characteristics that approached linearity. Similar improvements in the effectiveness of chord-extensions through the use of extensions with increased leading-edge radii were noted in the earlier work of reference 1.

As has been shown in this and the preceding section, the effectiveness of the leading-edge chord-extension is increased by an increase in the leading-edge radius and/or the projection of the extension. Thus, it can be seen that for a wing exhibiting only a moderate instability, the same linearization can probably be obtained through either the use of a large leading-edge radius chord-extension of small projection or a small leading-edge radius extension of large projection. Final selection for application to wings of this type will be dependent upon high speed, structure, or other considerations.

Although significant reductions in the nonlinearity of the basic wing pitching-moment characteristics were obtained, none of the undrooped extensions were able to prevent a rather marked forward aerodynamic-center shift at approximately the same angle of attack at which the basic wing instability occurred (see tables I, II, and III). Furthermore, addition of the undrooped extensions did not noticeably improve the flow at the wing tips.

From the results of the present tests it appears that although the undrooped extensions have succeeded in checking the boundary-layer outflow

(their design purpose), due to the high concentration of loading at the tip on the basic plan form the lift producing capacity of the tip sections (independent of boundary-layer outflow) have been surpassed and stalled flow still exists. For further improvements in the flow at the tip (and hence the stability characteristics), the stalling characteristics of the tip sections must be altered. The results of the addition of forward camber in the form of a  $12^\circ$  drooped extension (see table III and fig. 5(c)) seem to confirm the foregoing and indicate droop is an important variable in the design of chord-extensions for use on the present wings.

Buffeting.— What appeared to be rather severe buffeting was encountered during the present chord-extension investigation. Although no measurements of the intensity were made, audiovisual observation of the model during the tests indicated that buffeting was most severe when the reduction in the destabilizing pitching moment was the greatest.

Inasmuch as poor buffeting characteristics could possibly severely limit or prohibit the use of leading-edge chord-extensions as a longitudinal stability "fix" it appears that further investigation of the buffeting characteristics of wings equipped with chord-extensions would be desirable.

### CONCLUSIONS

The following conclusions are based on the results of tests of various leading-edge chord-extensions on three  $45^\circ$  sweptback, aspect-ratio 5 wings incorporating different airfoil sections:

1. Although complete linearity of the pitching-moment curve was not achieved, large reductions in the longitudinal instability of the basic wings were obtained through the use of leading-edge chord-extensions. For a given chord-extension the reduction was the largest on the wing with smallest leading-edge radius.
2. For the wings with smaller leading-edge radii the most nearly linear pitching-moment characteristics were obtained with the inboard end of the extensions located near the 55-percent wing semispan station. On the wing with the largest leading-edge radius the optimum position varied from 57.5 to 70 percent of the wing semispan depending upon the extension geometry.
3. The greatest improvements in the longitudinal stability obtained through the use of undrooped extensions were produced by the largest leading-edge radius, largest projection chord-extension.

4. Additional improvements in the longitudinal stability characteristics of the wing with the largest leading-edge radius were obtained through the use of drooped chord-extensions.

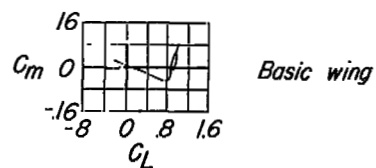
Langley Aeronautical Laboratory,  
National Advisory Committee for Aeronautics,  
Langley Field, Va., August 1, 1955.

#### REFERENCES

1. Furlong, G. Chester: Exploratory Investigation of Leading-Edge Chord-Extensions To Improve the Longitudinal Stability Characteristics of Two  $52^\circ$  Sweptback Wings. NACA RM L50A30, 1950.
2. Furlong, G. Chester, and McHugh, James G.: A Summary and Analysis of the Low-Speed Longitudinal Characteristics of Swept Wings at High Reynolds Number. NACA RM L52D16, 1952.
3. Sivells, James C., and Salmi, Rachel M.: Jet-Boundary Corrections for Complete and Semispan Swept Wings in Closed Circular Wind Tunnels. NACA TN 2454, 1951.
4. Foster, Gerald V., and Schneider, William C.: Effects of Leading-Edge Radius on the Longitudinal Stability of Two  $45^\circ$  Sweptback Wings As Influenced by Reynolds Numbers up to  $8.20 \times 10^6$  and Mach numbers up to 0.303. NACA RM L55F06, 1955.
5. Goodson, Kenneth W., and Few, Albert G., Jr.: Effect of Leading-Edge Chord-Extensions on Subsonic and Transonic Aerodynamic Characteristics of Three Models Having  $45^\circ$  Sweptback Wings of Aspect Ratio 4. NACA RM L52K21, 1953.

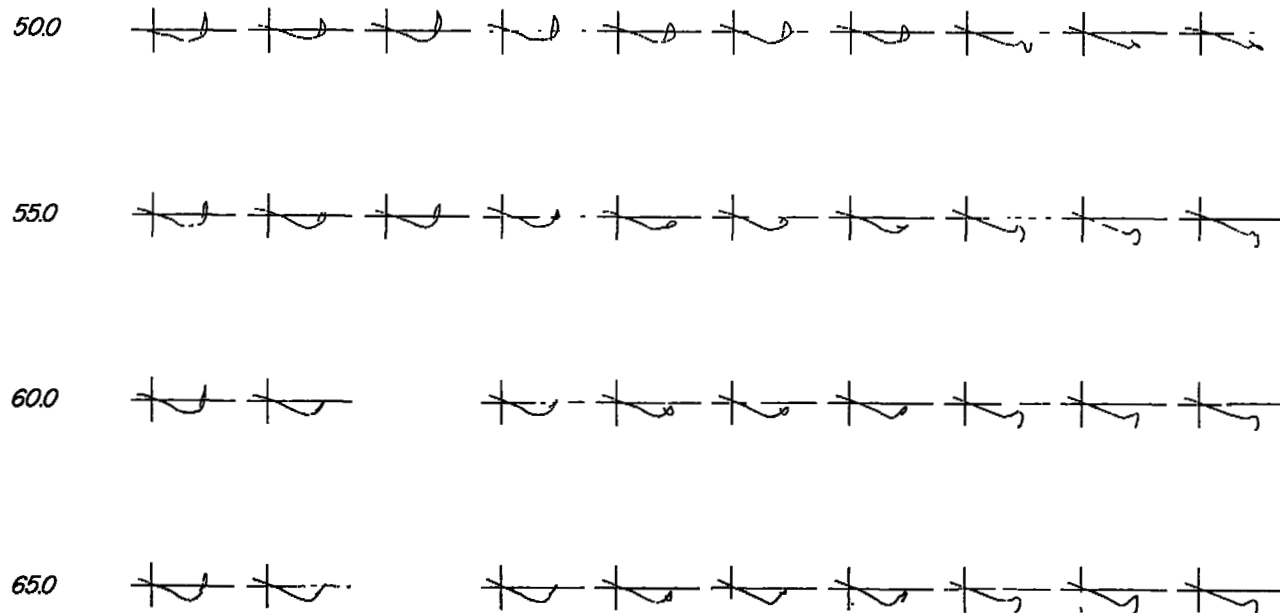
TABLE I - CHARACTERISTICS OF THE  $0.0025c$  LEADING-EDGE RADIUS WING WITH CHORD EXTENSIONS  
(a)  $C_m$  against  $C_L$ .

10



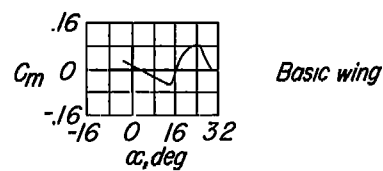
L.E. Radius, %c	0		0.125			0.250		0.445		
Extension, %c	13.0	19.8	6.4	13.0	19.8	13.0	19.8	6.4	13.0	19.8

Inboard end  
position, % b/2



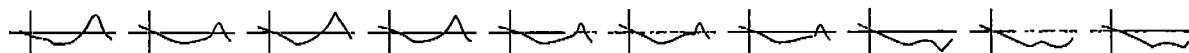
NACA RM L55H19

TABLE I.- Concluded  
(b)  $C_m$  against  $\alpha$ .

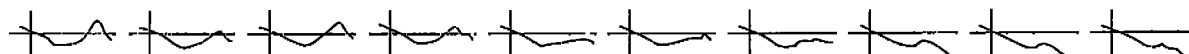


L.E. Radius, %c	0		0.125			0.250		0.445		
Extension, %c	130	198	6.4	130	198	130	198	6.4	130	198
Inboard end position, %b/2										

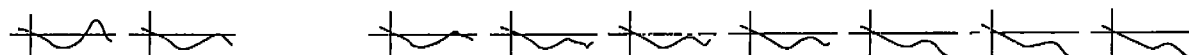
50.0



55.0



60.0



65.0

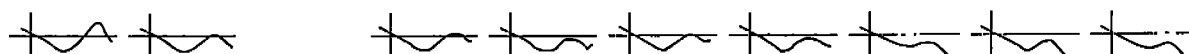
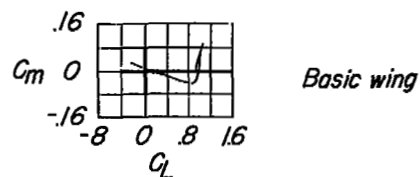


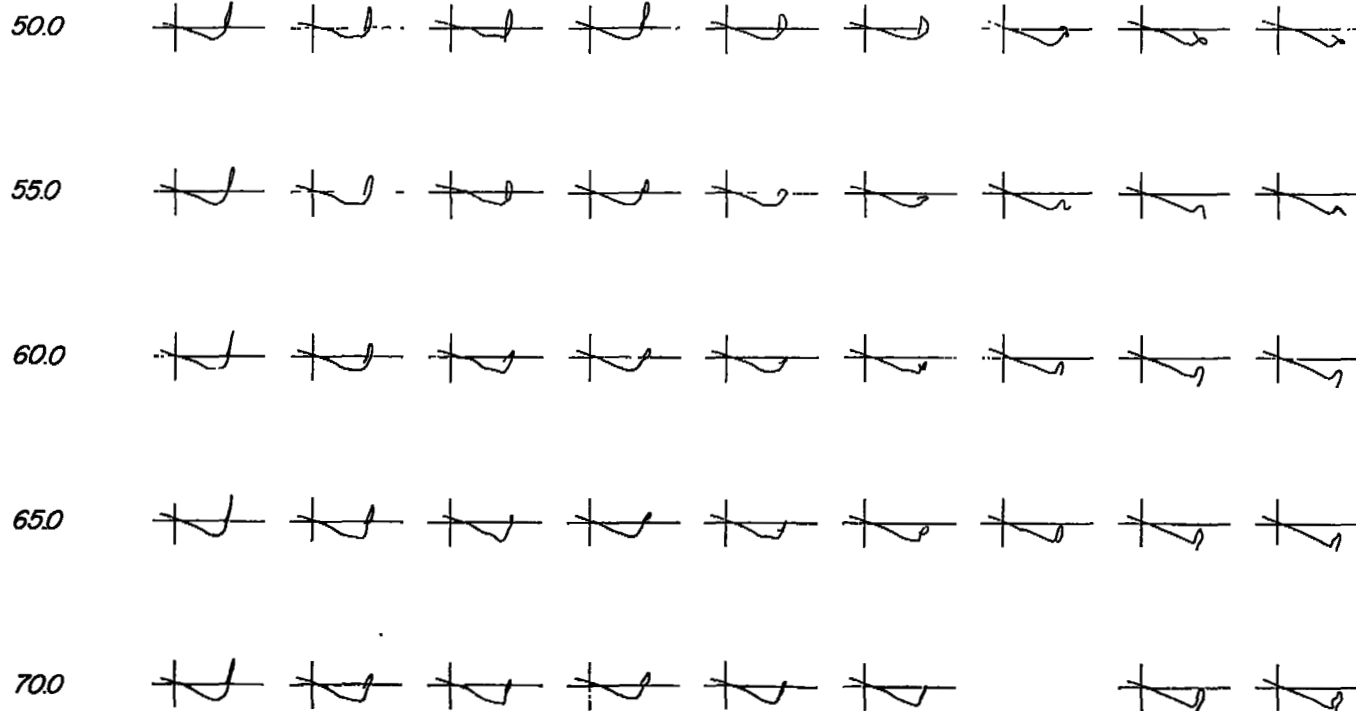
TABLE II.- CHARACTERISTIC OF THE 0.0050c LEADING-EDGE RADIUS WING WITH CHORD EXTENSIONS  
(a)  $C_m$  against  $C_L$ .

12



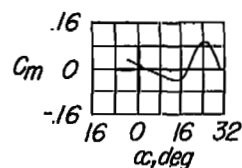
L.E. Radius, %c	0			0.250			0.445		
Extension, %c	6.4	13.0	19.8	6.4	13.0	19.8	6.4	13.0	19.8

Inboard end  
position, %b/2



NACA RM L55H19

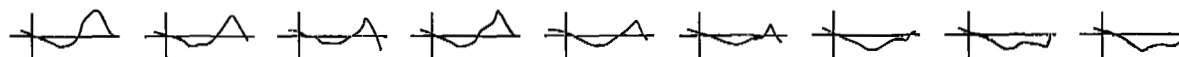
TABLE II.- Concluded  
(b)  $C_m$  against  $\alpha$ .



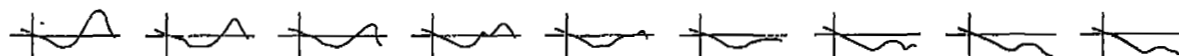
L.E. Radius, %c	0			0.250			0.445		
Extension, %c	6.4	13.0	19.8	6.4	13.0	19.8	6.4	13.0	19.8

Inboard end  
position, %b/2

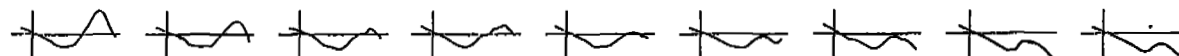
50.0



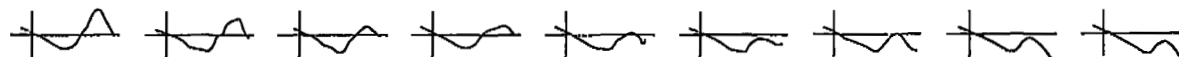
55.0



60.0



65.0



70.0

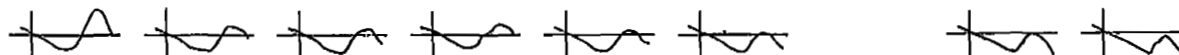
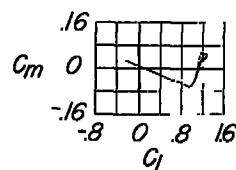


TABLE III.- CHARACTERISTICS OF THE 0.0089c LEADING-EDGE RADIUS WING WITH CHORD EXTENSIONS  
(a)  $C_m$  against  $C_L$ .

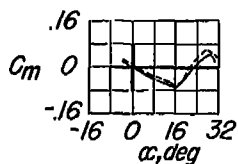


Basic wing

---  $R=4.9 \times 10^6$   
—  $R=4.6 \times 10^6$

L.E. Radius, %c	0			0.445			0.890			
Extension, %c	6.4	13.0	19.8	6.4	13.0	19.8	6.4	13.0	19.8	18.0 drooped
Inboard end position, % b/2										
500										
550										
575										
600										
625										
650										
700										
750										

TABLE III.- Concluded  
(b)  $C_m$  against  $\alpha$ .



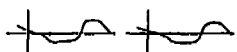
Basic wing

---  $R=4.9 \times 10^6$   
—  $R=4.6 \times 10^6$

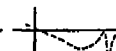
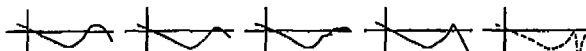
L.E. Radius, %c	0			0.445			0.890			
Extension, %c	6.4	13.0	19.8	6.4	13.0	19.8	6.4	13.0	19.8	18.0 drooped

Inboard end  
position, % b/2

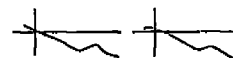
50.0



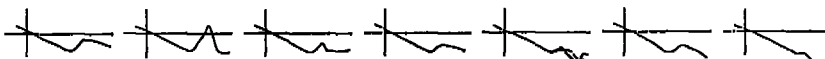
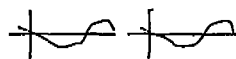
55.0



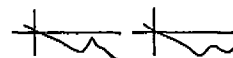
57.5



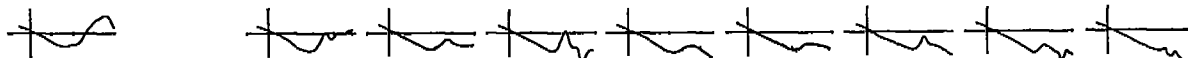
60.0



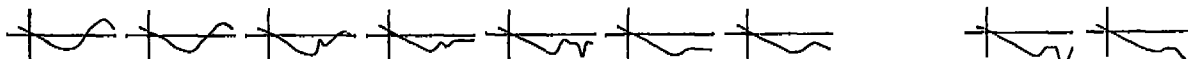
62.5



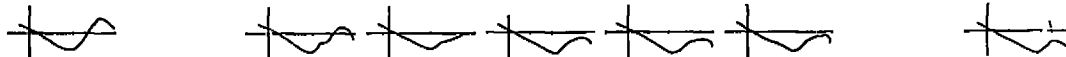
65.0

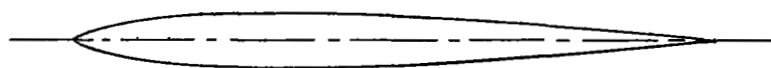
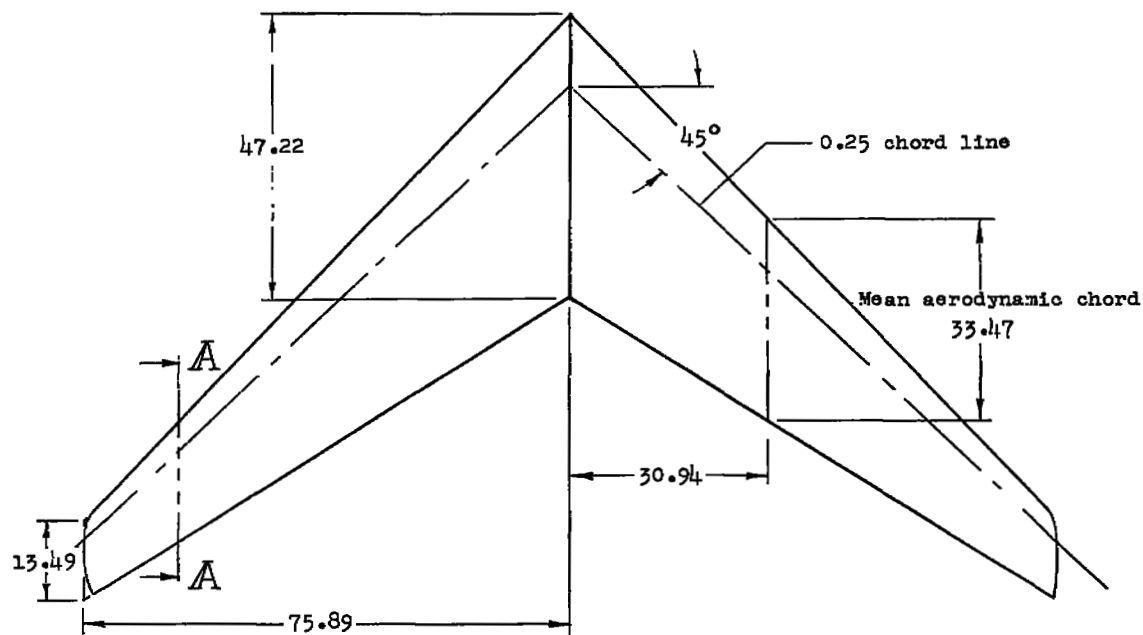


70.0

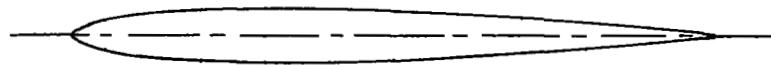


75.0

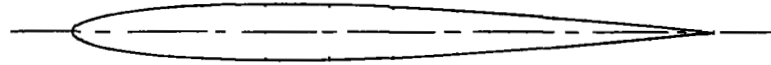




NACA 0009-(3.18)3 airfoil



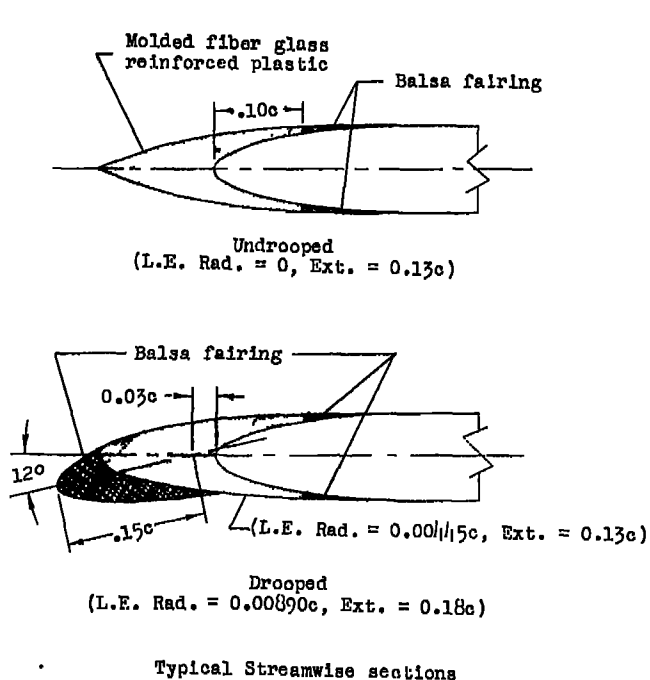
NACA 0009-(4.53)3 airfoil



NACA 0009-63 airfoil

Section A-A (enlarged)

Figure 1.- Geometric characteristics of the basic wings. (Dimensions in inches except as noted.)



L.E. Rad. (fraction c)	Airfoil (streamwise)	Extension (fraction c)
0	NACA 0009-03	0.064, 0.130, 0.198
0.00125	NACA 0009-(2.25)3	0.064, 0.130, 0.198
.00250	NACA 0009-(3.18)3	0.064, 0.130, 0.198
.00450	NACA 0009-(4.24)3	0.064, 0.130, 0.198
.00890	NACA 0009-63	0.064, 0.130, 0.198, 0.180 (drooped)

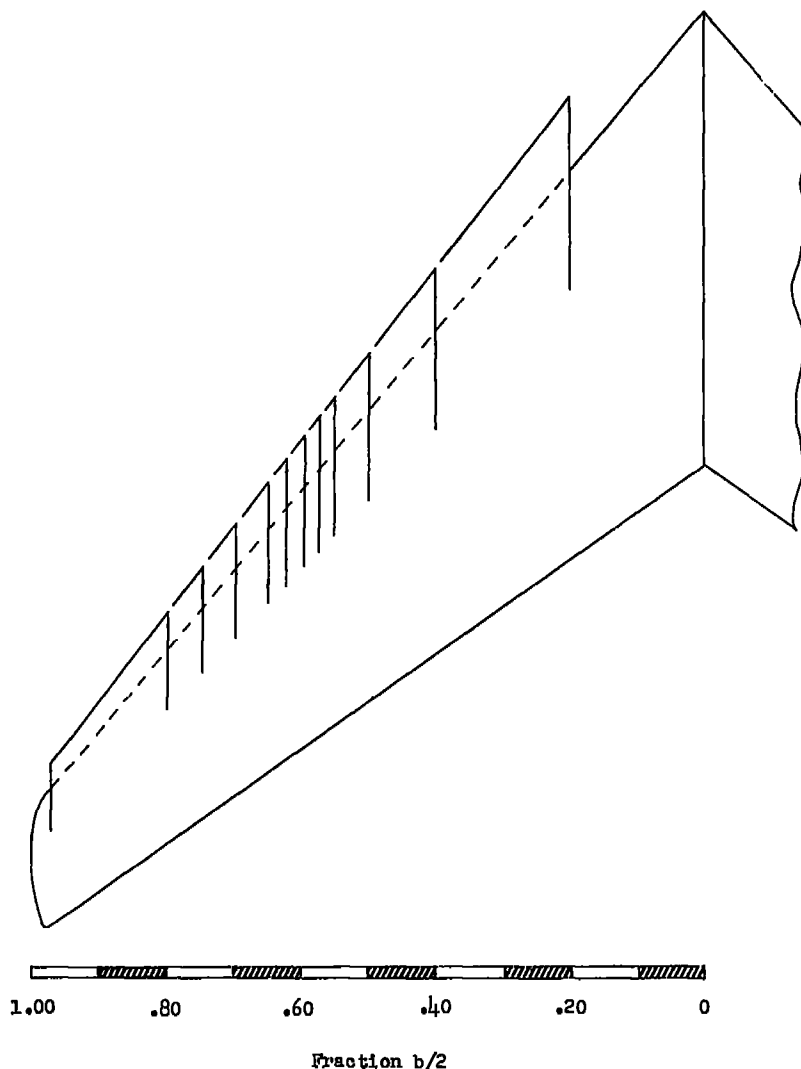
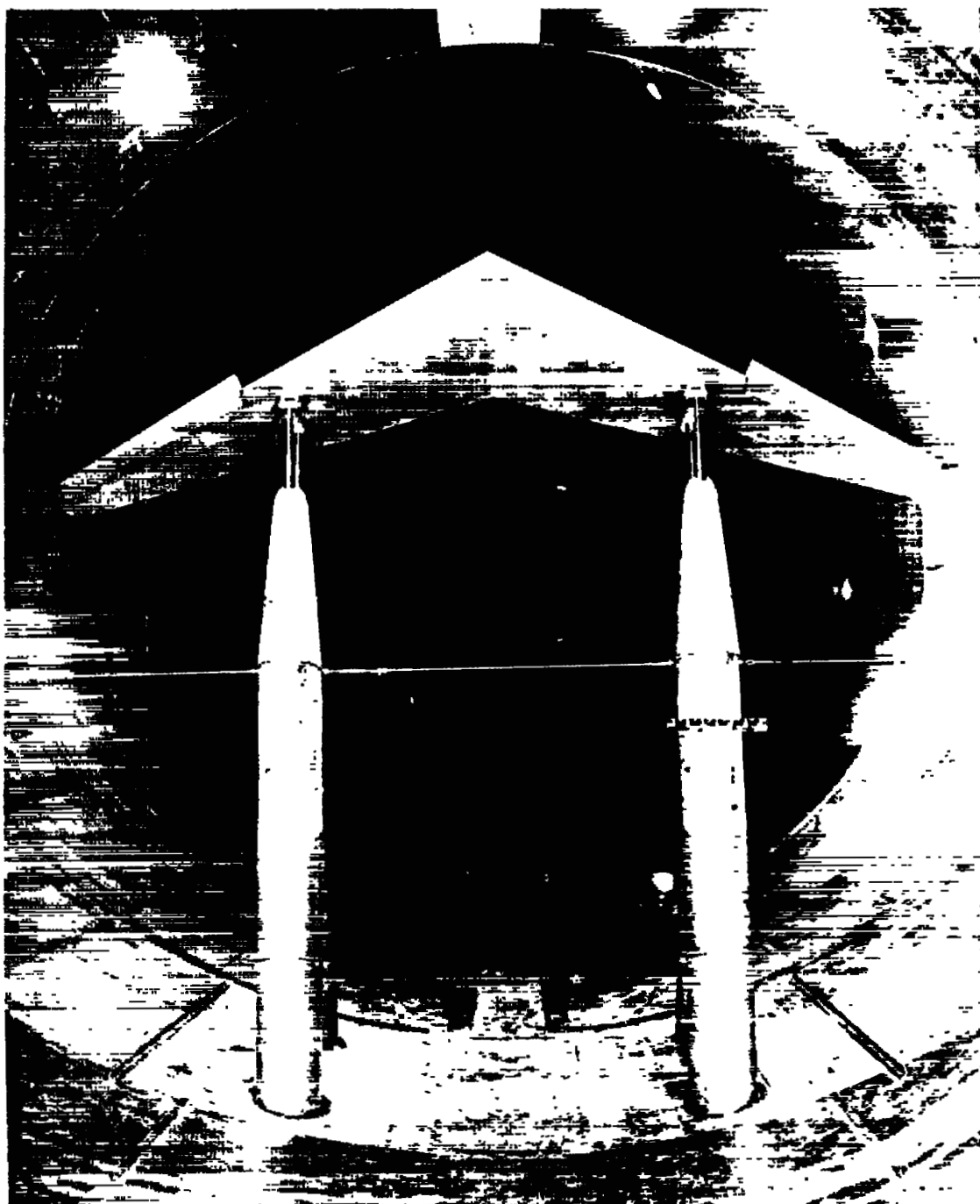


Figure 2.- Details of the leading-edge chord-extensions.



L-87178

Figure 3.- A  $45^\circ$  sweptback, aspect ratio 5 wing equipped with leading-edge chord-extensions mounted in the Langley 19-foot pressure tunnel.

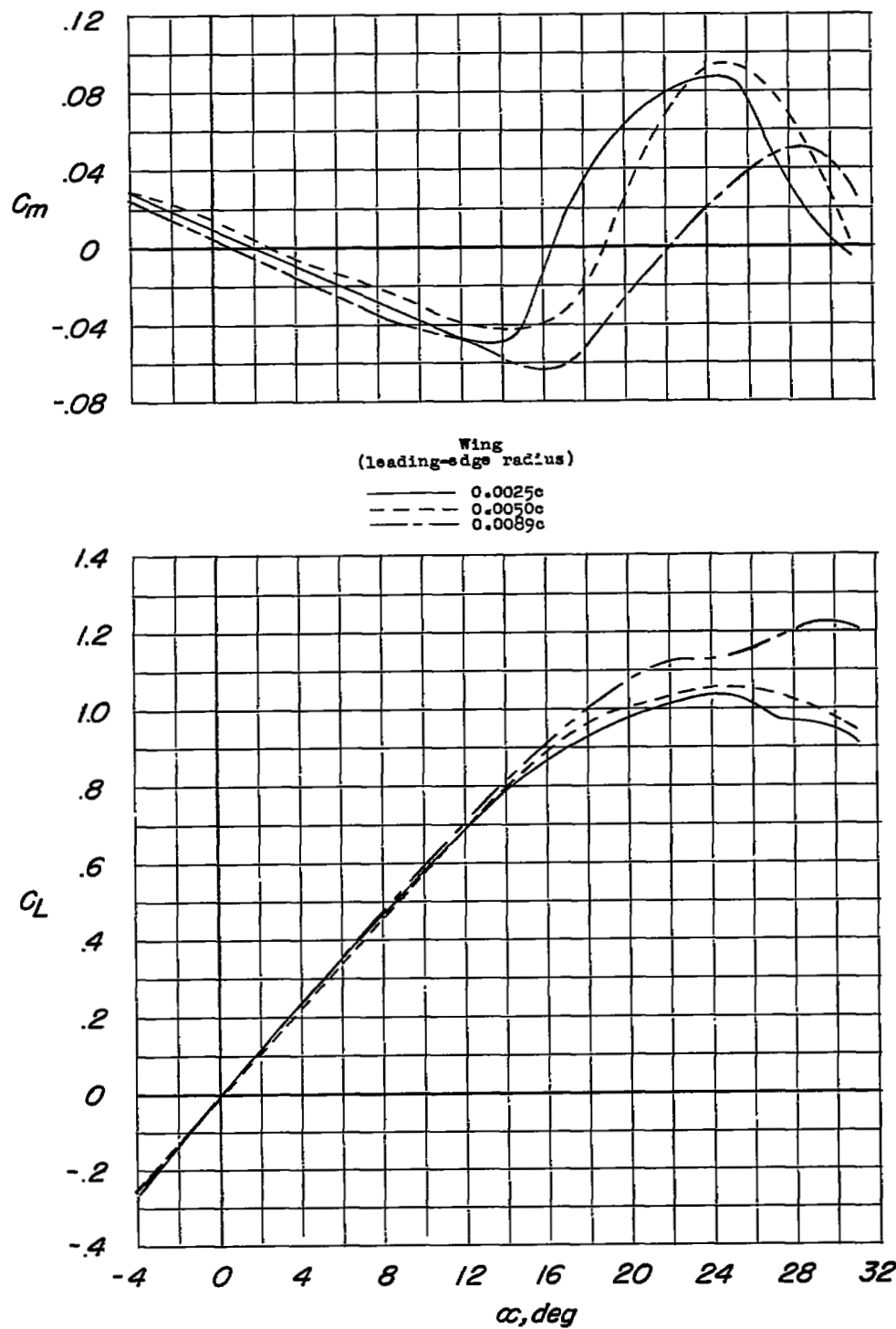
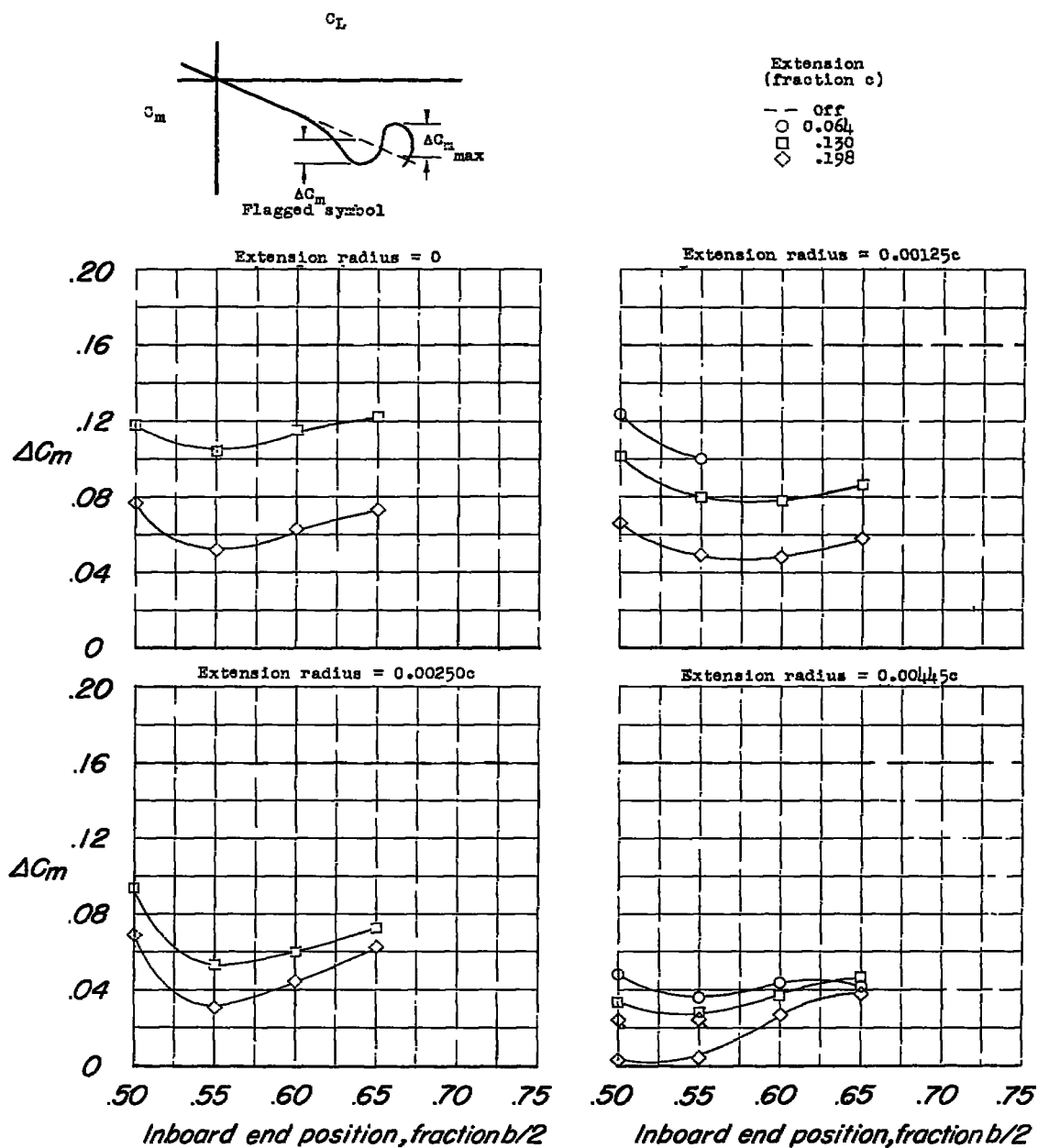
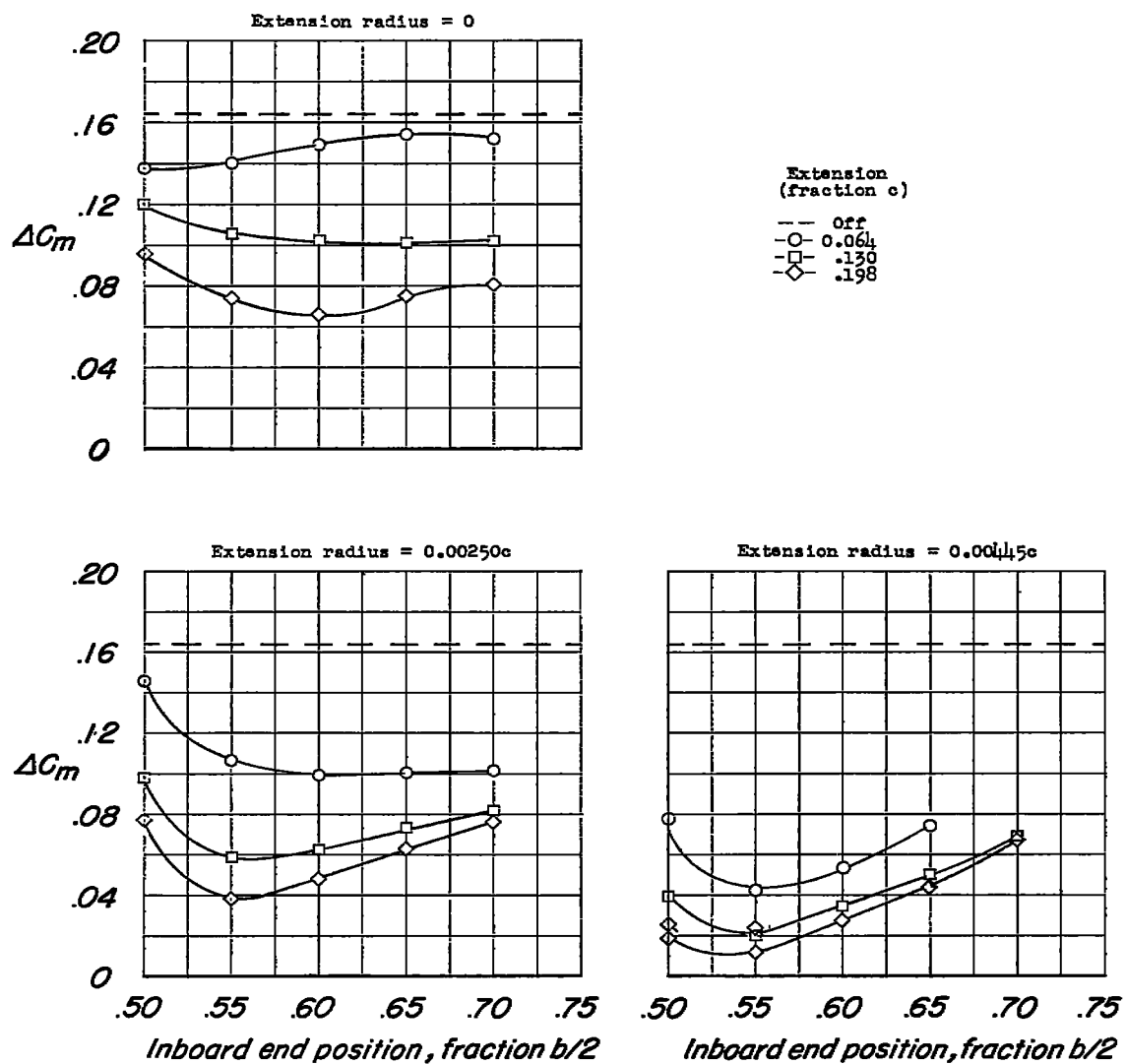


Figure 4.- Lift and pitching-moment characteristics of the basic wing.



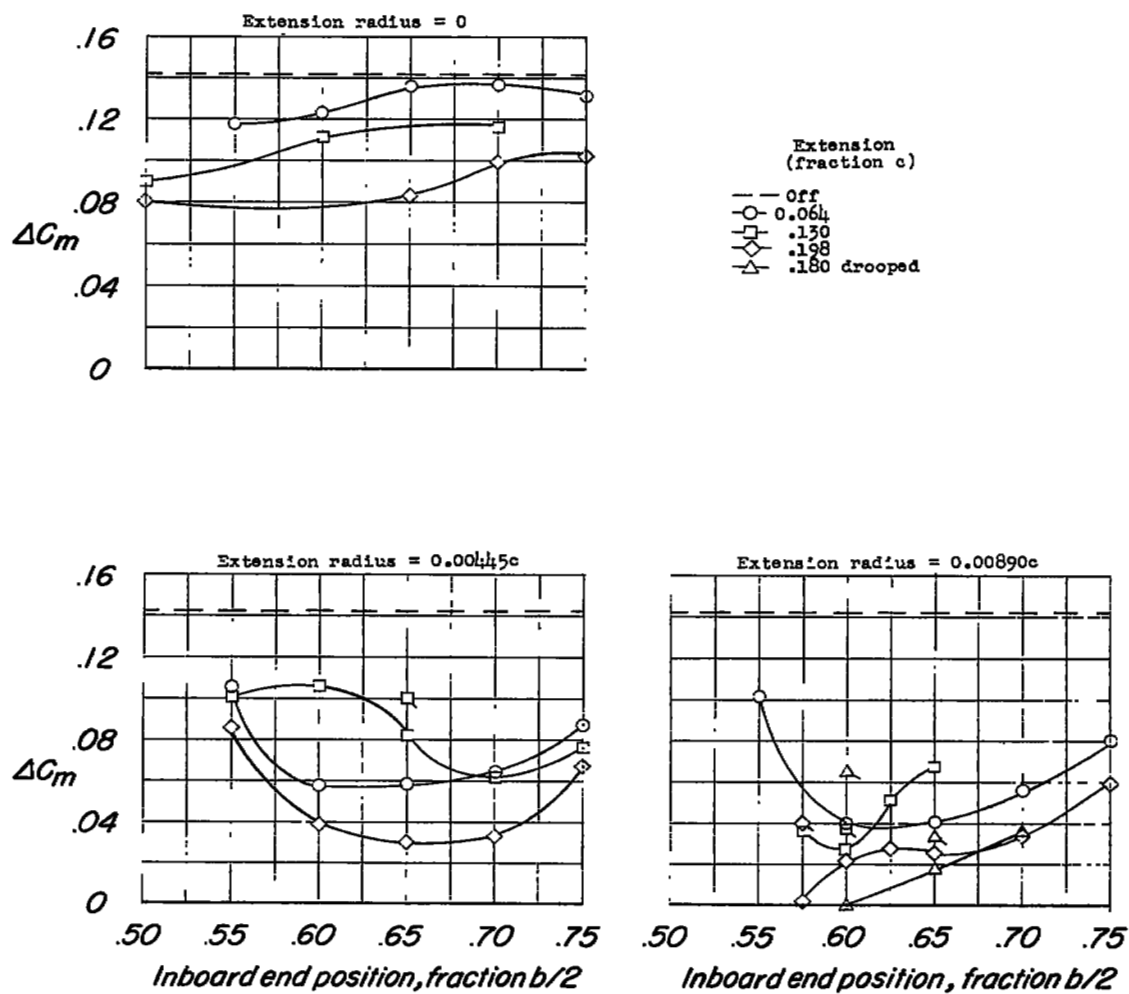
(a) 0.0025c-leading-edge-radius wing.

Figure 5.- Maximum pitching-moment deviations  $\Delta C_m$  for various chord-extension configurations. Flagged symbols denote large stabilizing deviations prior to maximum lift.



(b) 0.0050c-leading-edge-radius wing.

Figure 5.- Continued.



(c) 0.0089c-leading-edge-radius wing.

Figure 5.- Concluded.

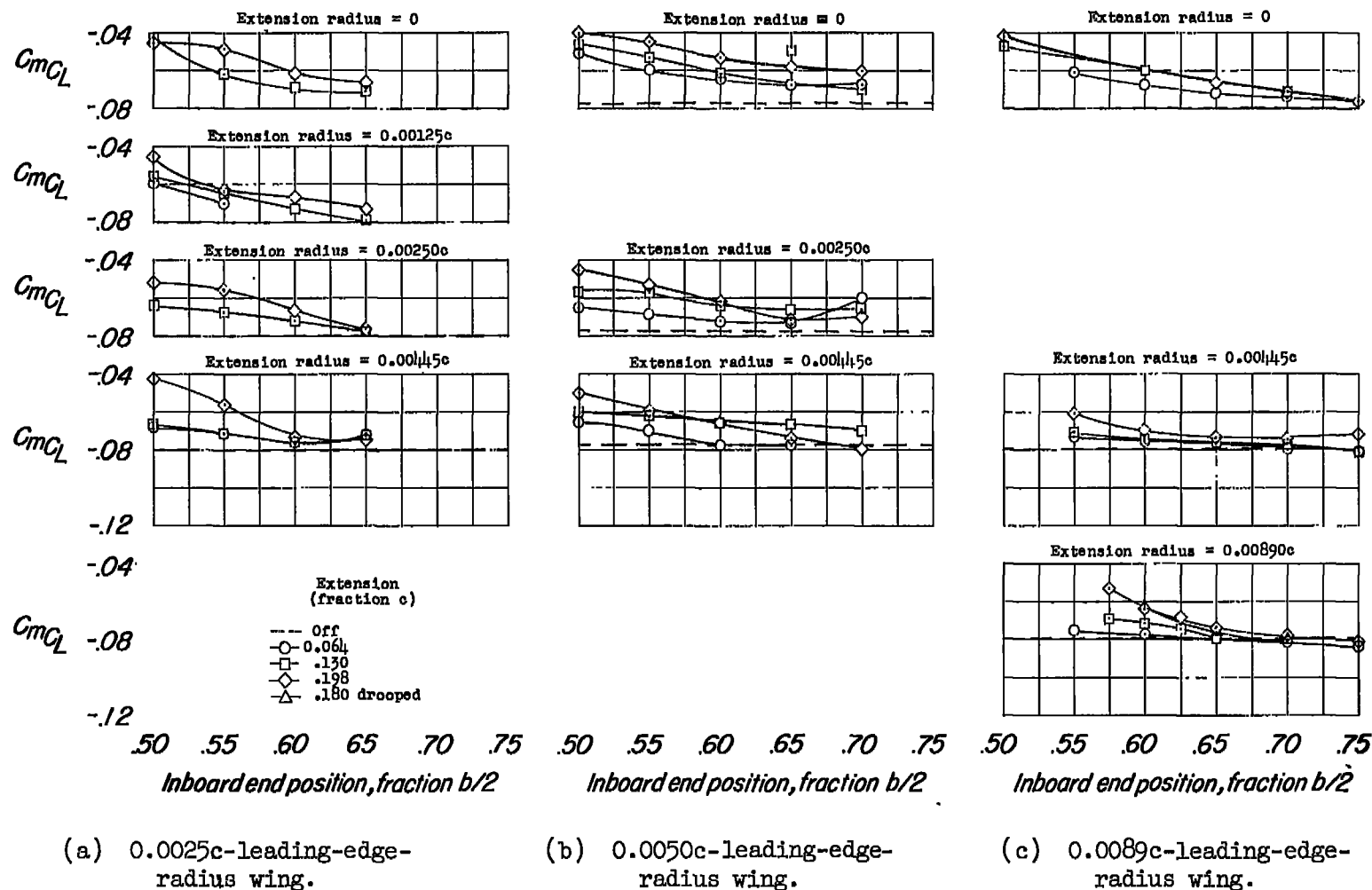


Figure 6.- Rate of change of pitching moment with lift at  $C_L = 0$  for various chord-extension configurations.

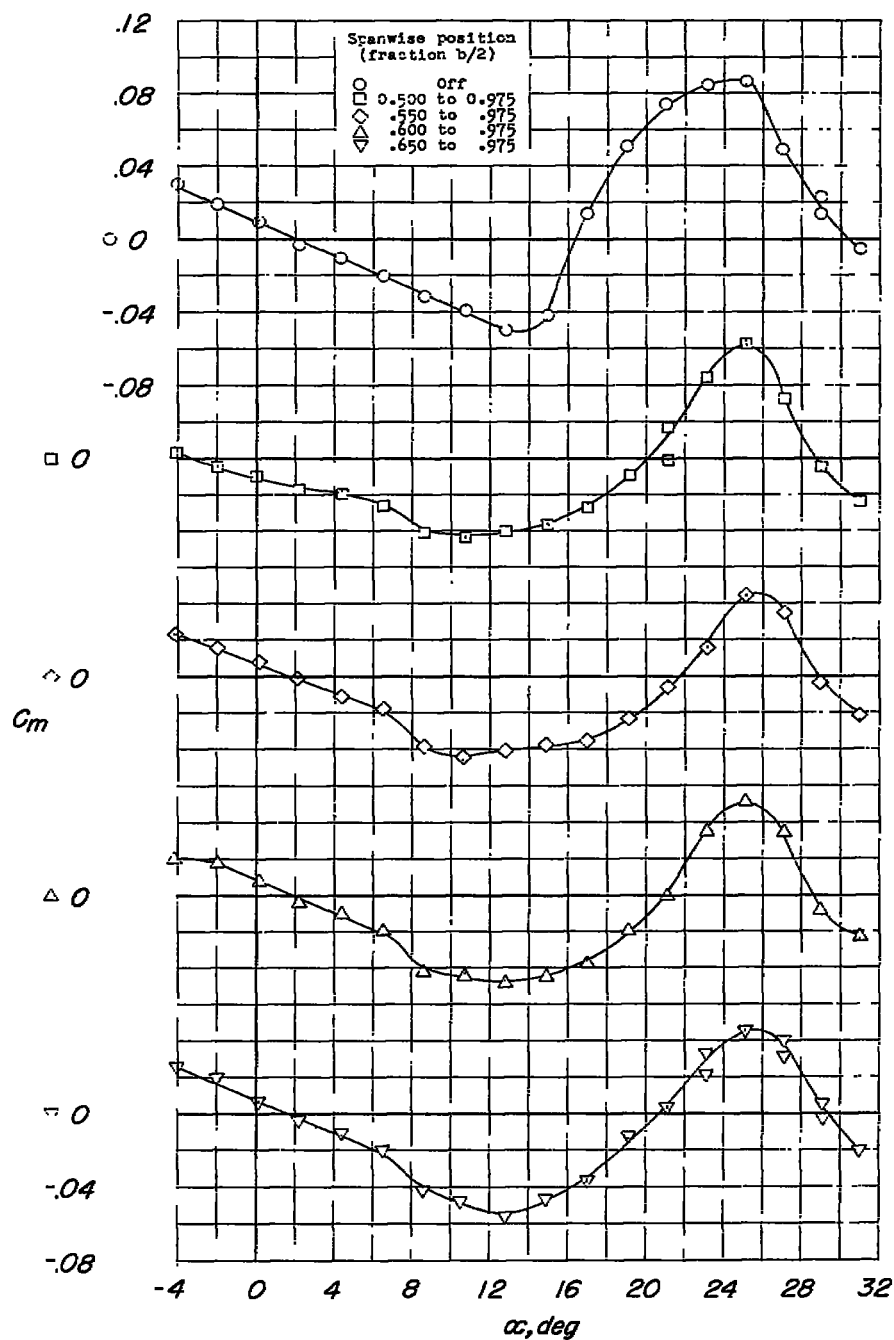
(a)  $C_m$  against  $\alpha$ .

Figure 7.- Lift and pitching-moment characteristics of wing with chord-extensions. Wing leading-edge radius,  $0.0025c$ ; chord-extension, 13.0 percent; chord-extension leading-edge radius,  $0c$ .

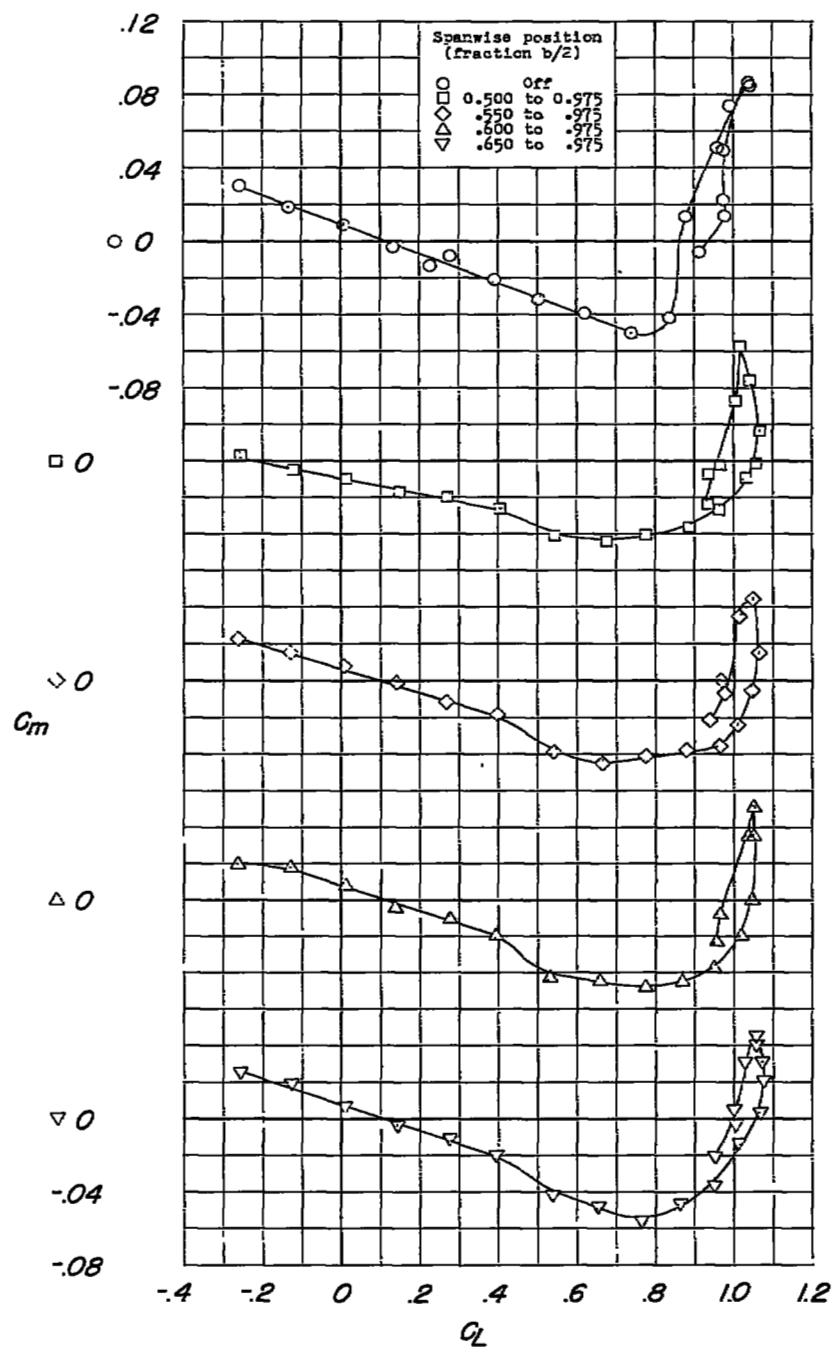
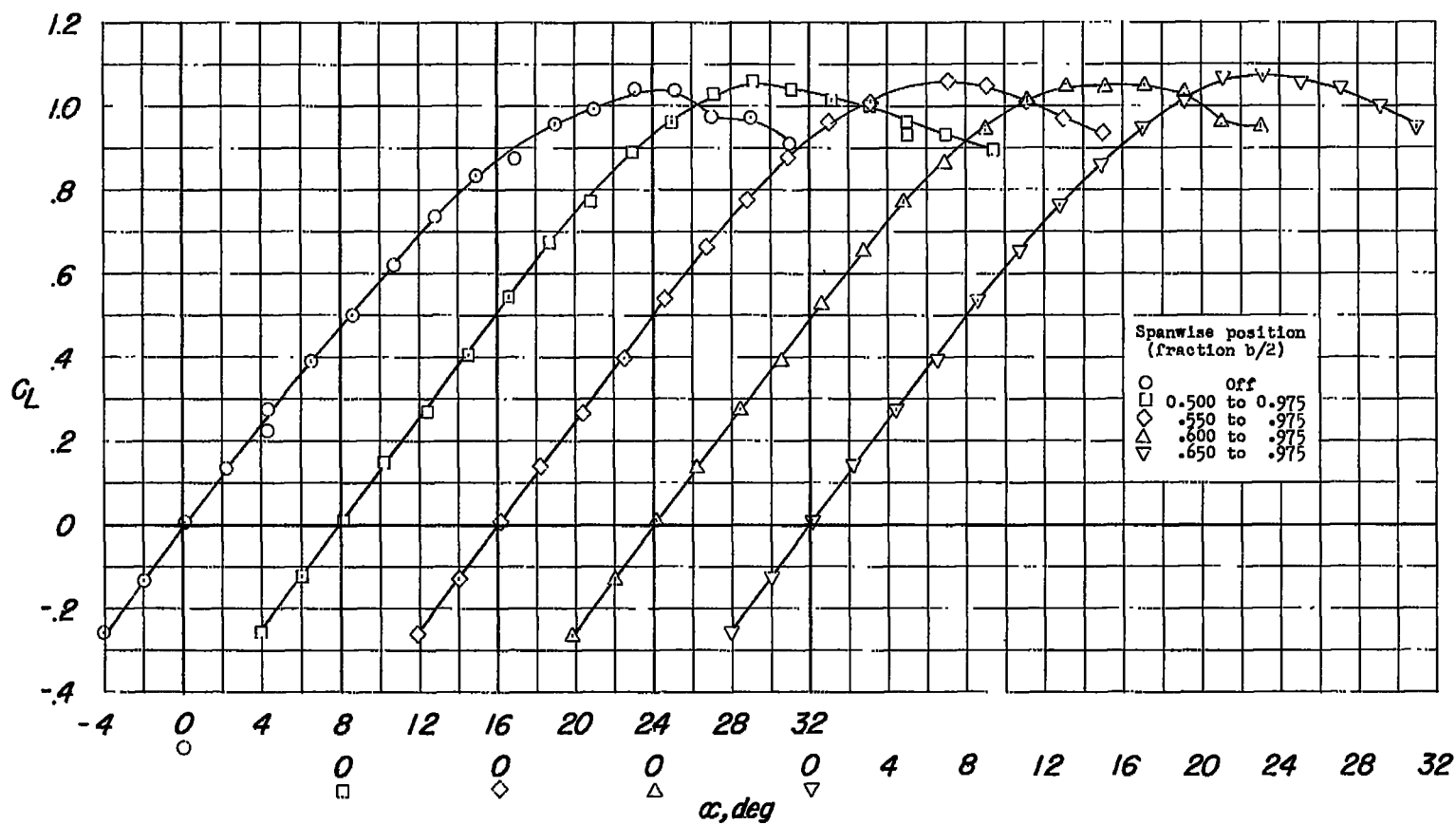
(b)  $C_m$  against  $C_L$ .

Figure 7.- Continued.



(c)  $C_L$  against  $\alpha$ .

Figure 7.- Concluded.

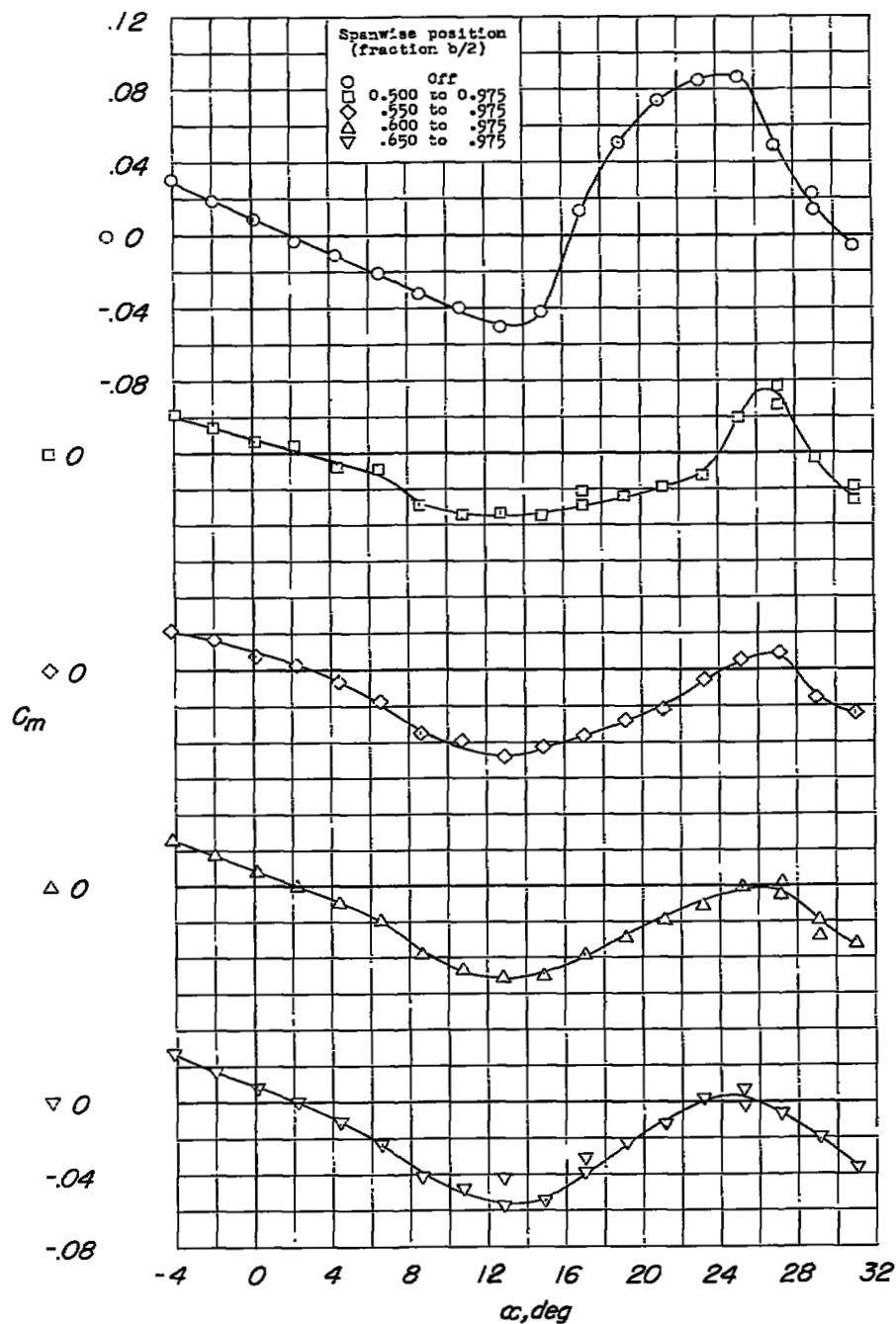
(a)  $C_m$  against  $\alpha$ .

Figure 8.- Lift and pitching-moment characteristics of wing with chord-extensions. Wing leading-edge radius, 0.0025c; chord-extension, 19.8 percent; chord-extension leading-edge radius, 0c.

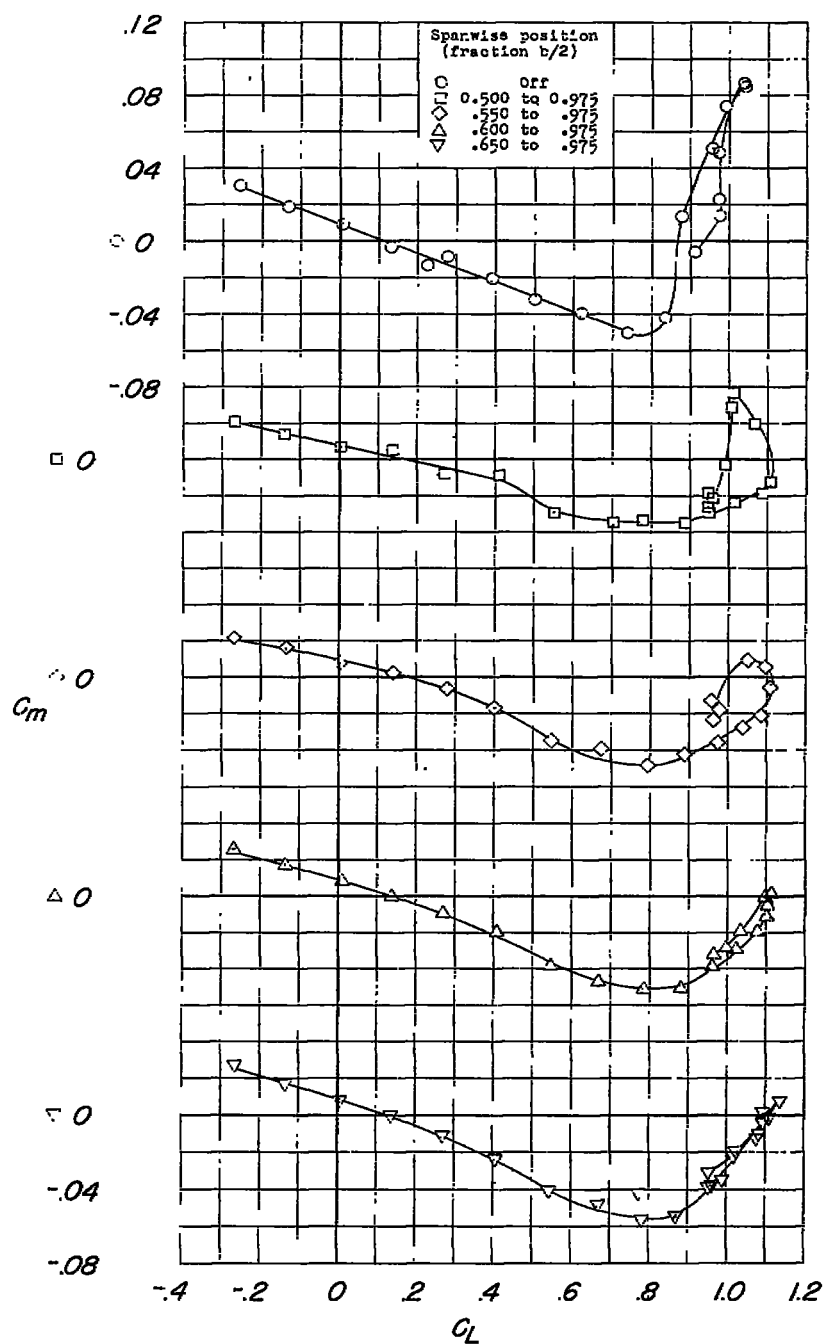
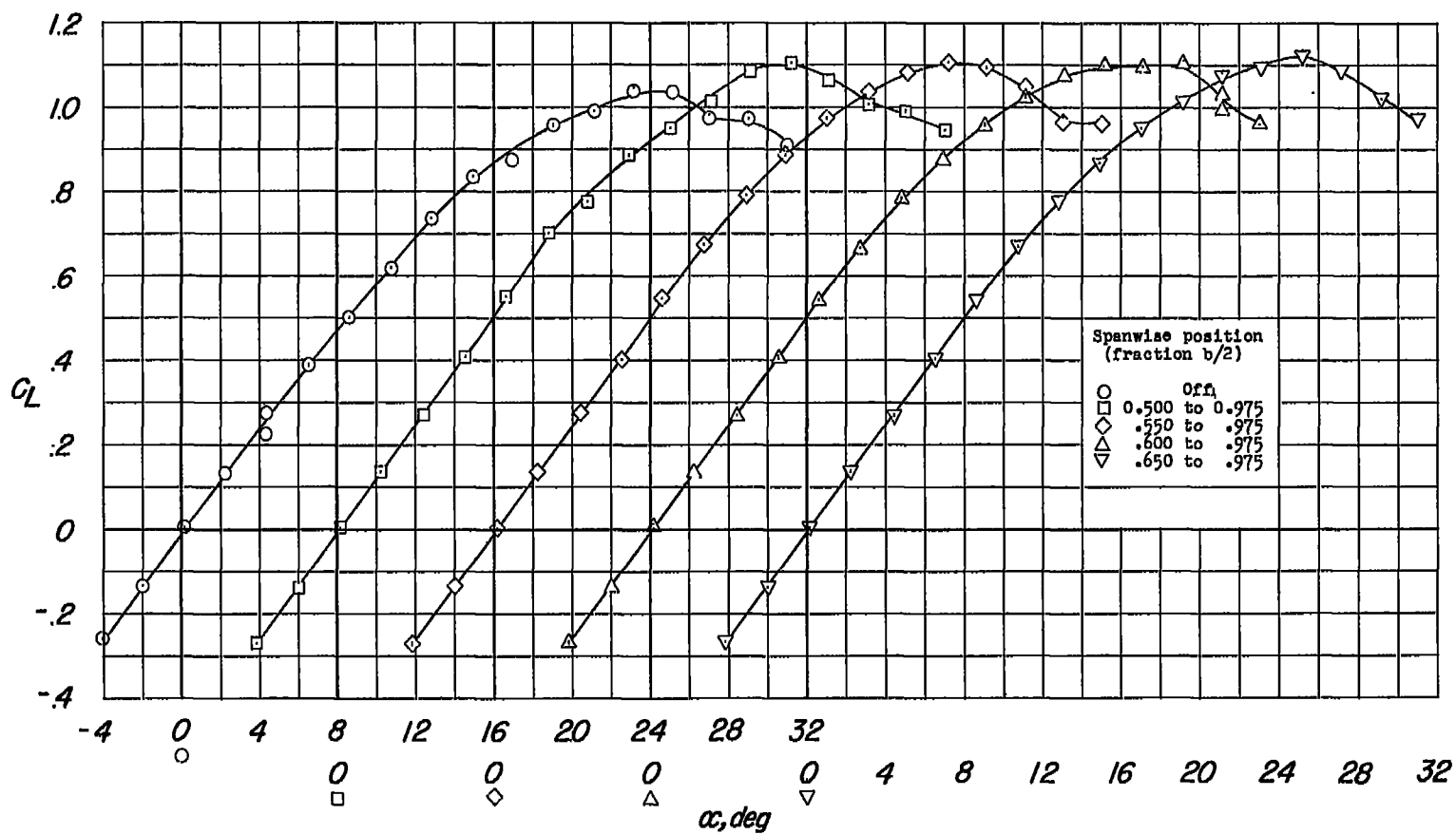
(b)  $C_m$  against  $C_L$ .

Figure 8.- Continued.



(c)  $C_L$  against  $\alpha$ .

Figure 8.- Concluded.

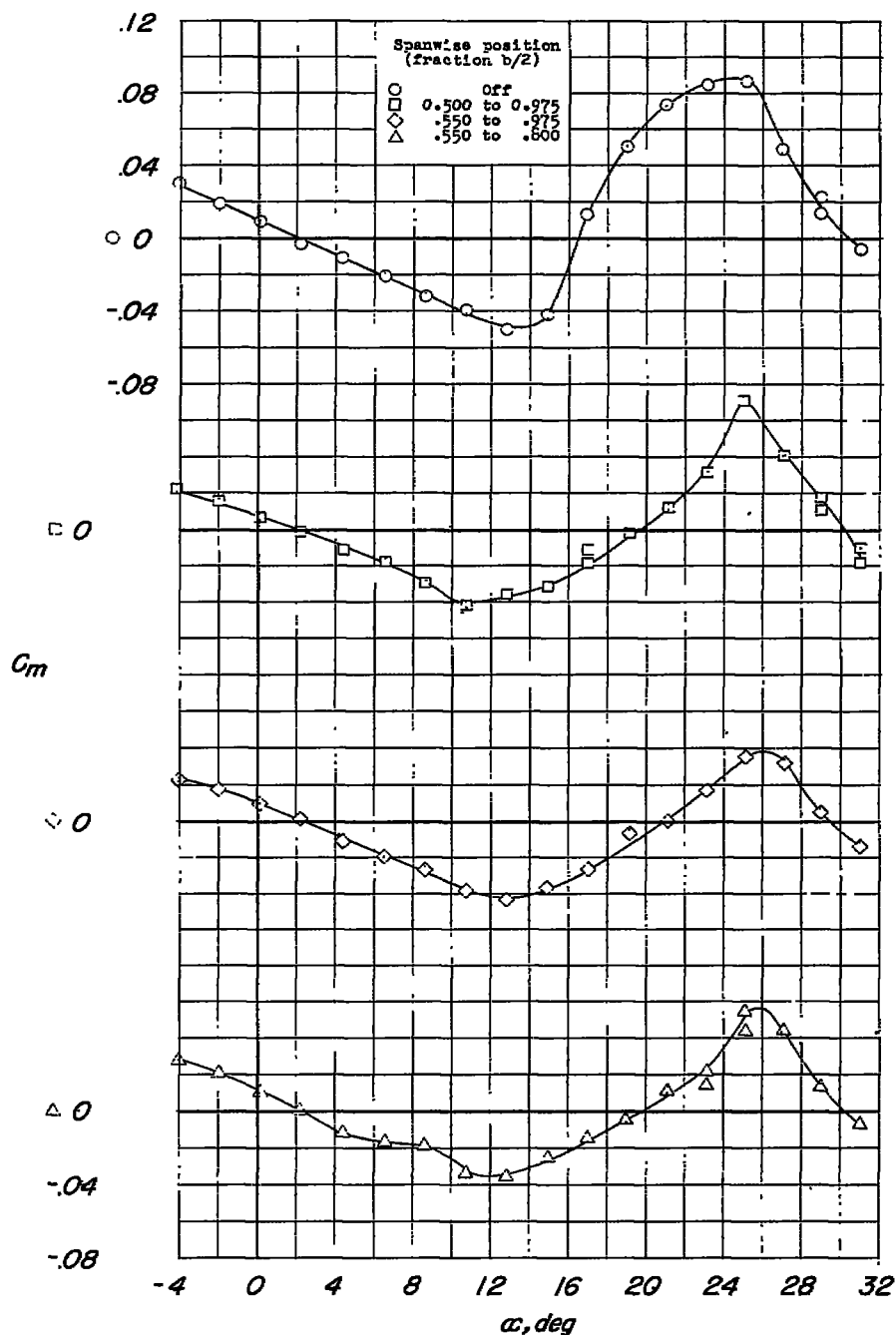
(a)  $C_m$  against  $\alpha$ .

Figure 9.- Lift and pitching-moment characteristics of wing with chord-extensions. Wing leading-edge radius, 0.0025c; chord-extension, 6.4 percent; chord-extension leading-edge radius, 0.00125c.

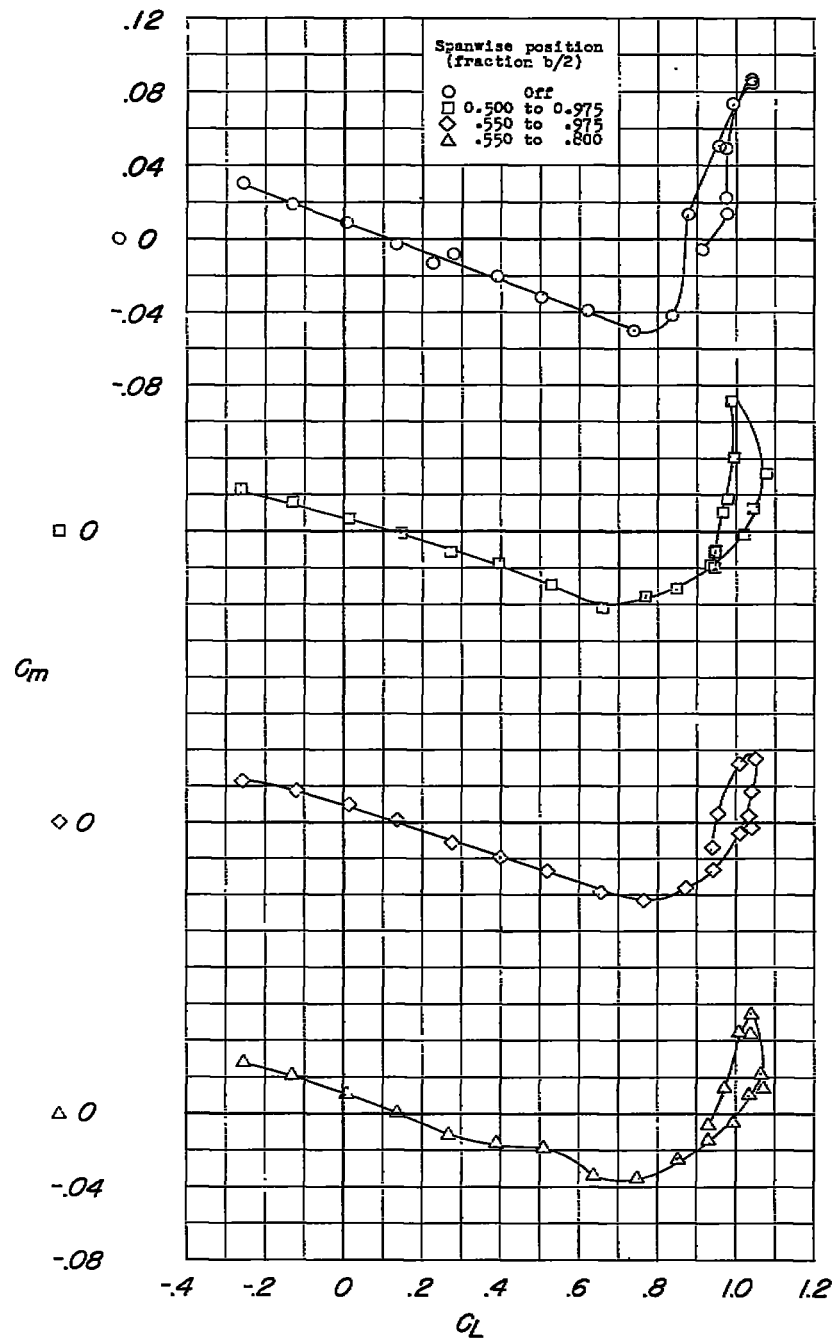
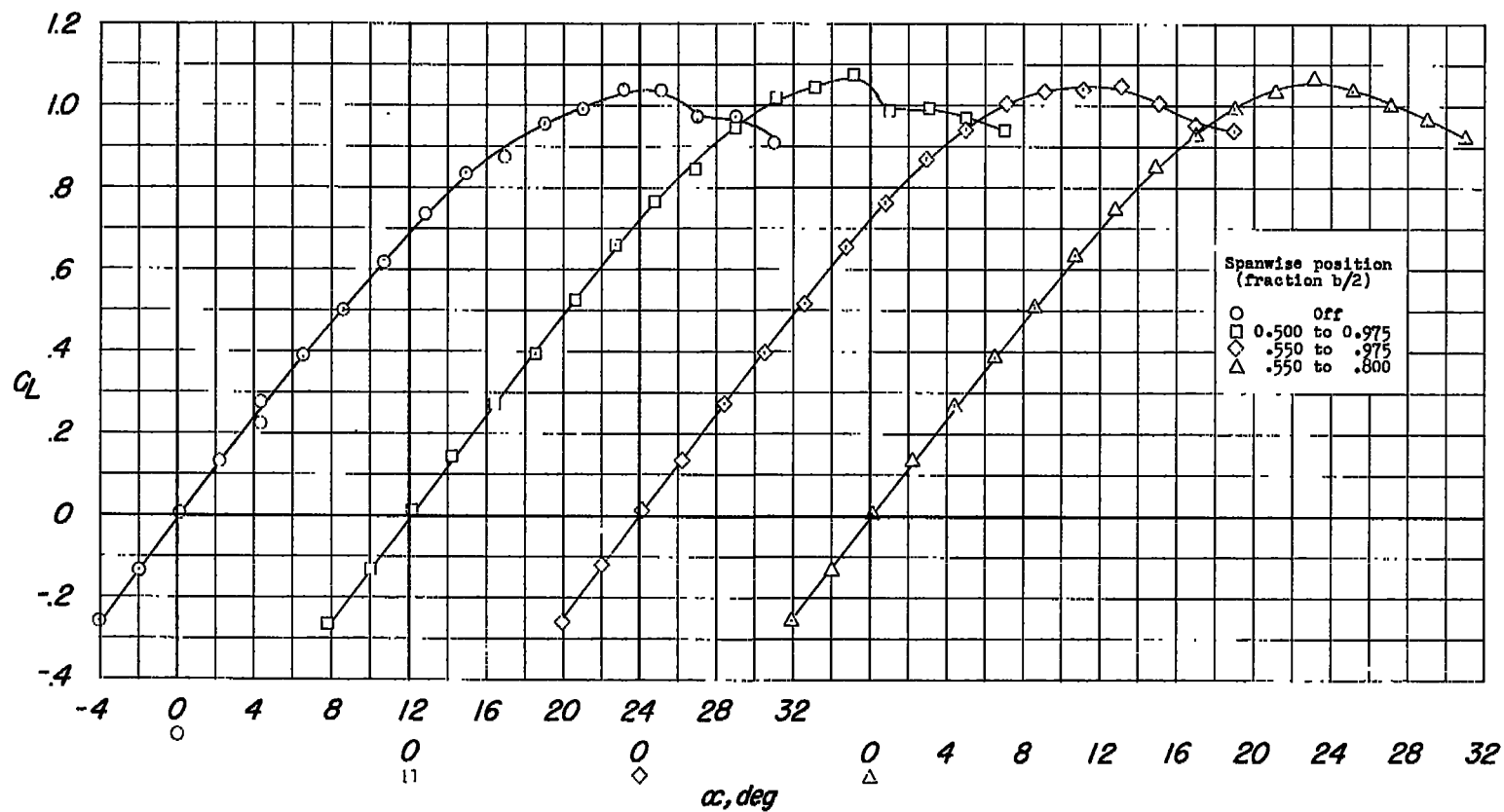
(b)  $C_m$  against  $C_L$ .

Figure 9.- Continued.



(c)  $C_L$  against  $\alpha$ .

Figure 9.- Concluded.

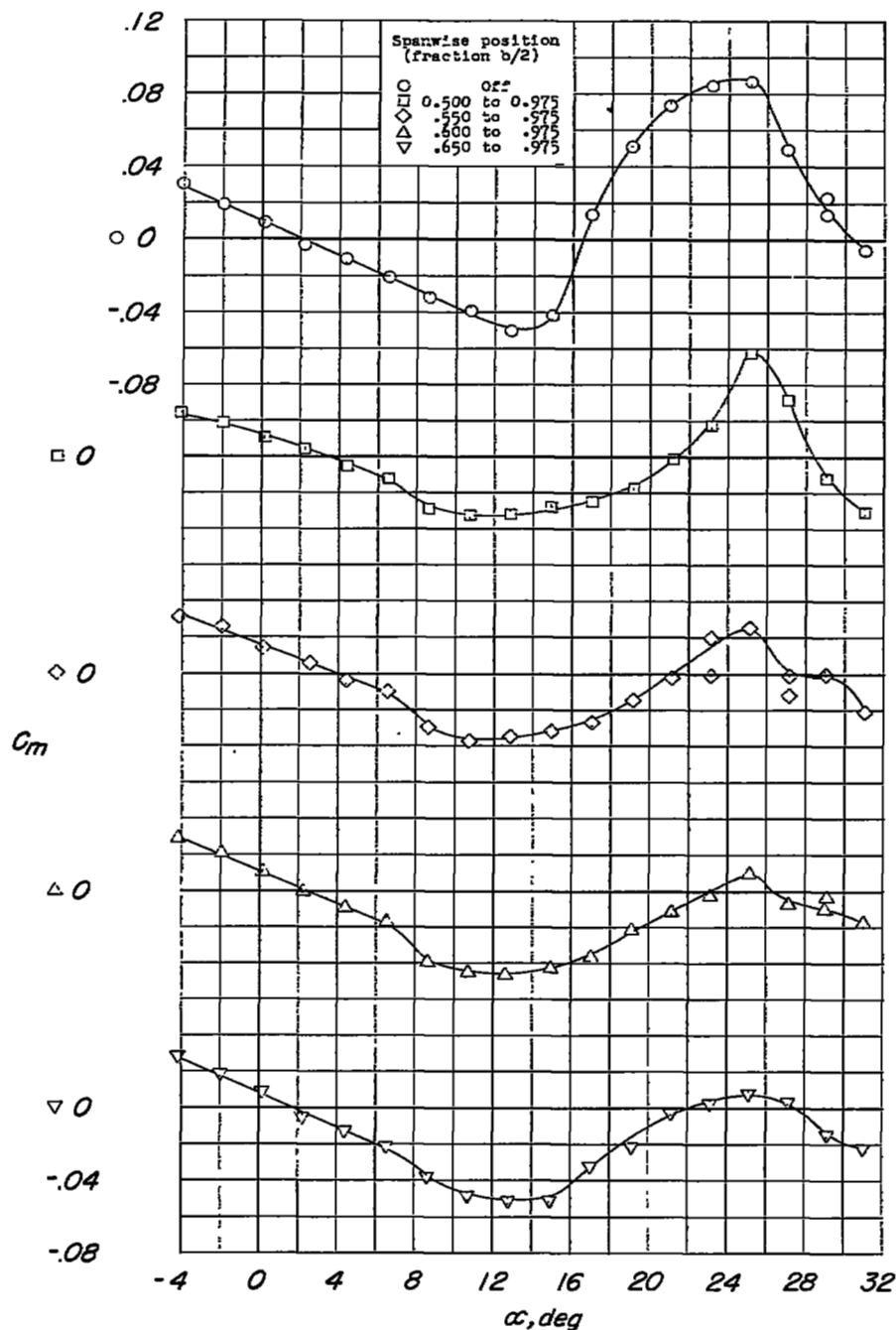
(a)  $C_m$  against  $\alpha$ .

Figure 10.- Lift and pitching-moment characteristics of wing with chord-extensions. Wing leading-edge radius, 0.0025c; chord-extension, 13.0 percent; chord-extension leading-edge radius, 0.00125c.

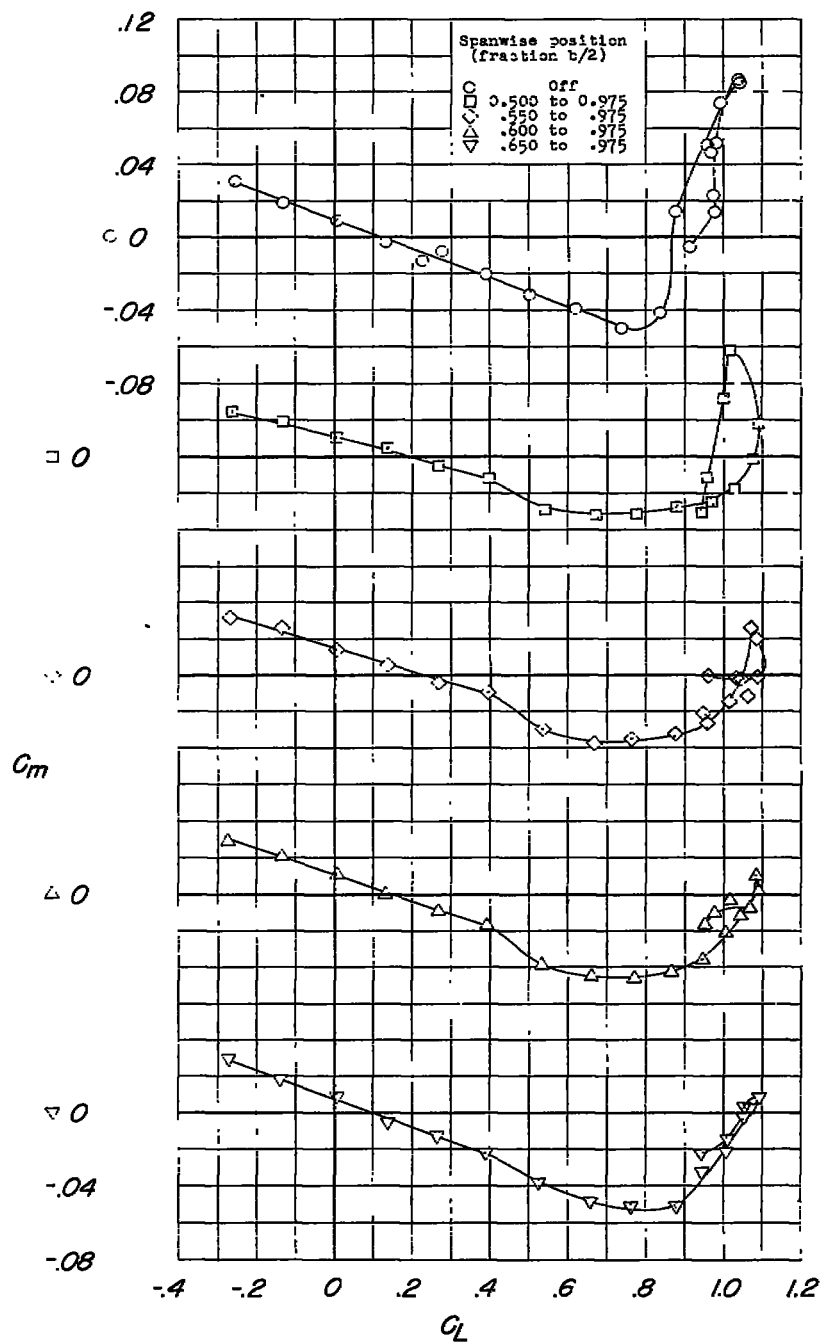
(b)  $C_m$  against  $C_L$ .

Figure 10.- Continued.

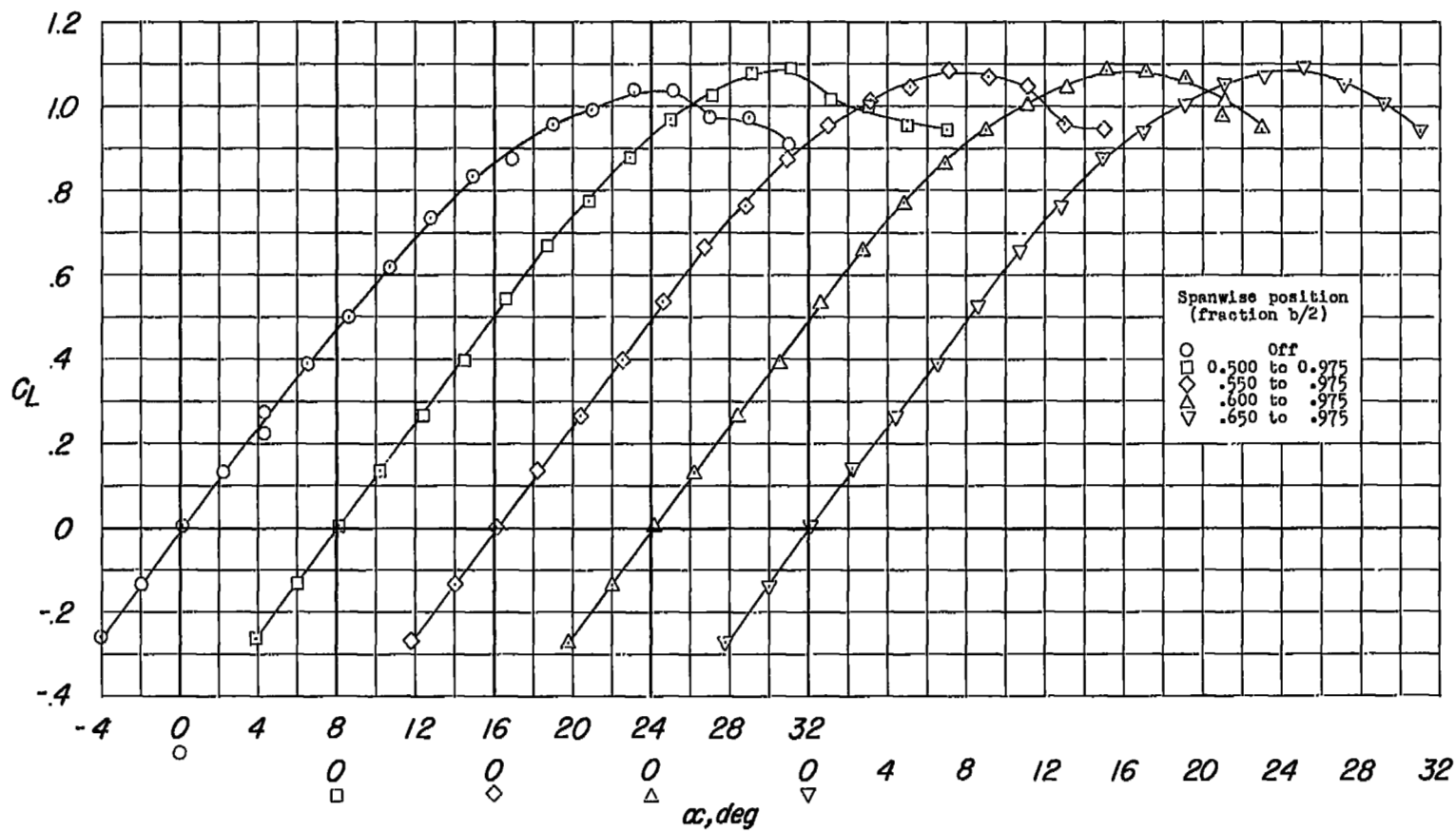
(c)  $C_L$  against  $\alpha$ .

Figure 10.- Concluded.

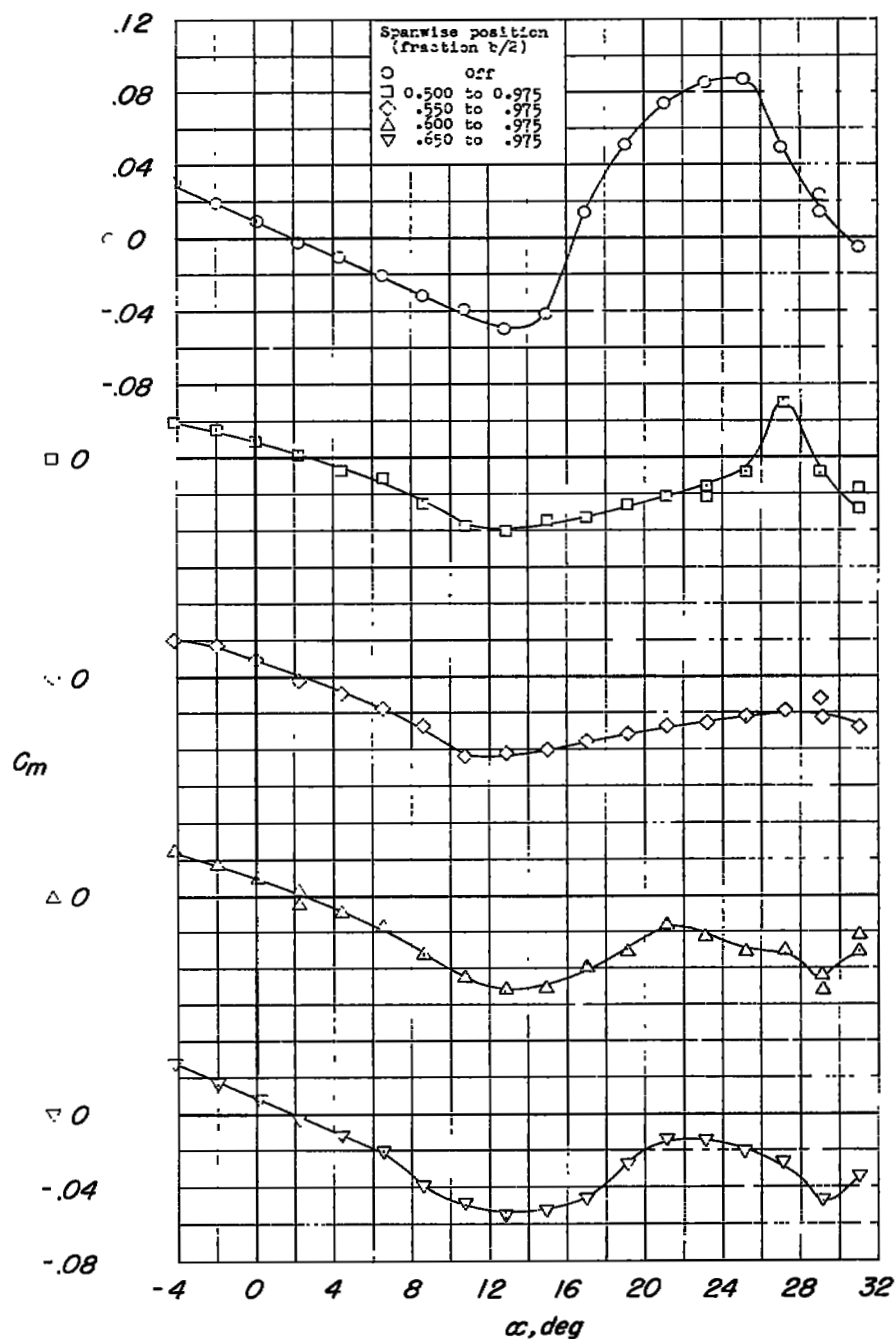
(a)  $C_m$  against  $\alpha$ .

Figure 11.- Lift and pitching-moment characteristics of wing with chord-extensions. Wing leading-edge radius, 0.0025c; chord-extension, 19.8 percent; chord-extension leading-edge radius, 0.00125c.

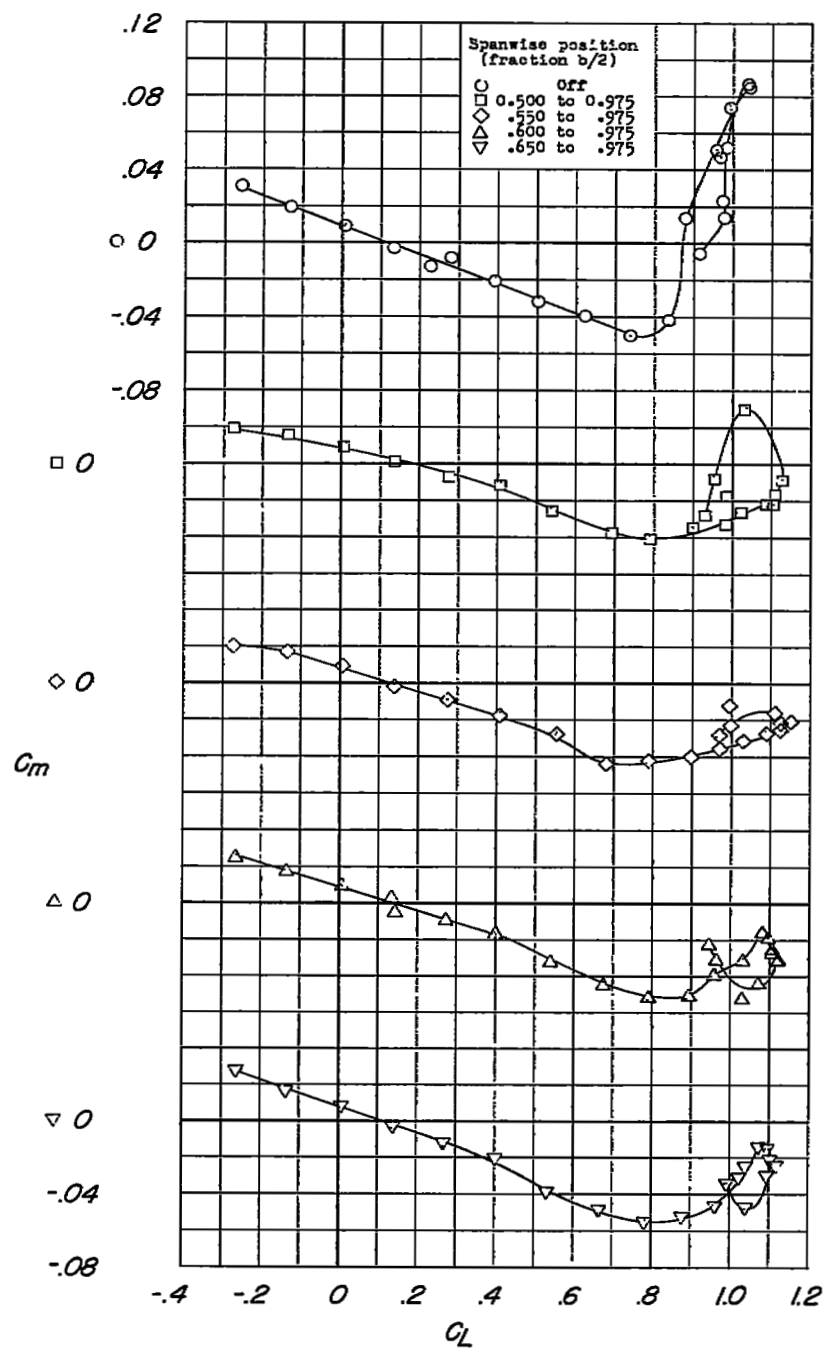
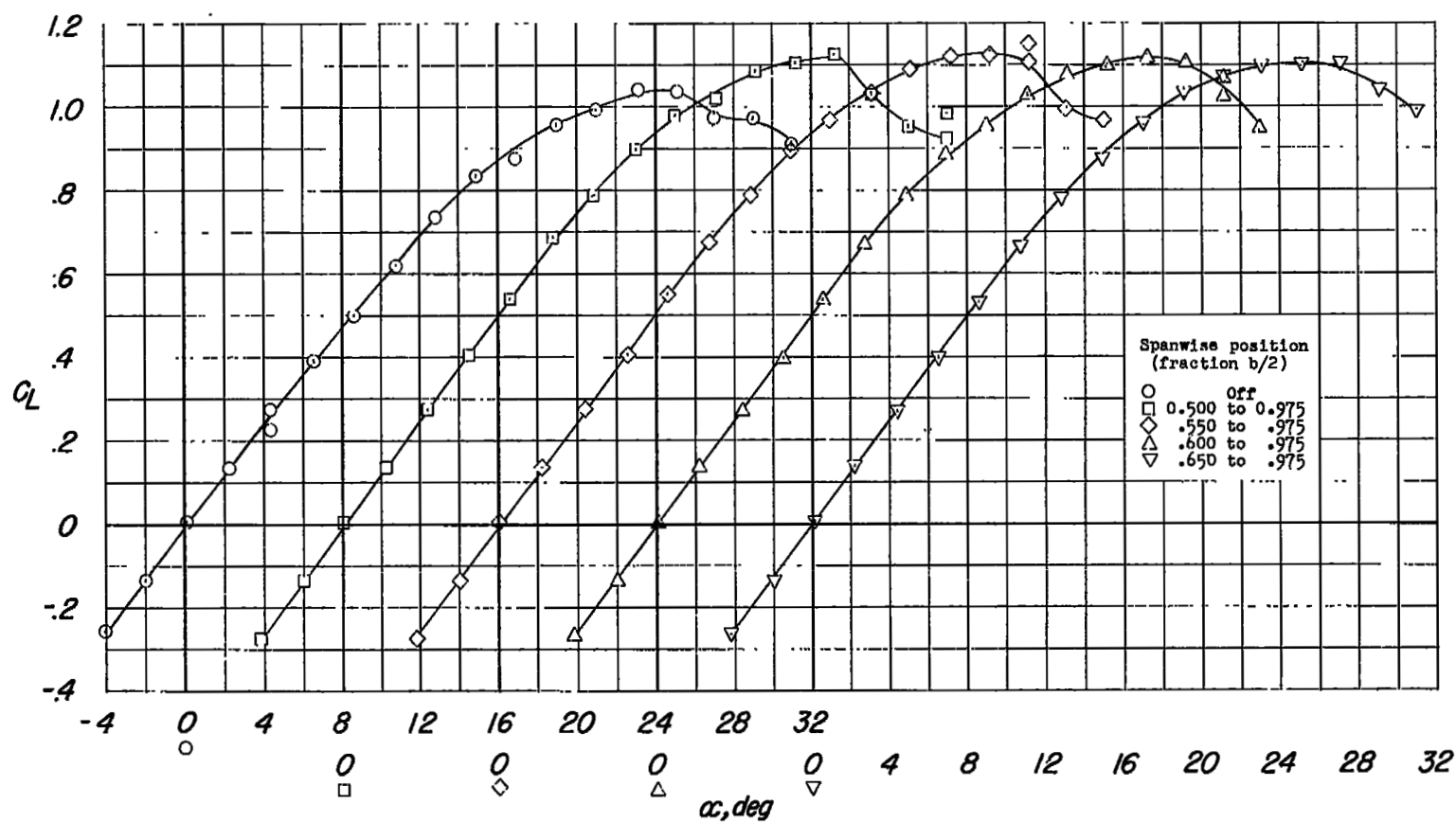
(b)  $C_m$  against  $C_L$ .

Figure 11.- Continued.



(c)  $C_L$  against  $\alpha$ .

Figure 11.- Concluded.

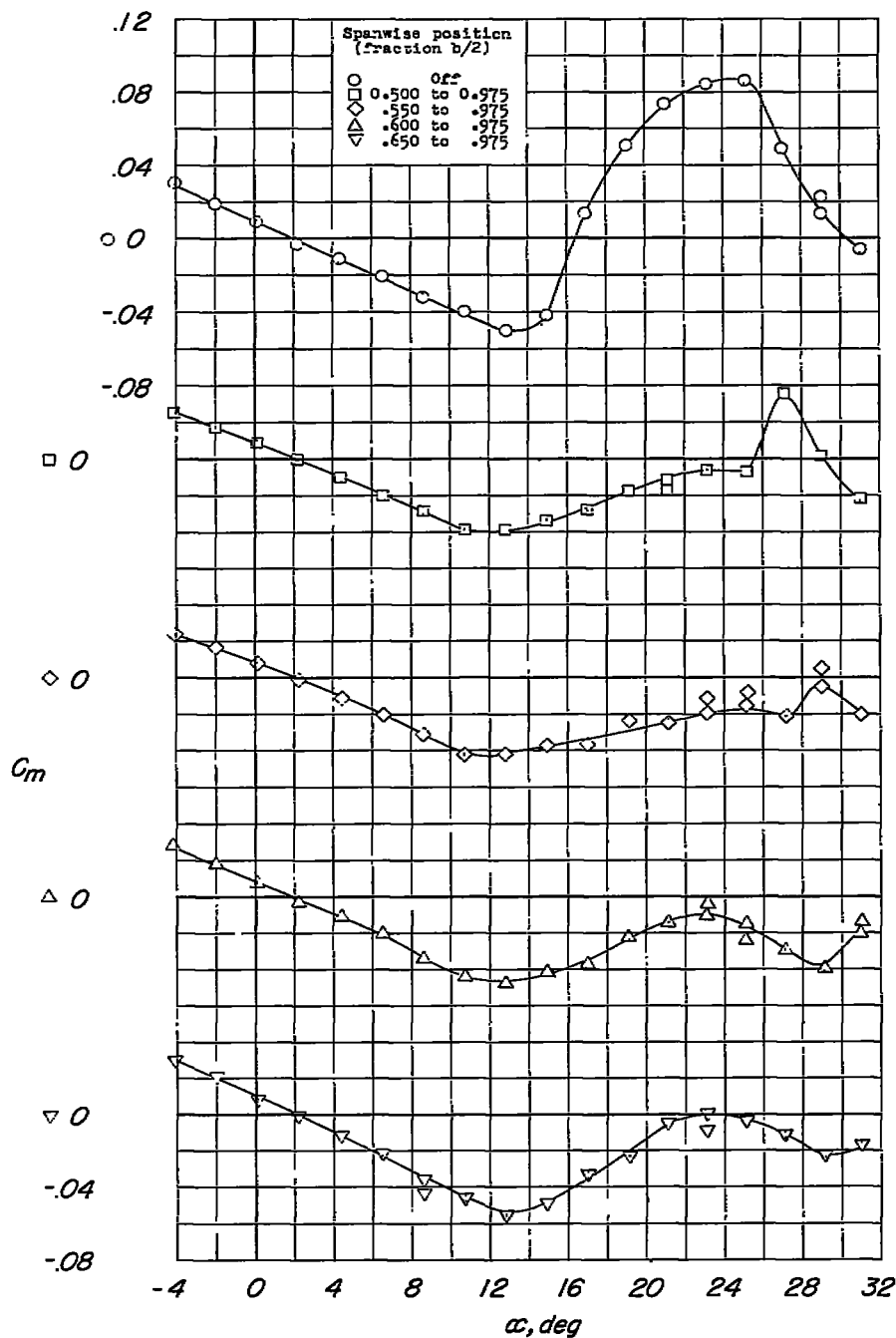
(a)  $C_m$  against  $\alpha$ .

Figure 12.- Lift and pitching-moment characteristics of wing with chord-extensions. Wing leading-edge radius, 0.0025c; chord-extension, 13.0 percent; chord-extension leading-edge radius, 0.00250c.

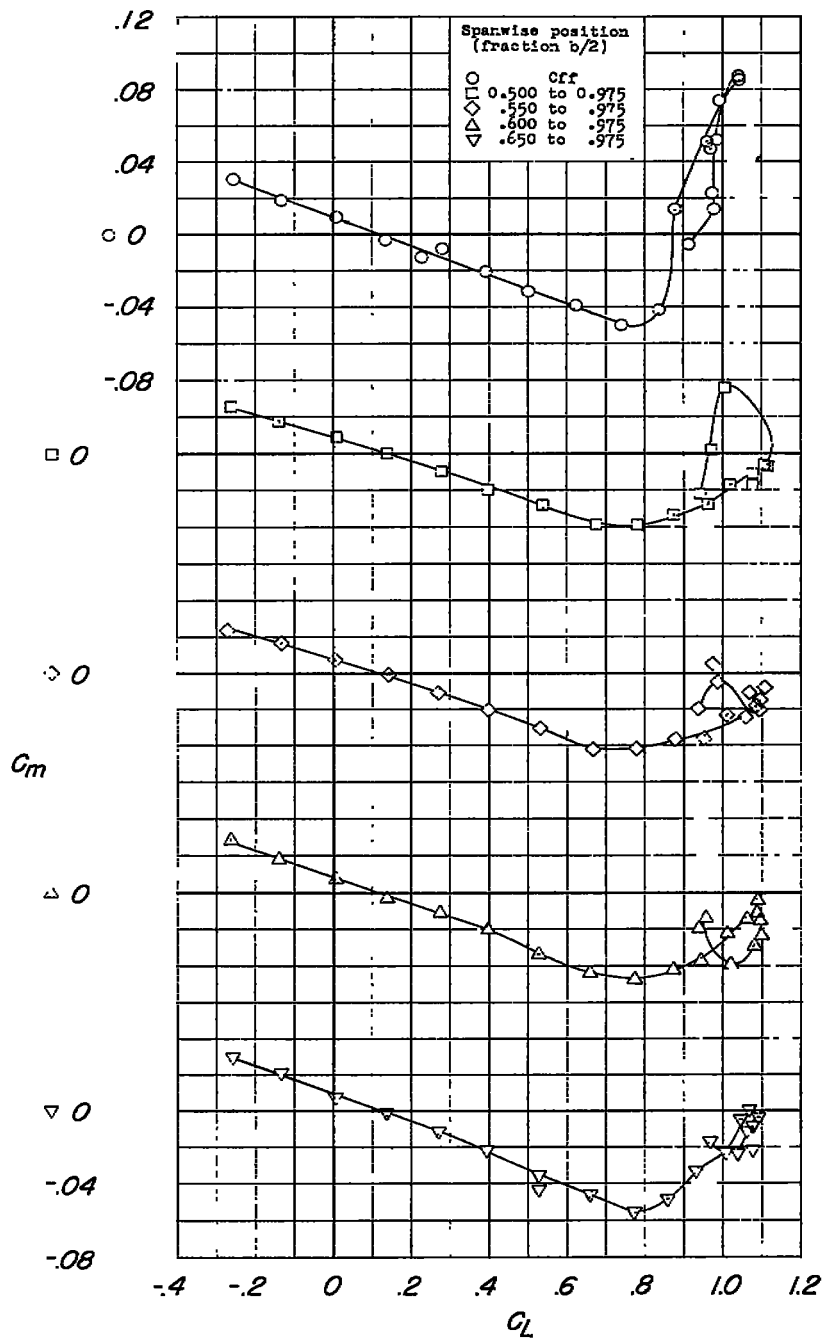
(b)  $C_m$  against  $C_L$ .

Figure 12.- Continued.

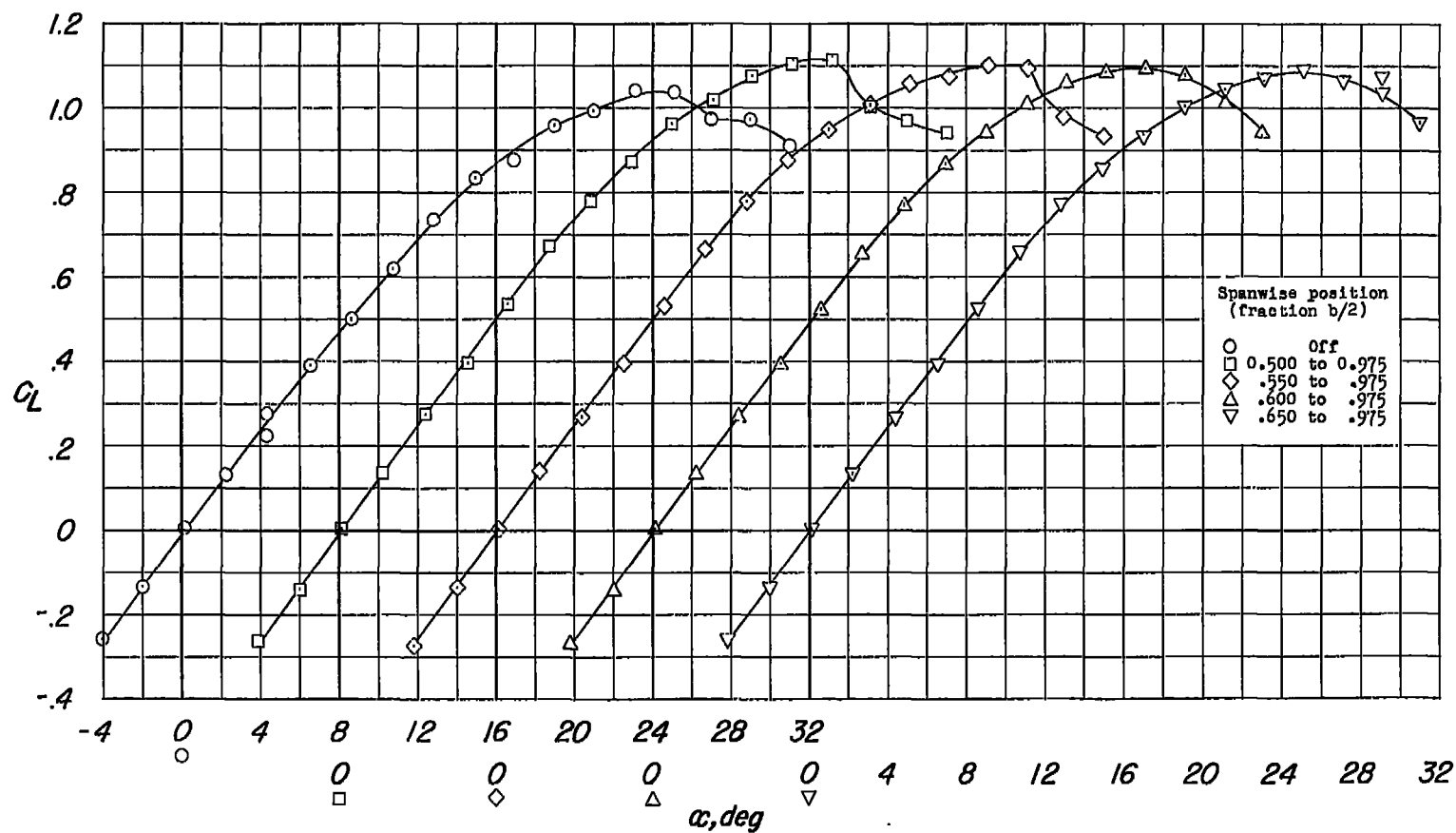
(c)  $C_L$  against  $\alpha$ .

Figure 12.- Concluded.

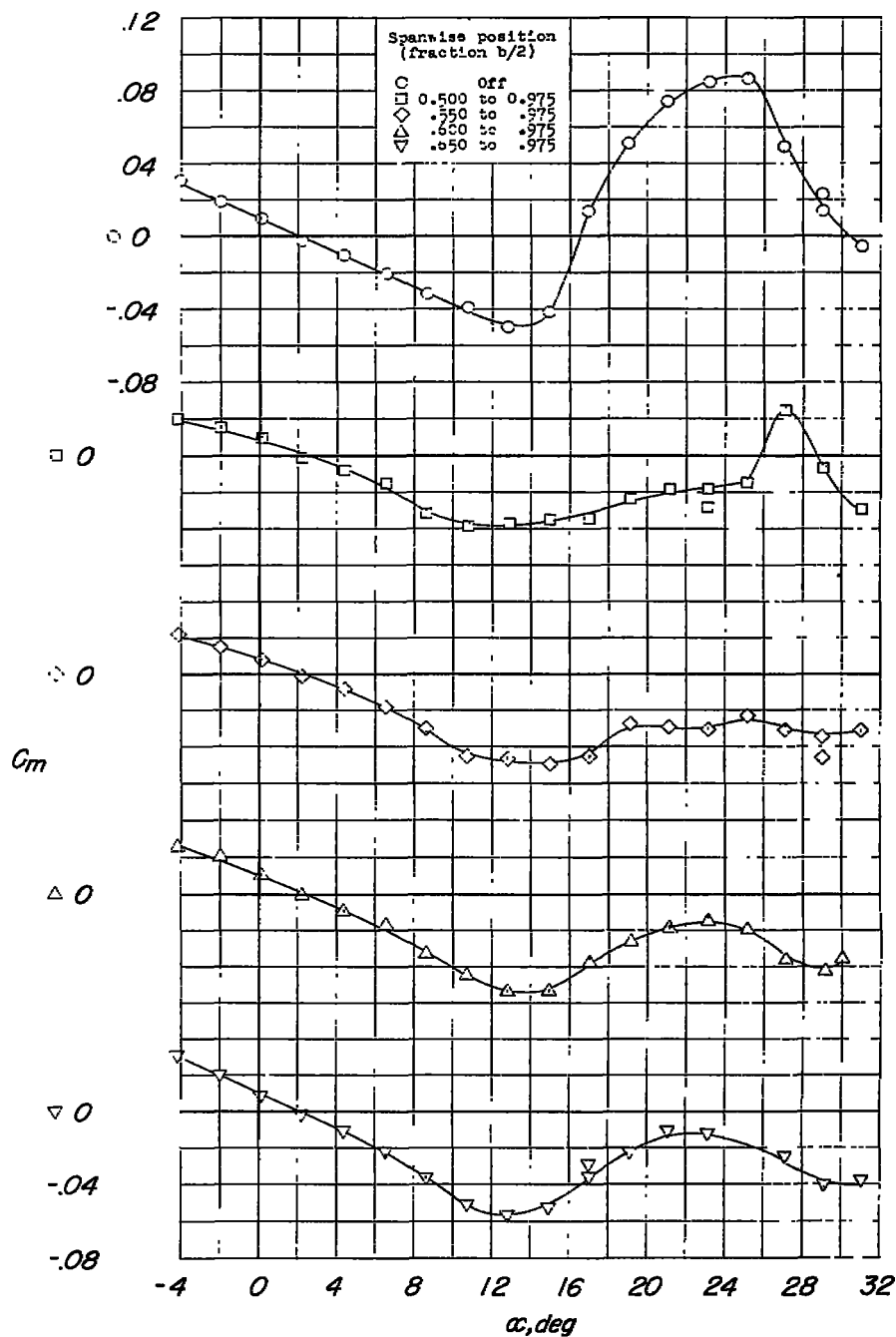
(a)  $C_m$  against  $\alpha$ .

Figure 13.- Lift and pitching-moment characteristics of wing with chord-extensions. Wing leading-edge radius, 0.0025c; chord extension, 19.8 percent; chord-extension leading-edge radius, 0.00250c.

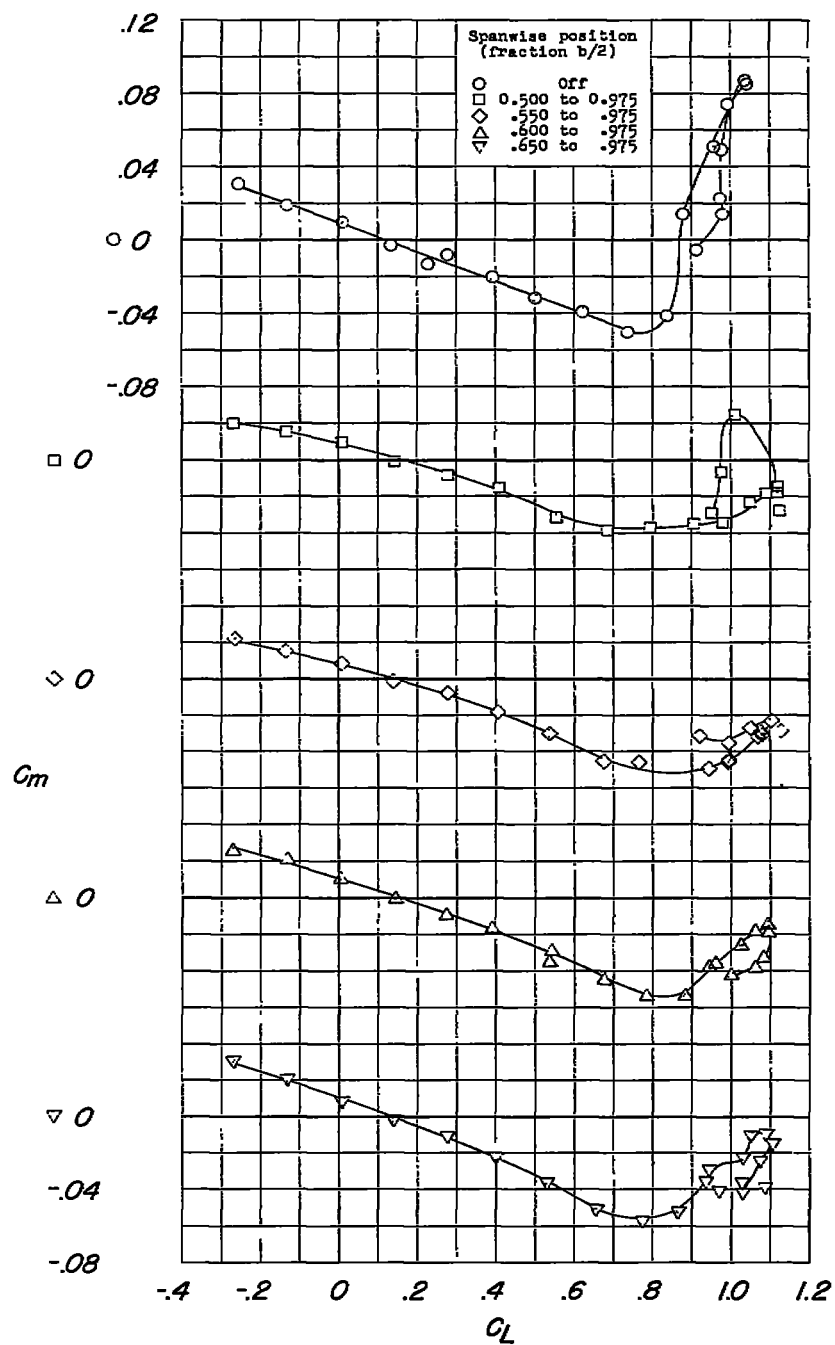
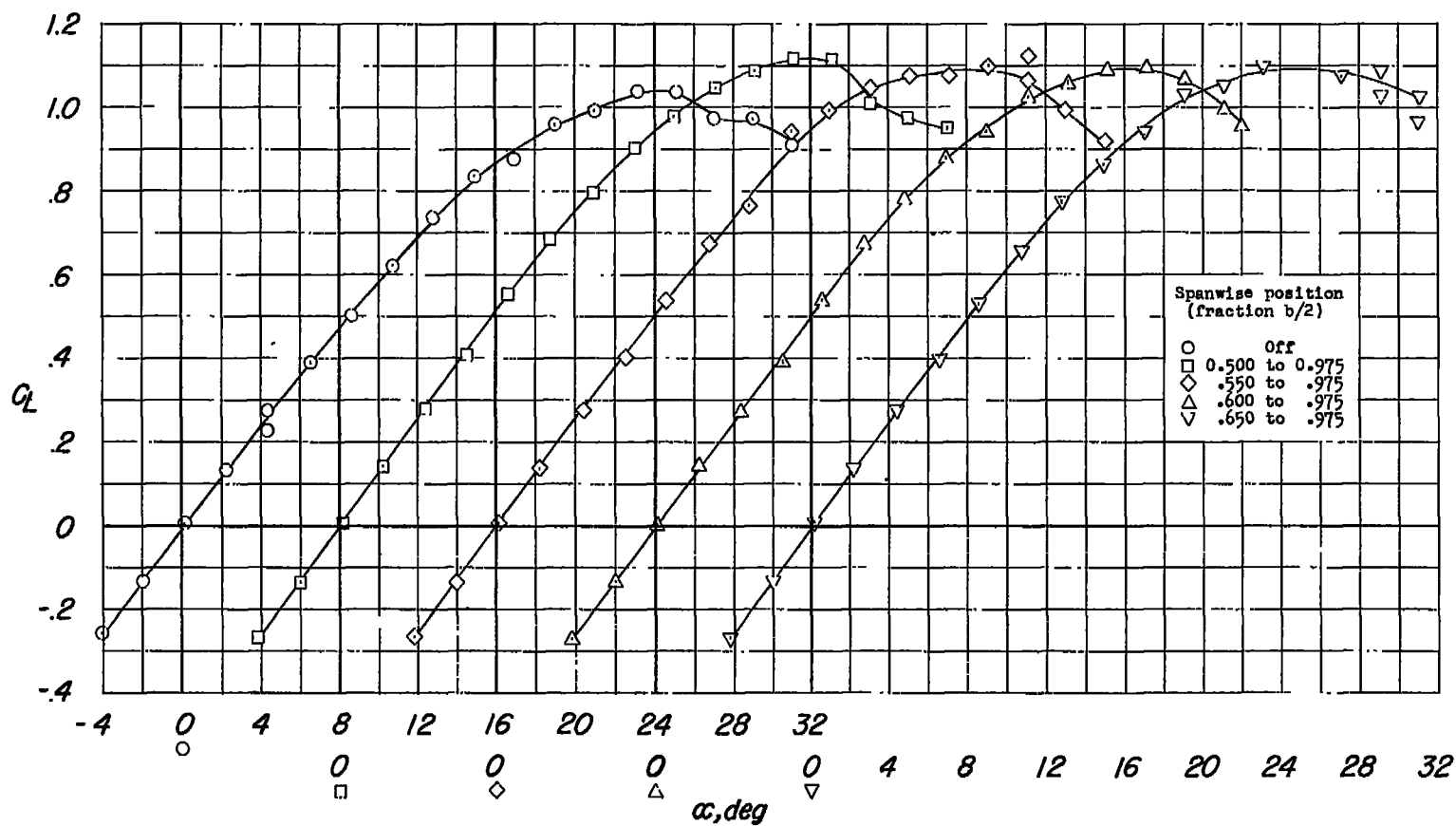
(b)  $C_m$  against  $C_L$ .

Figure 13.- Continued.



(c)  $C_L$  against  $\alpha$ .

Figure 13.- Concluded.

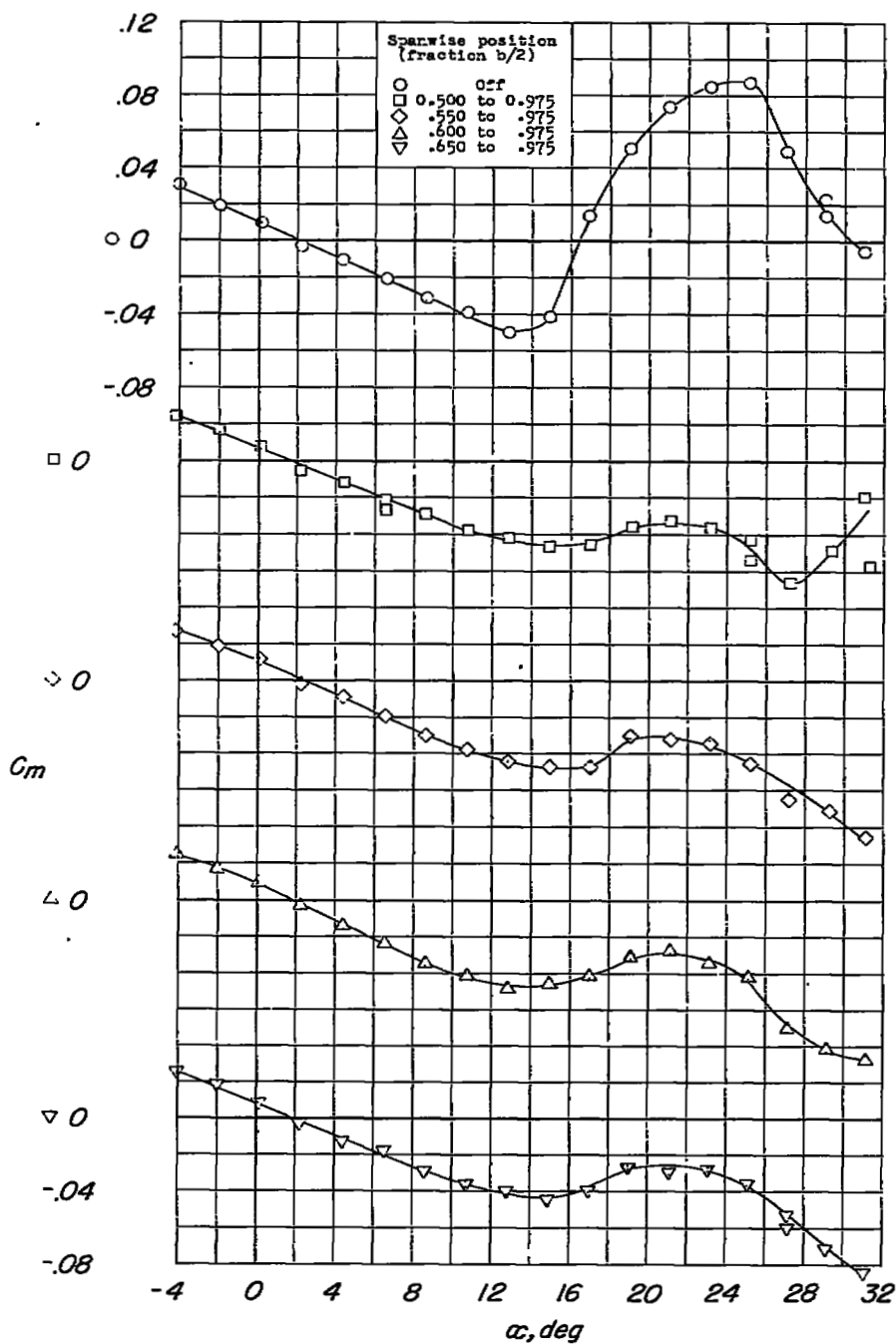
(a)  $C_m$  against  $\alpha$ .

Figure 14.- Lift and pitching-moment characteristics of wing with chord-extensions. Wing leading-edge radius, 0.0025c; chord-extension, 6.4 percent; chord-extension leading-edge radius, 0.0045c.

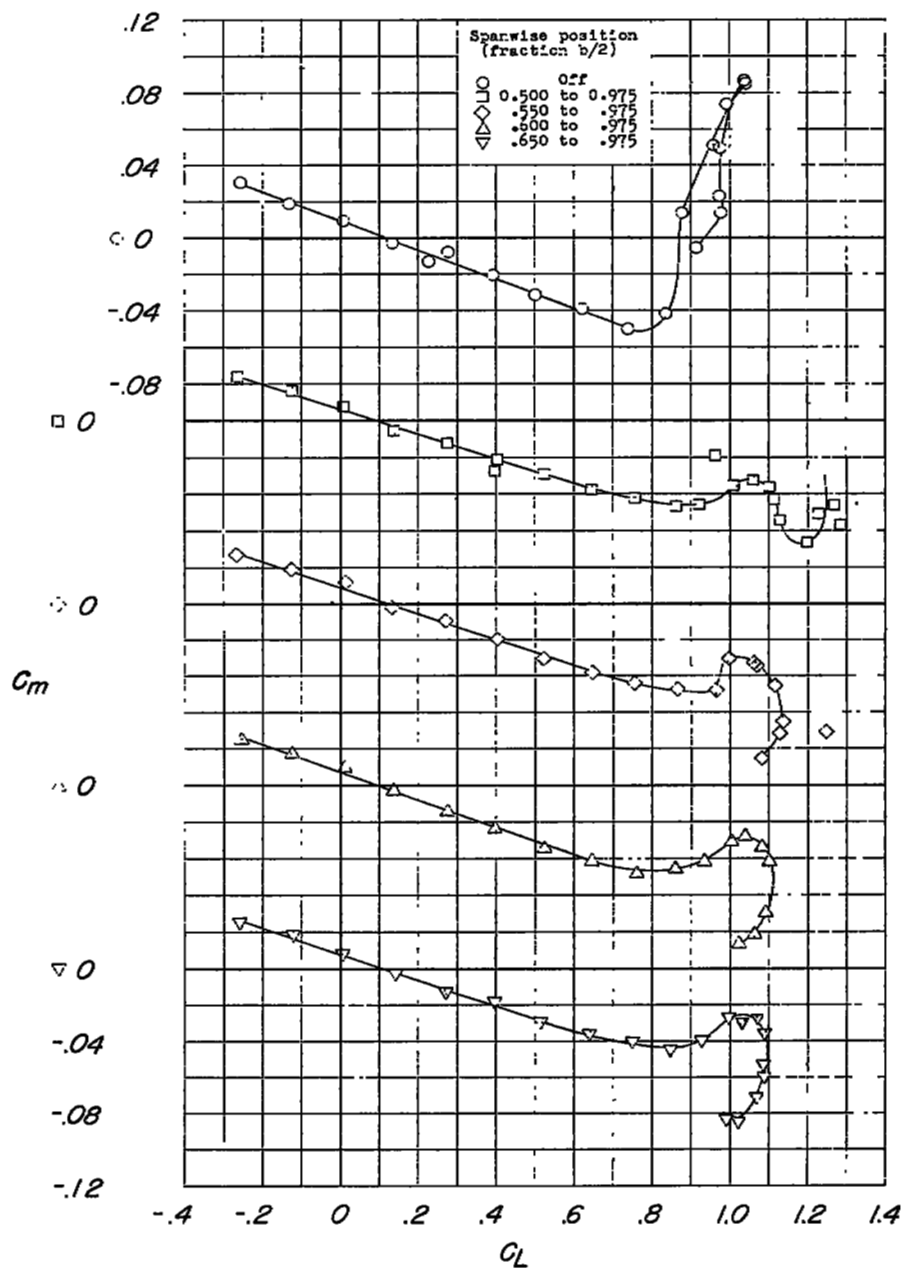
(b)  $C_m$  against  $C_L$ .

Figure 14.- Continued.

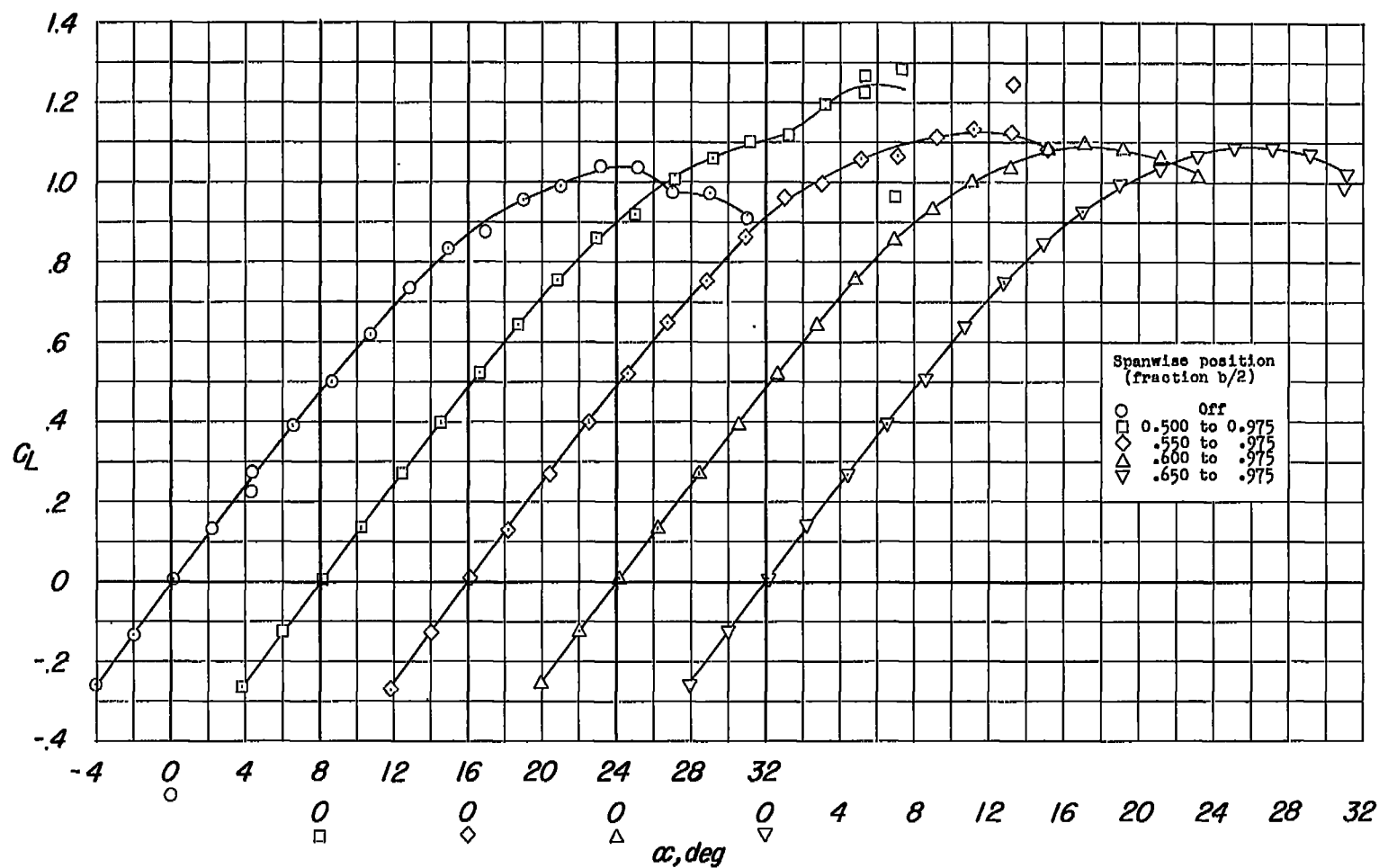
(c)  $C_L$  against  $\alpha$ .

Figure 14.- Concluded.

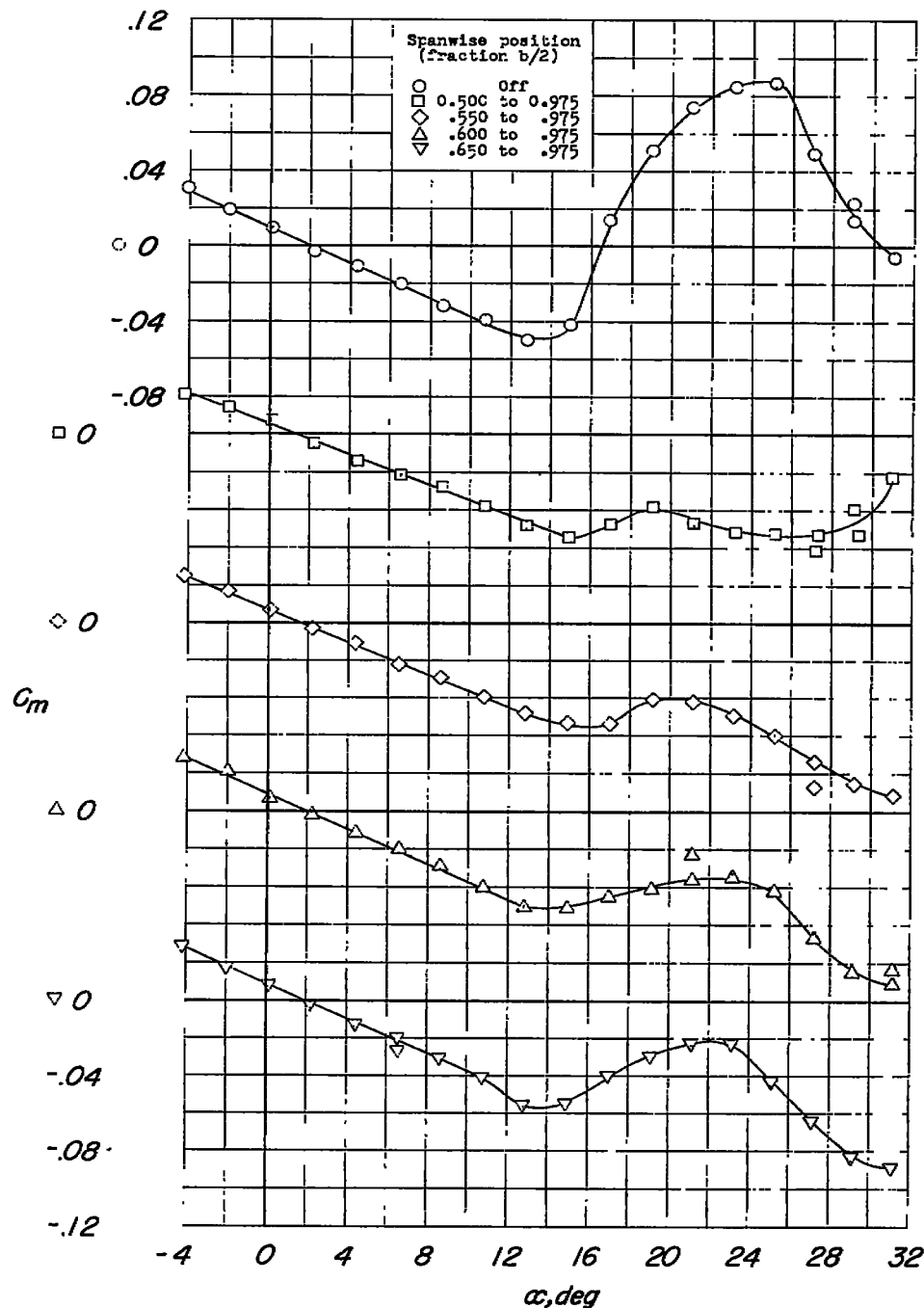
(a)  $C_m$  against  $\alpha$ .

Figure 15.- Lift and pitching-moment characteristics of wing with chord-extensions. Wing leading-edge radius, 0.0025c; chord-extension, 13 percent; chord-extension leading-edge radius, 0.00445c.

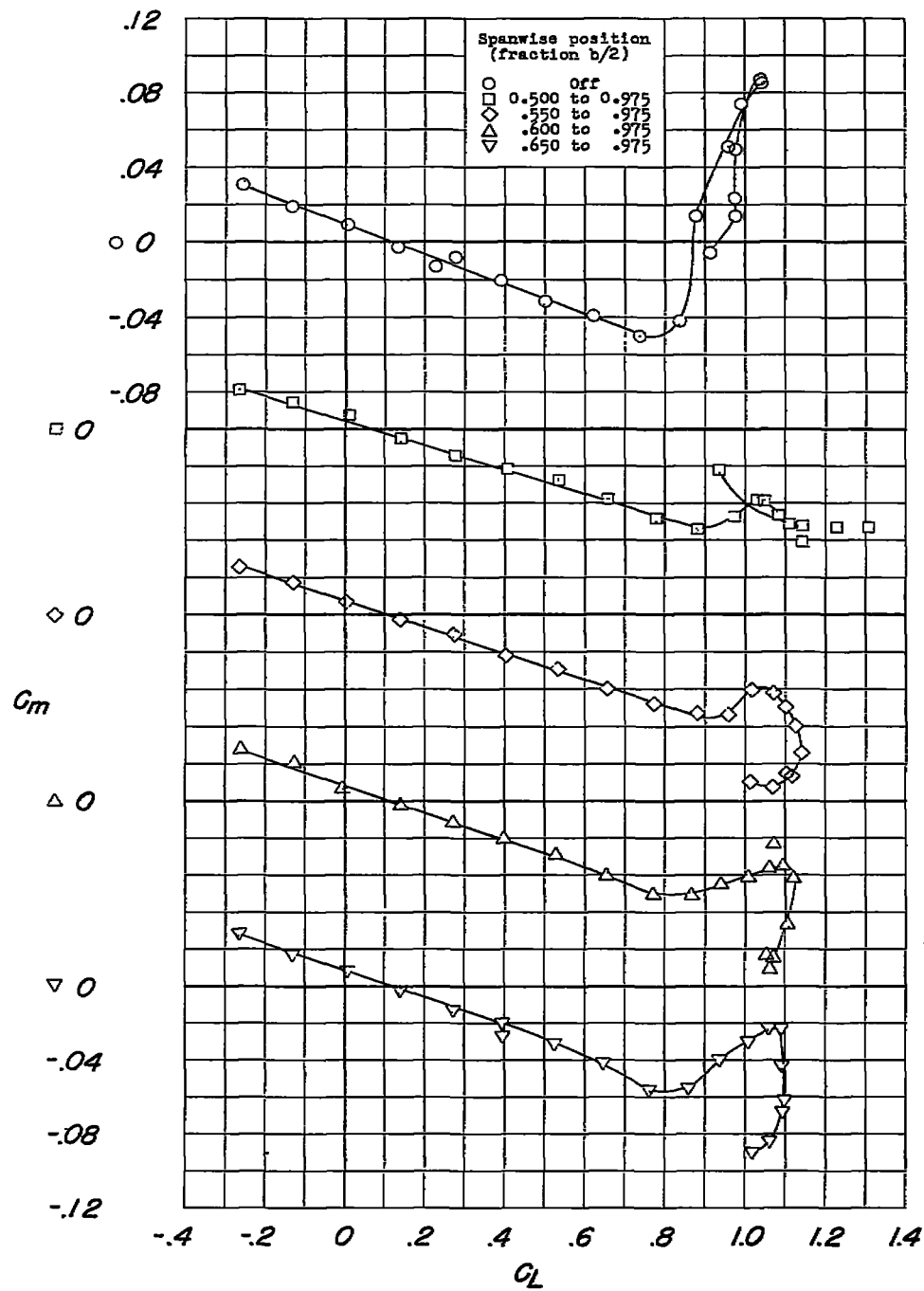
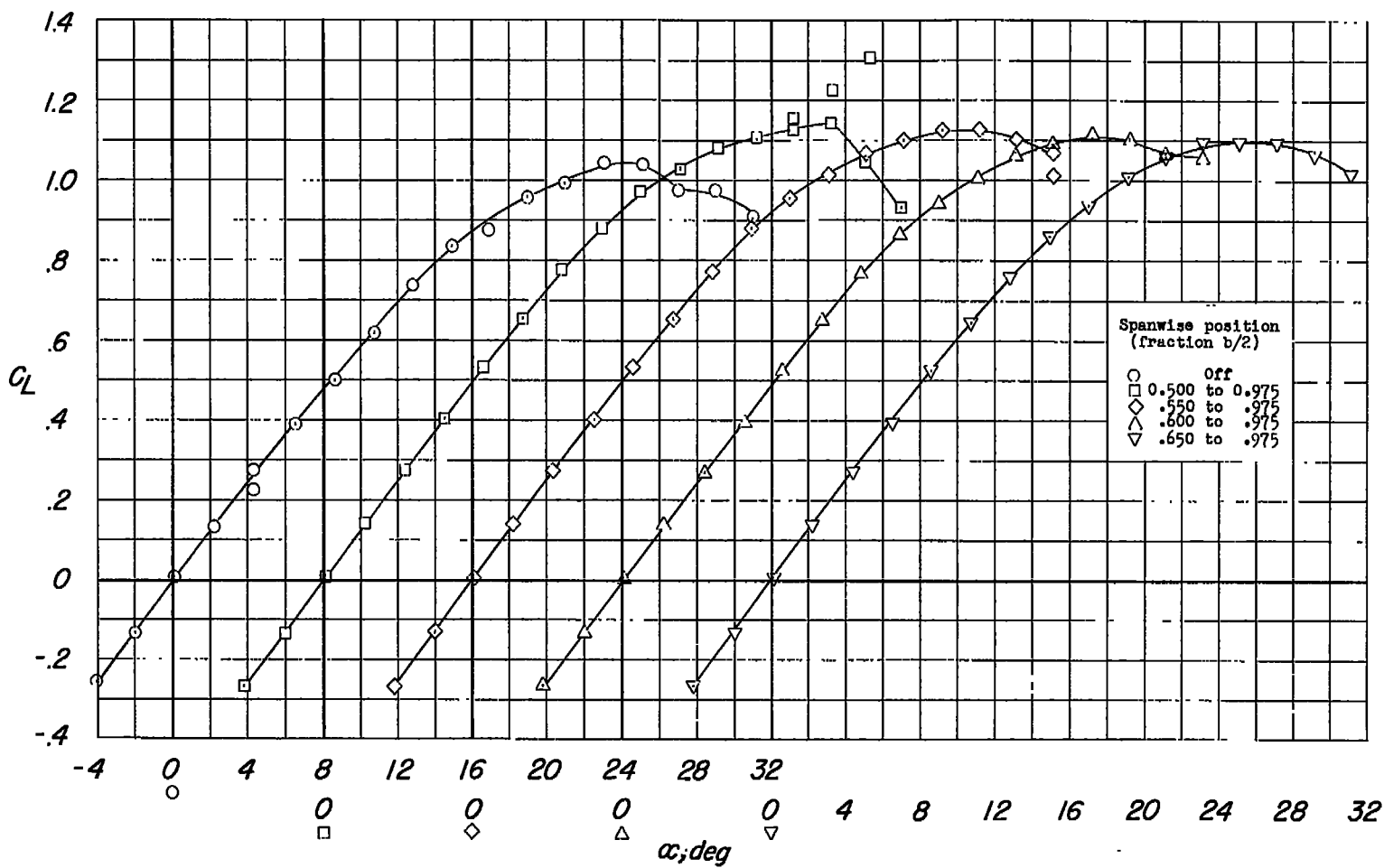
(b)  $C_m$  against  $C_L$ .

Figure 15.- Continued.



(c)  $C_L$  against  $\alpha$ .

Figure 15.- Concluded.

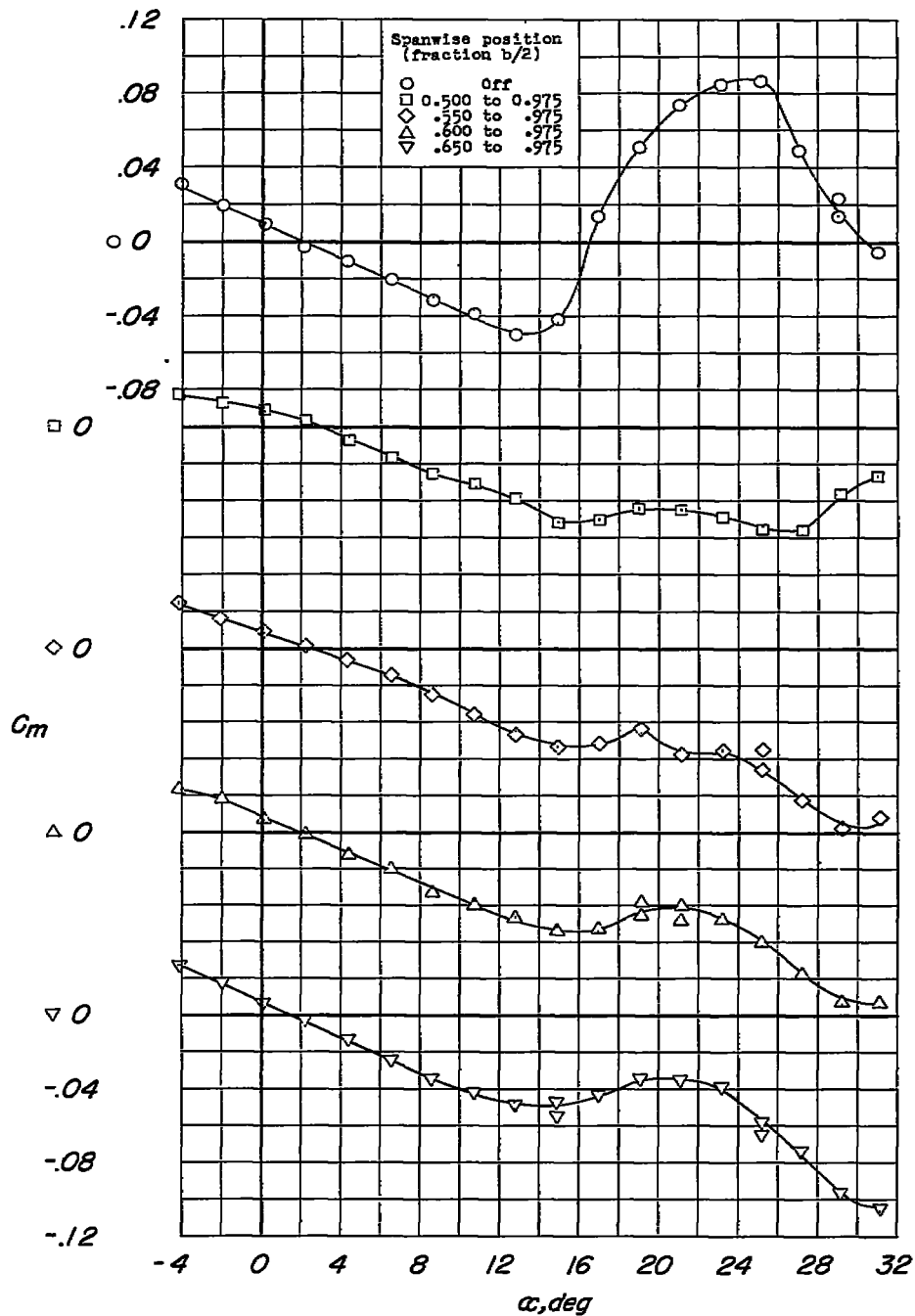
(a)  $C_m$  against  $\alpha$ .

Figure 16.- Lift and pitching-moment characteristics of wing with chord-extensions. Wing leading-edge radius, 0.0025c; chord-extension, 19.8 percent; chord-extension leading-edge radius, 0.00445c.

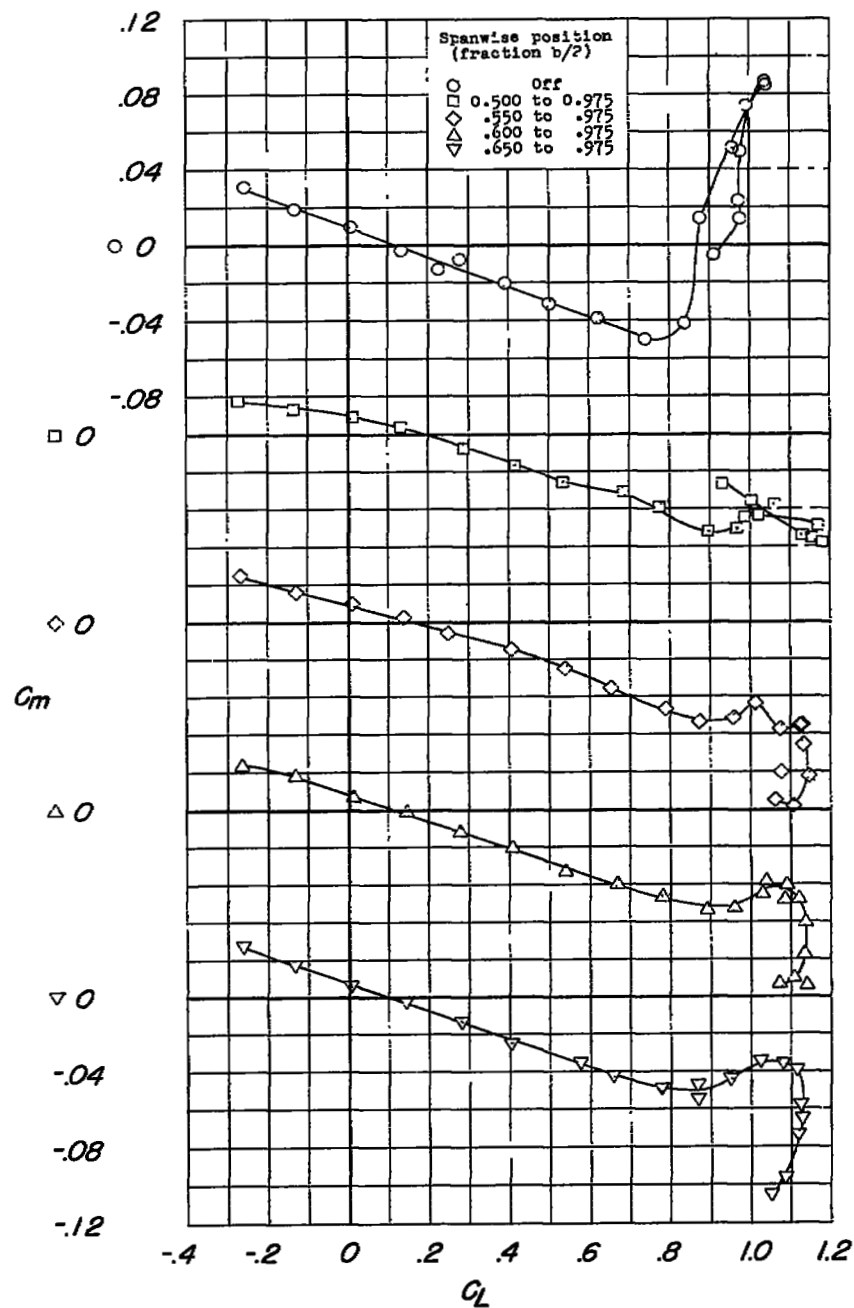
(b)  $C_m$  against  $C_L$ .

Figure 16.- Continued.

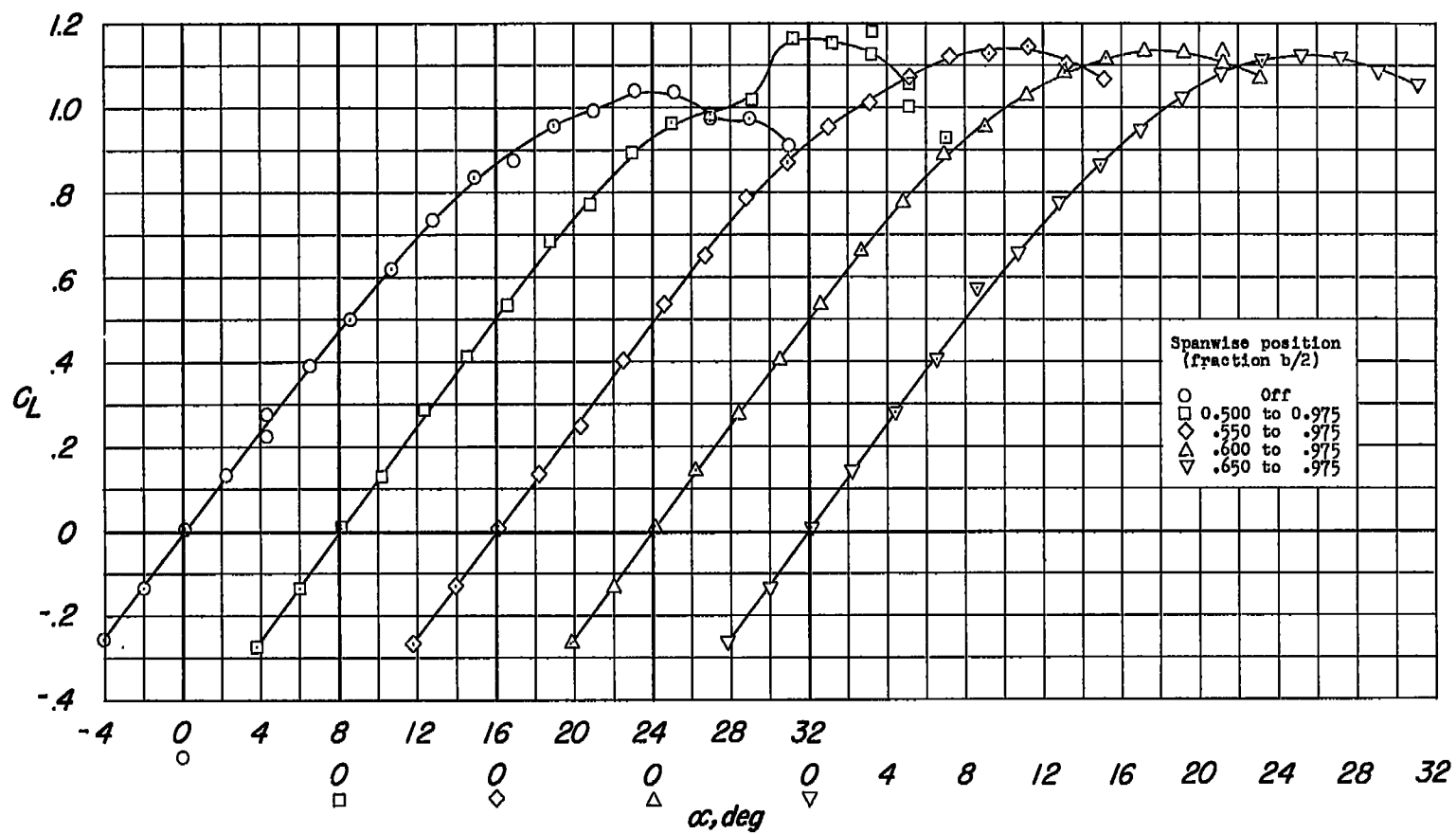
(c)  $C_L$  against  $\alpha$ .

Figure 16.- Concluded.

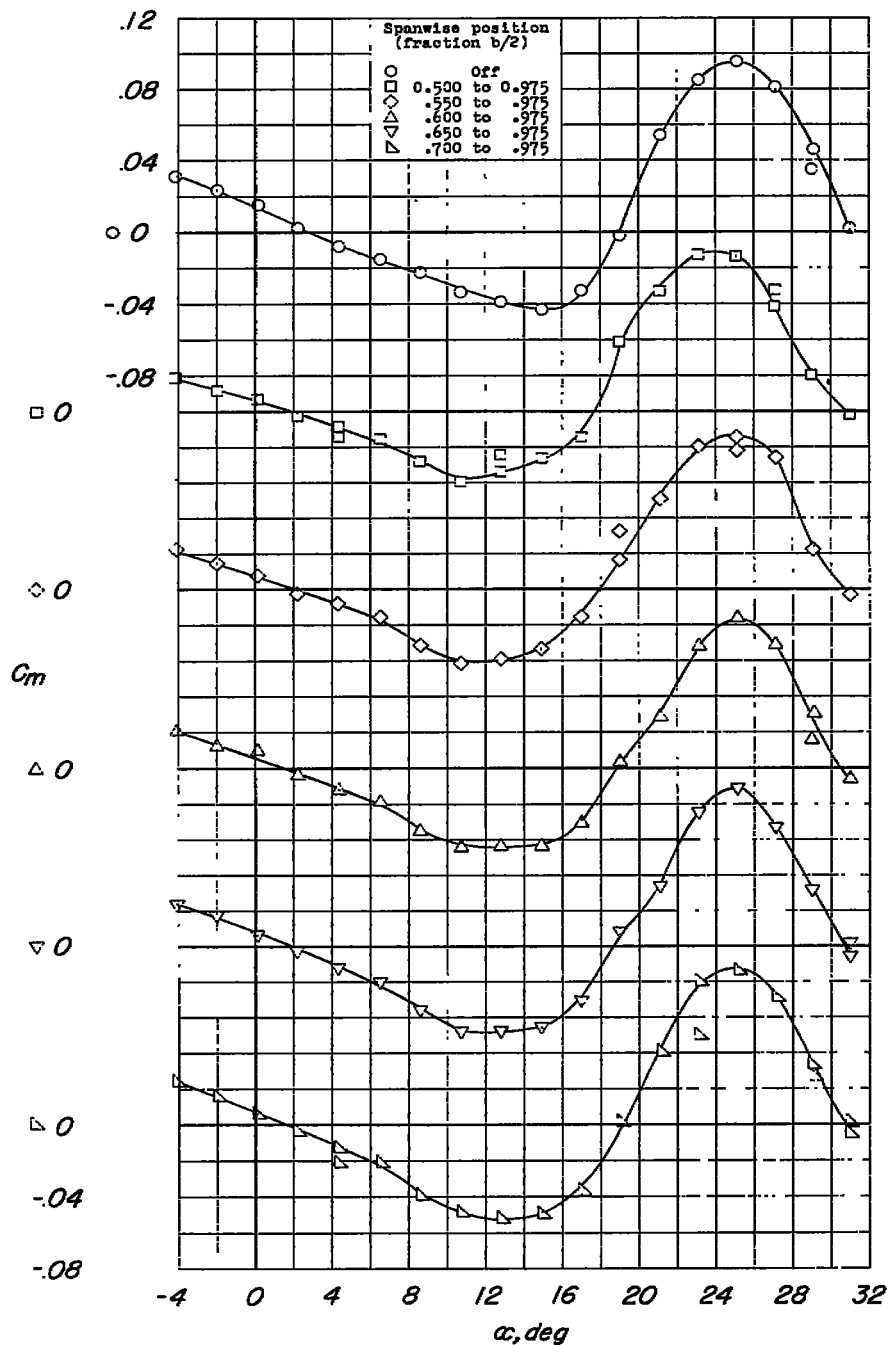
(a)  $C_m$  against  $\alpha$ .

Figure 17.- Lift and pitching-moment characteristics of wing with chord-extensions. Wing leading-edge radius,  $0.0050c$ ; chord-extension, 6.4 percent; chord-extension leading-edge radius,  $0c$ .

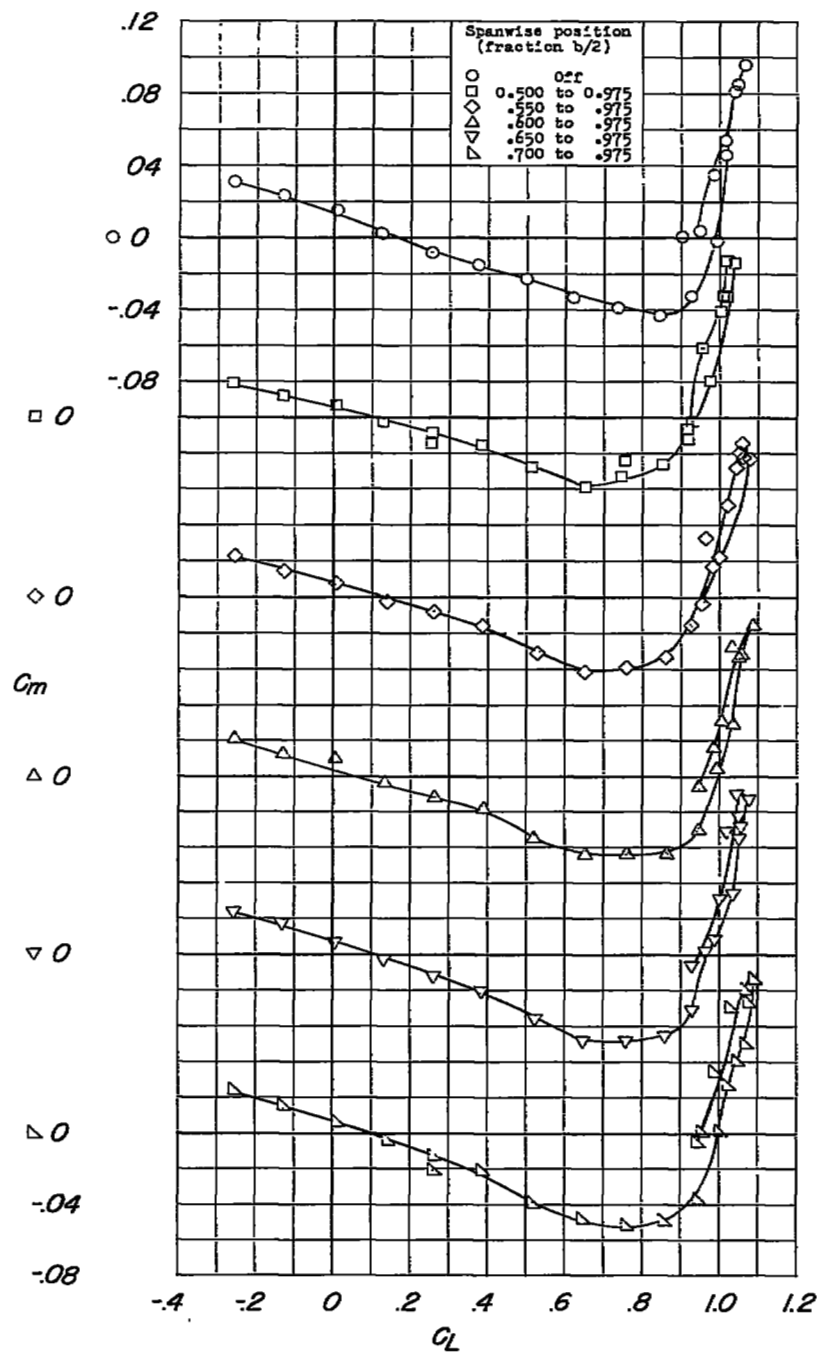
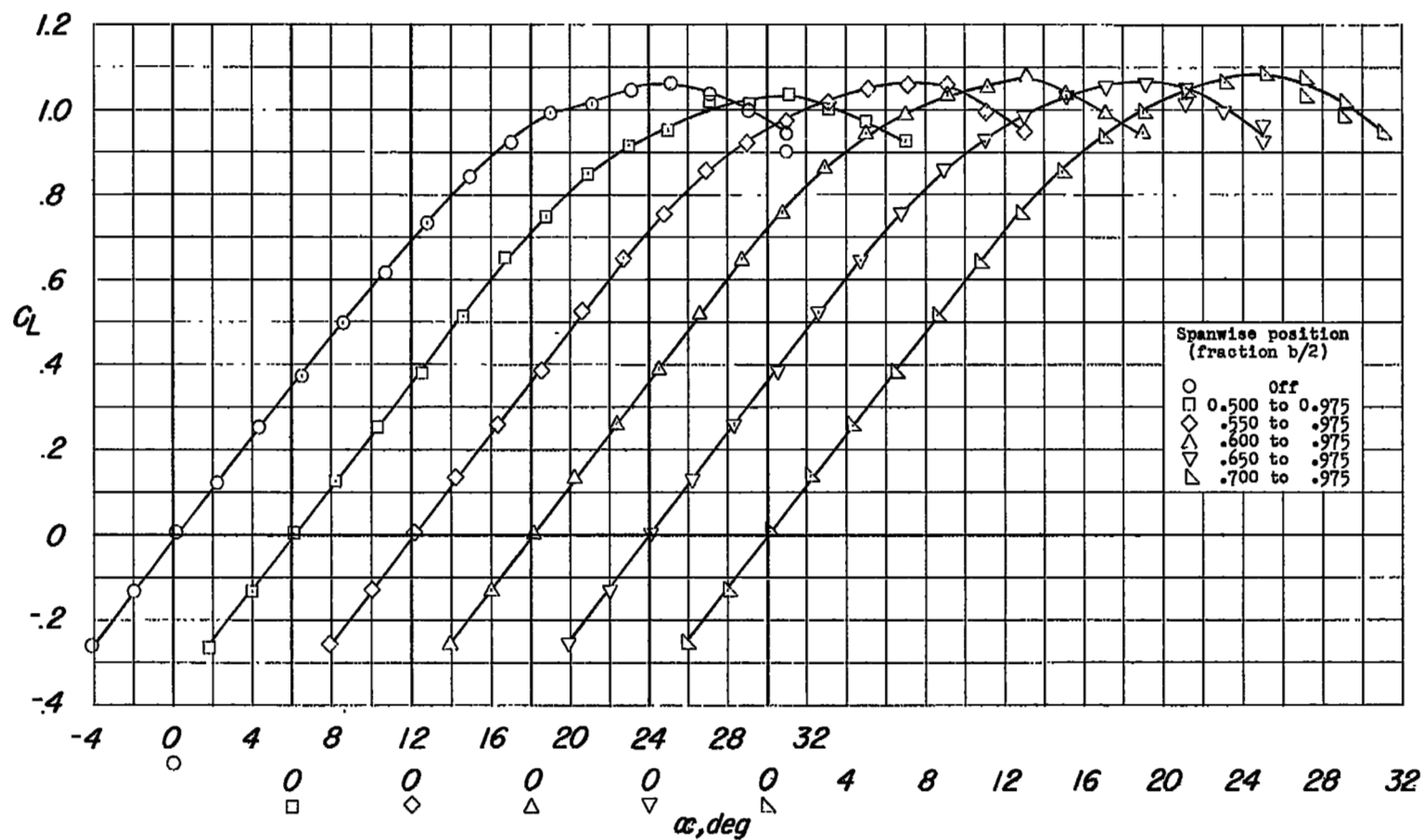
(b)  $C_m$  against  $C_L$ .

Figure 17.- Continued.



(c)  $C_L$  against  $\alpha$ .

Figure 17.- Concluded.

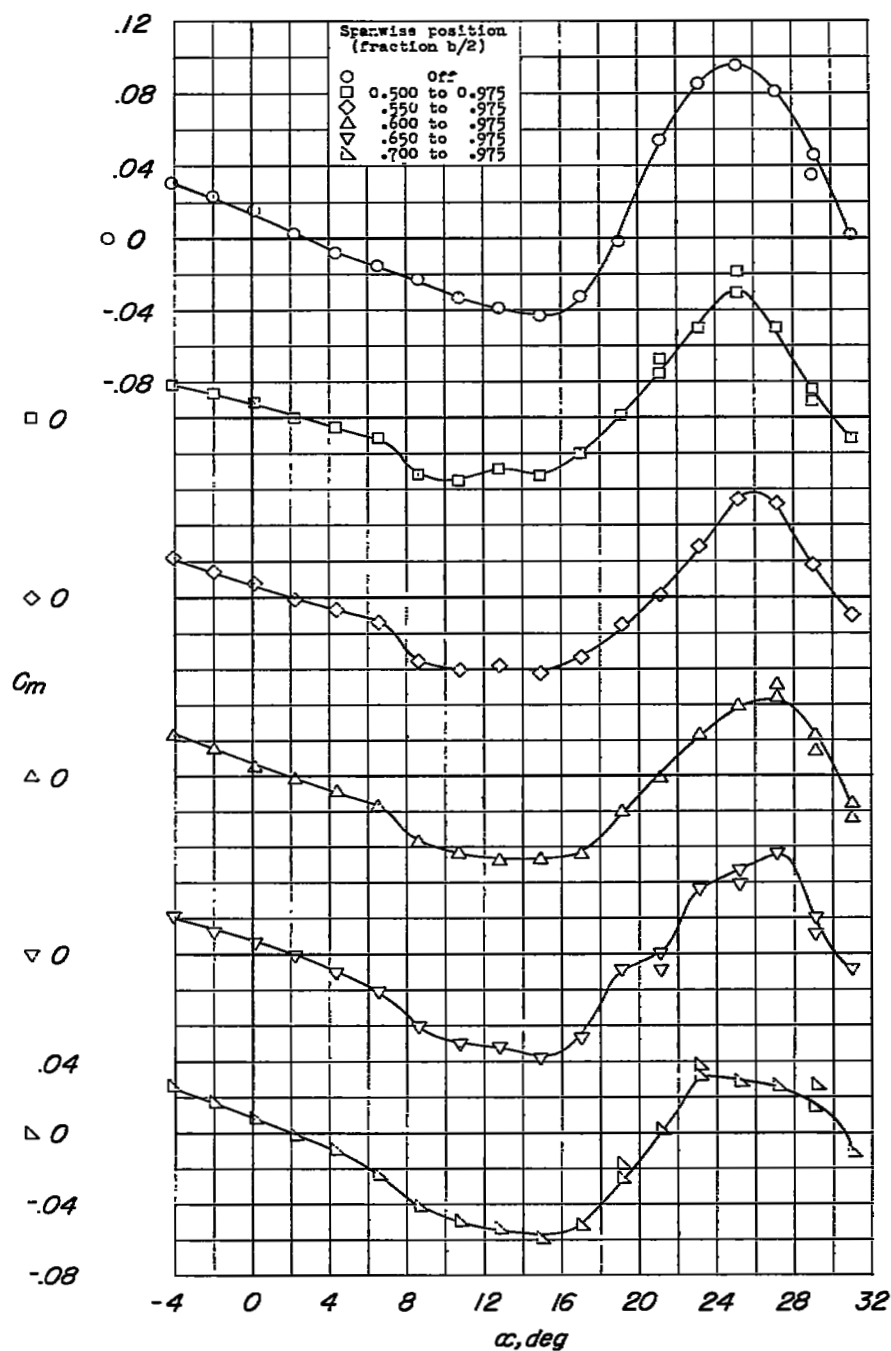
(a)  $C_m$  against  $\alpha$ .

Figure 18.- Lift and pitching-moment characteristics of wing with chord-extensions. Wing leading-edge radius, 0.0050c; chord-extension, 13.0 percent; chord-extension leading-edge radius, 0c.

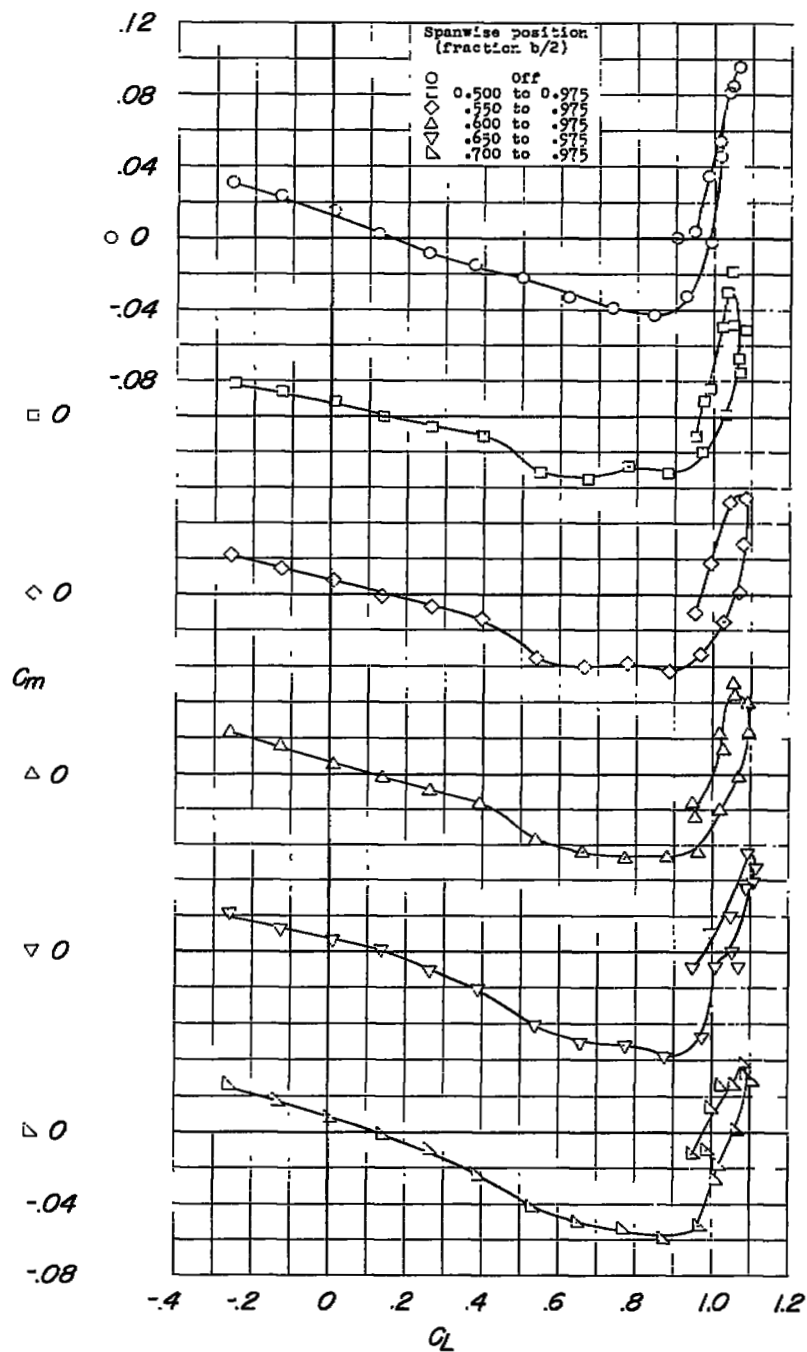
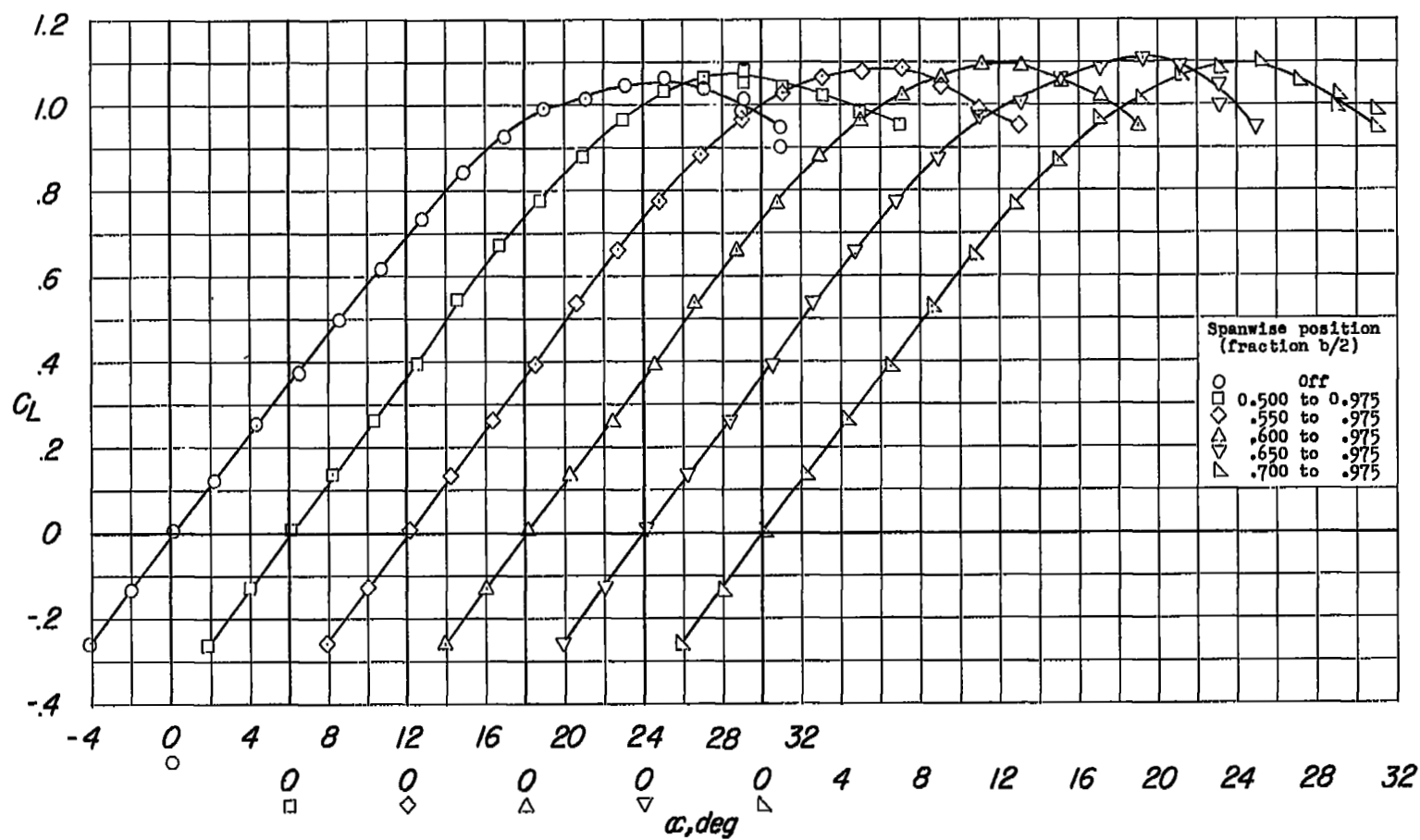
(b)  $C_m$  against  $C_L$ .

Figure 18.- Continued.



(c)  $C_L$  against  $\alpha$ .

Figure 18.- Concluded.

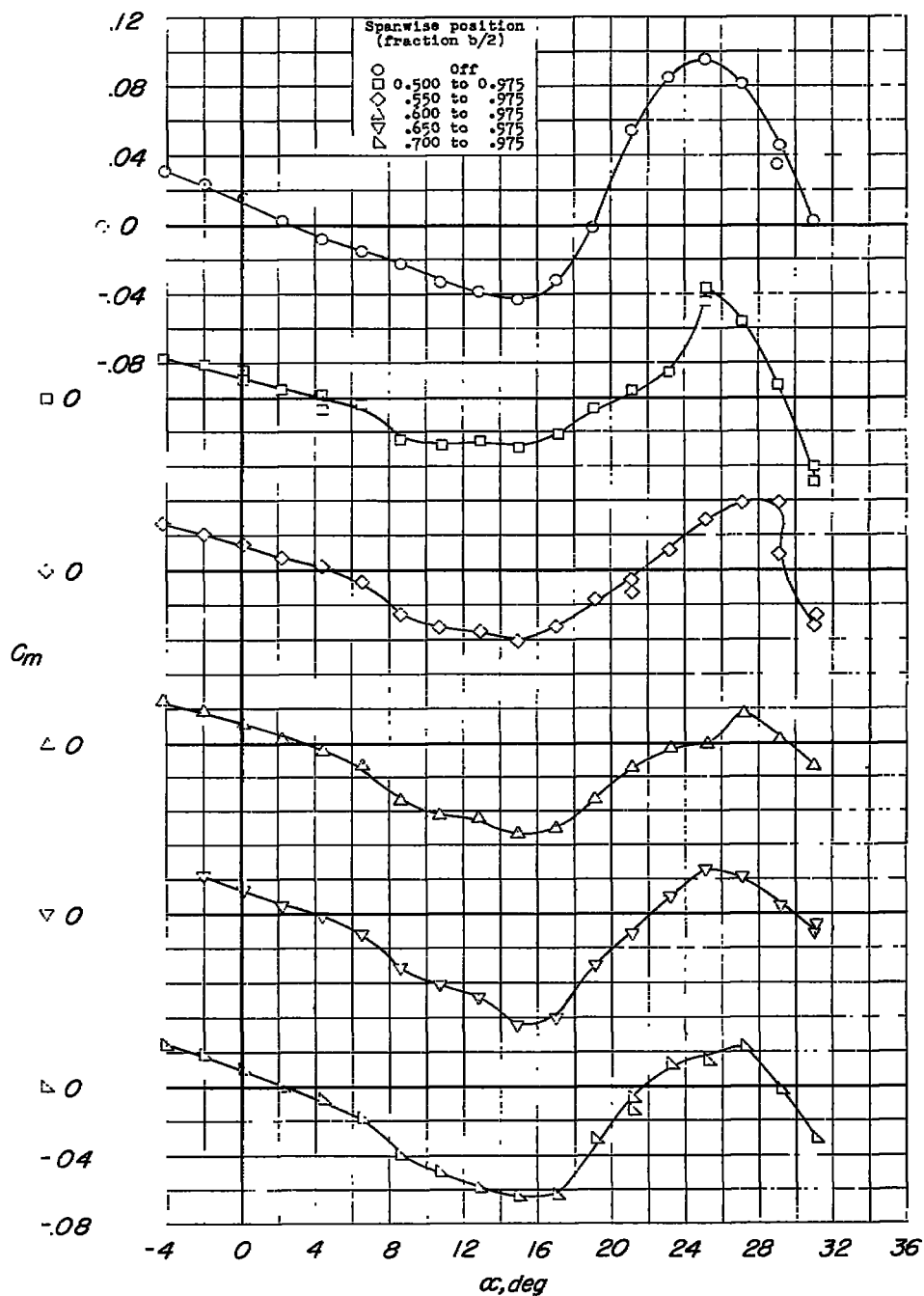
(a)  $C_m$  against  $\alpha$ .

Figure 19.- Lift and pitching-moment characteristics of wing with chord-extensions. Wing leading-edge radius,  $0.0050c$ ; chord-extension, 19.8 percent; chord-extension leading-edge radius,  $0c$ .

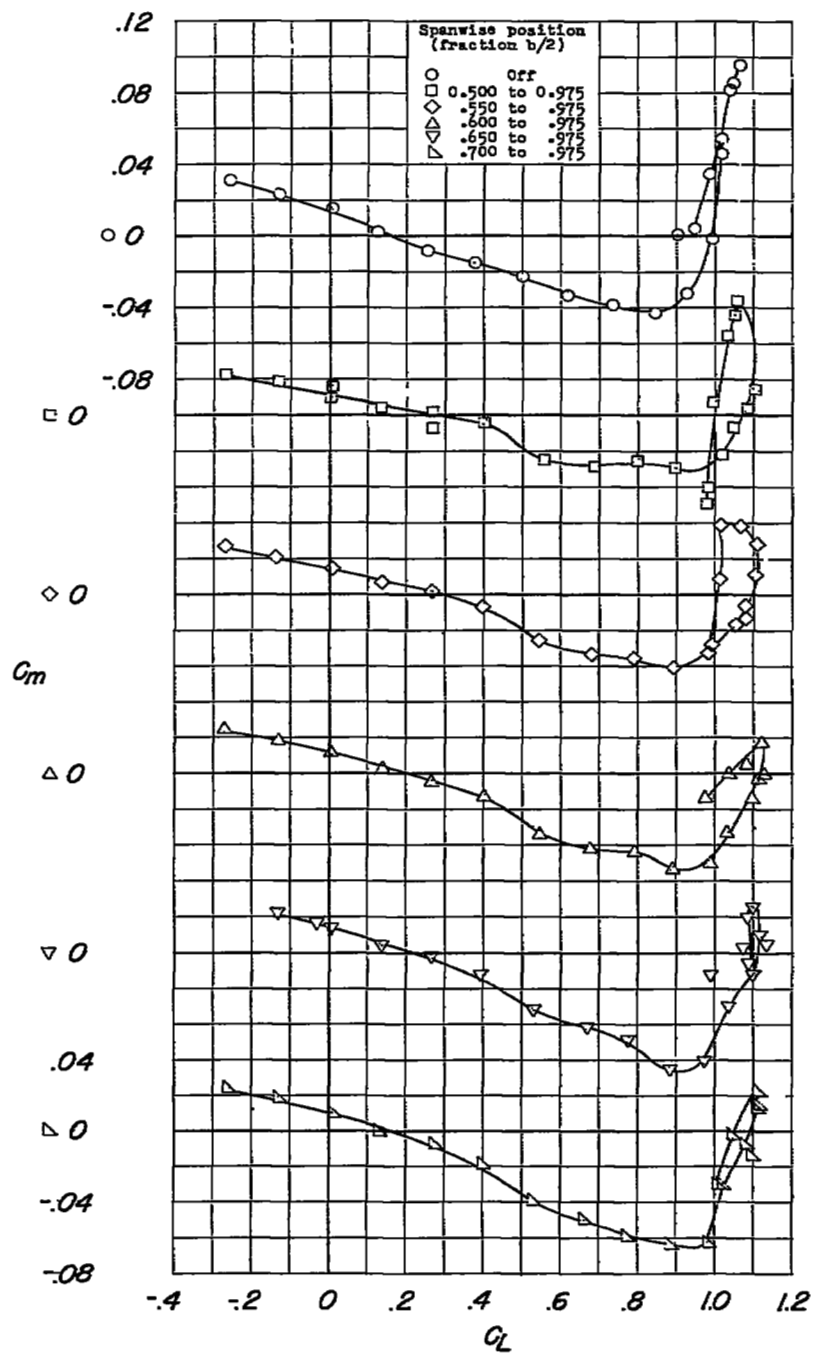
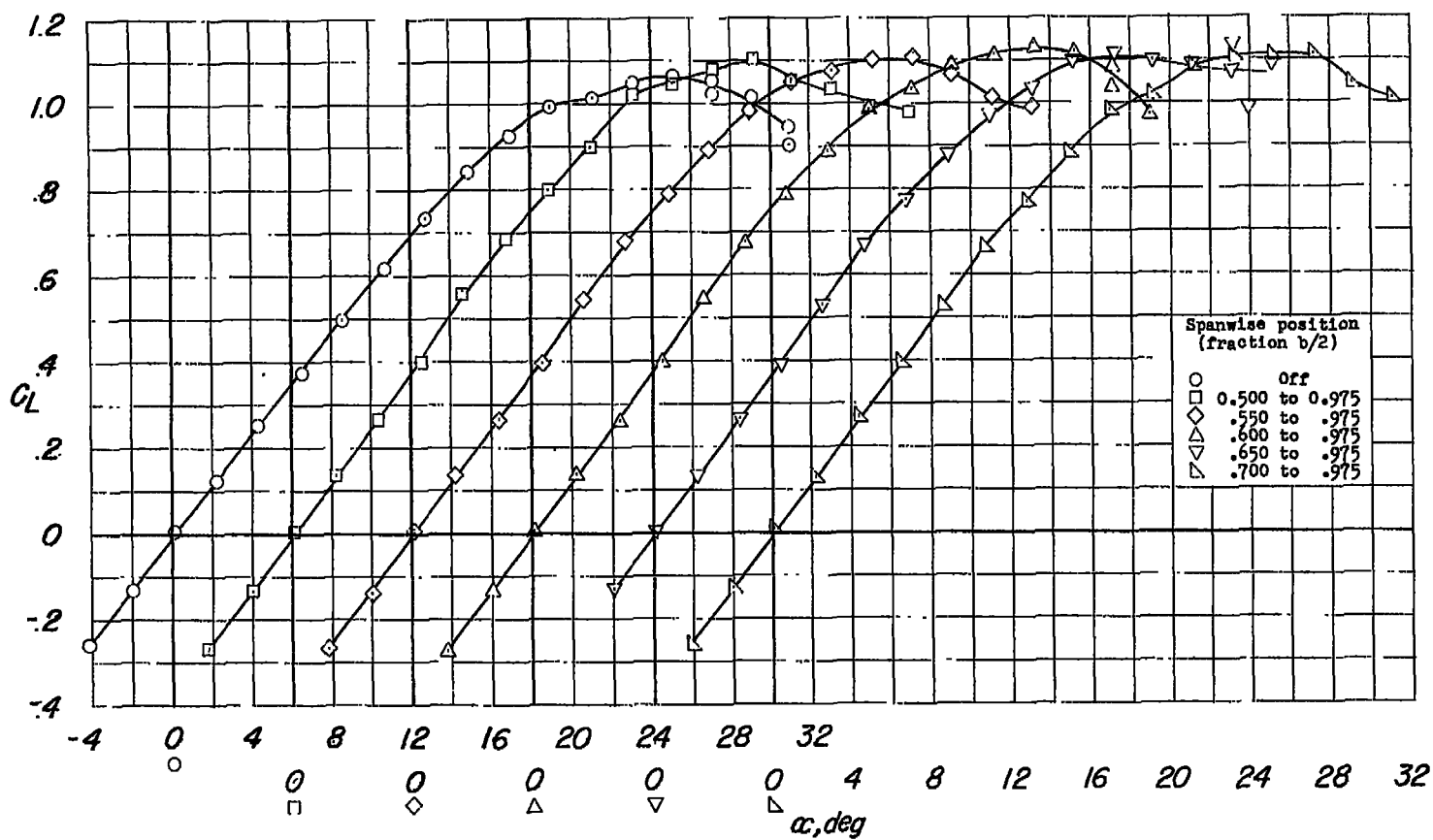
(b)  $C_m$  against  $C_L$ .

Figure 19.- Continued.



(c)  $C_L$  against  $\alpha$ .

Figure 19.- Concluded.

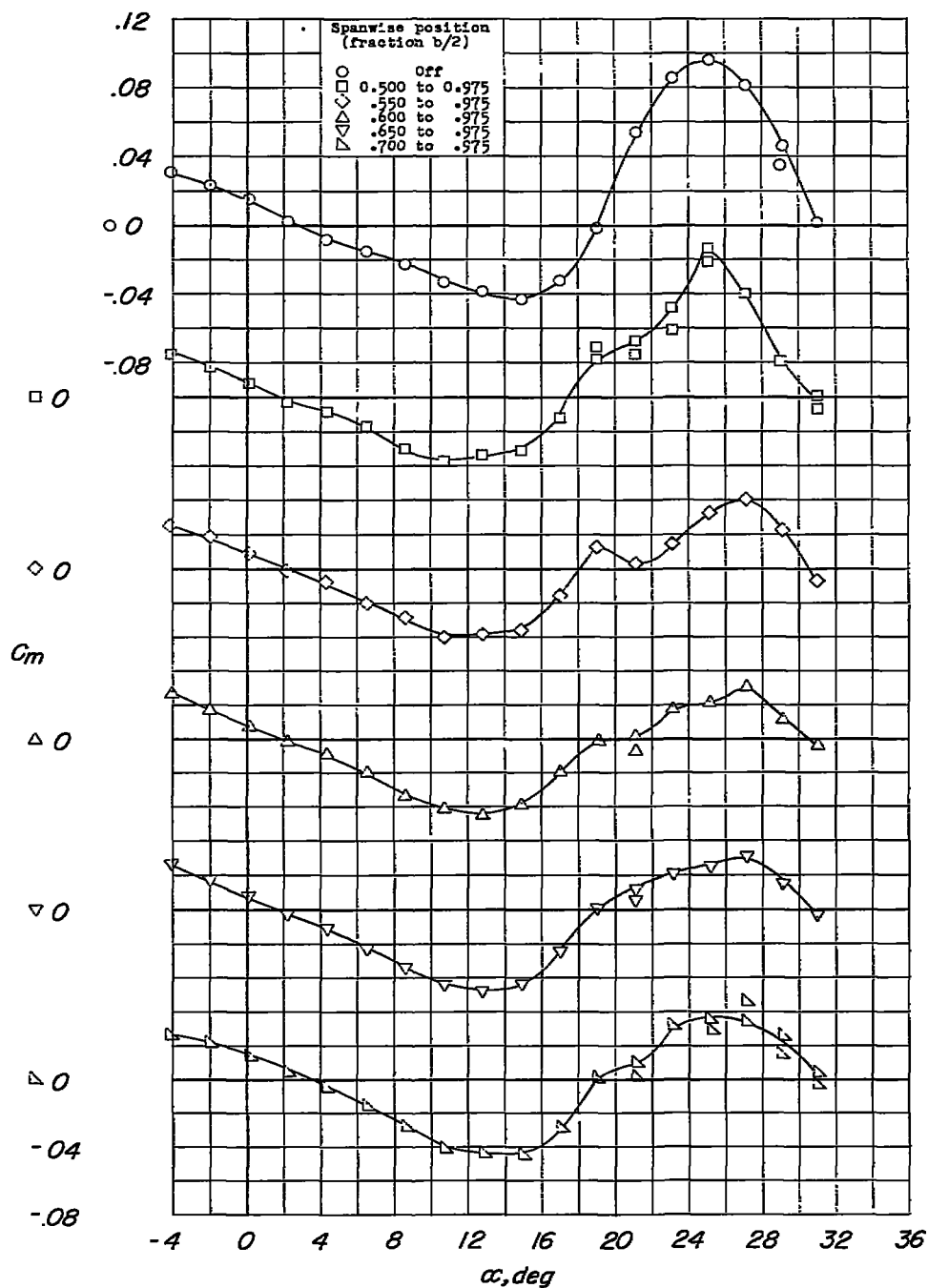
(a)  $C_m$  against  $\alpha$ .

Figure 20.- Lift and pitching-moment characteristics of wing with chord-extensions. Wing leading-edge radius, 0.0050c; chord-extension, 6.4 percent; chord-extension leading-edge radius, 0.00250c.

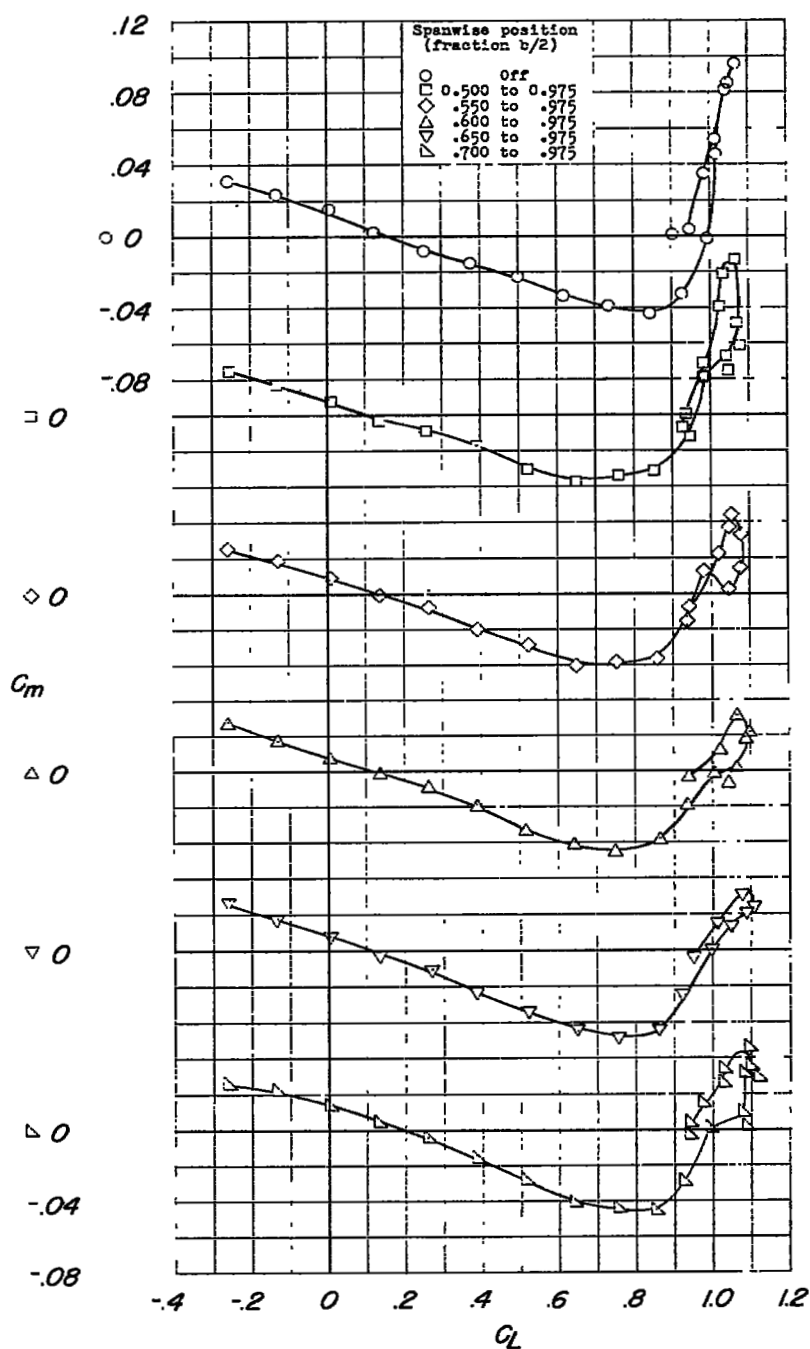
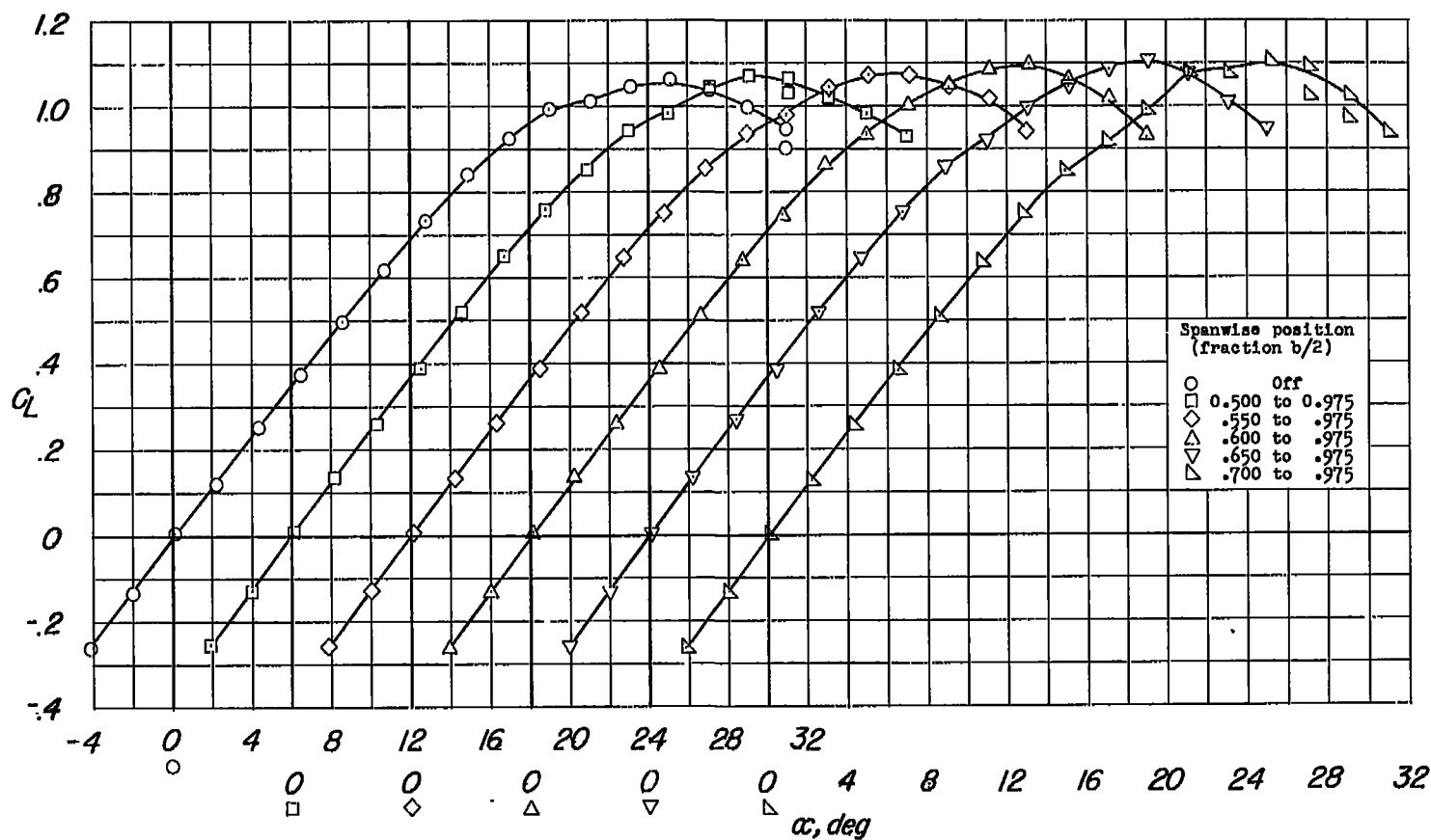
(b)  $C_m$  against  $C_L$ .

Figure 20.- Continued.



(c)  $C_L$  against  $\alpha$ .

Figure 20.- Concluded.

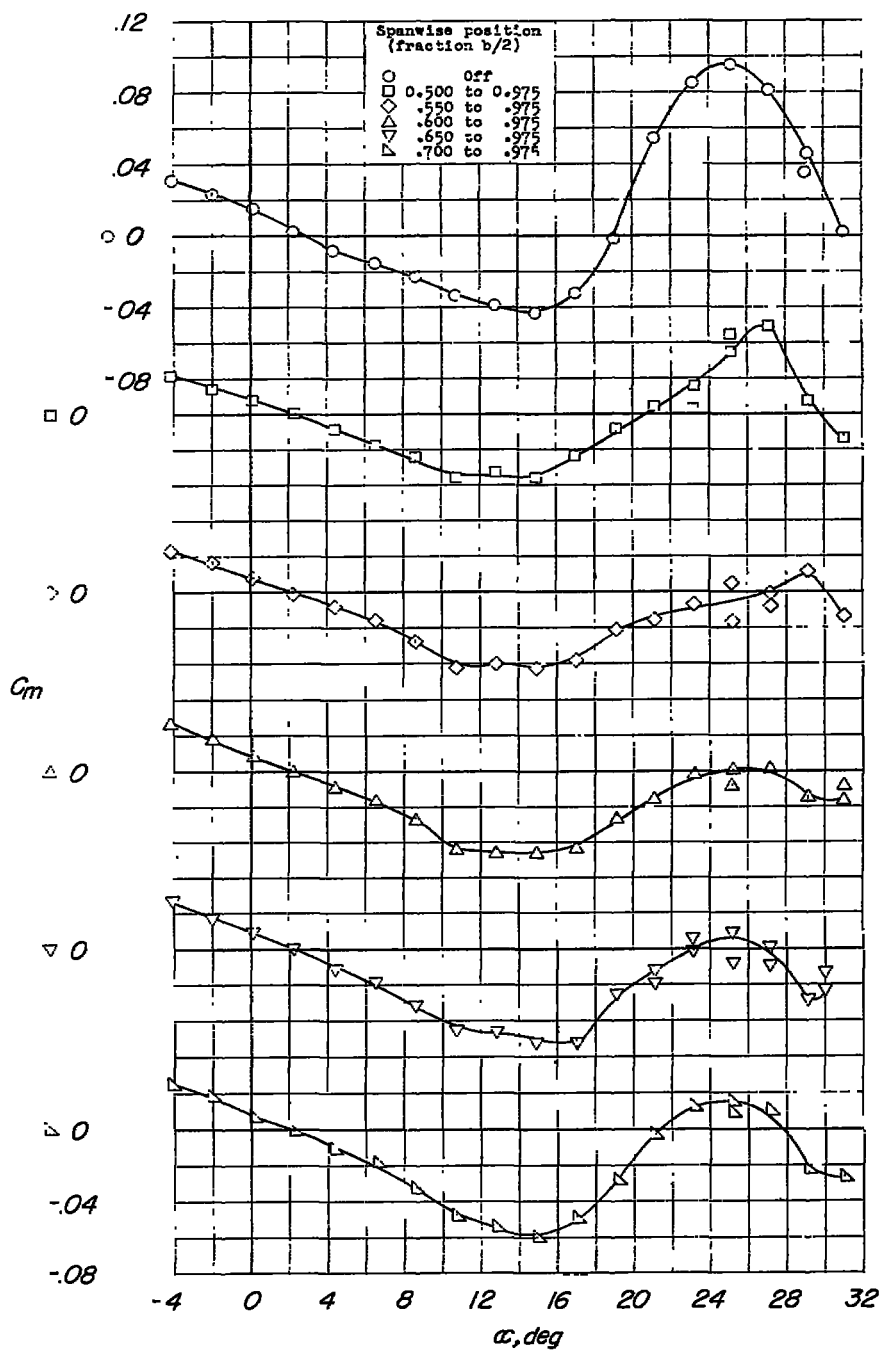
(a)  $C_m$  against  $\alpha$ .

Figure 21.- Lift and pitching-moment characteristics of wing with chord-extensions. Wing leading-edge radius, 0.0050c; chord-extension, 13.0 percent; chord-extension leading-edge radius, 0.00250c.

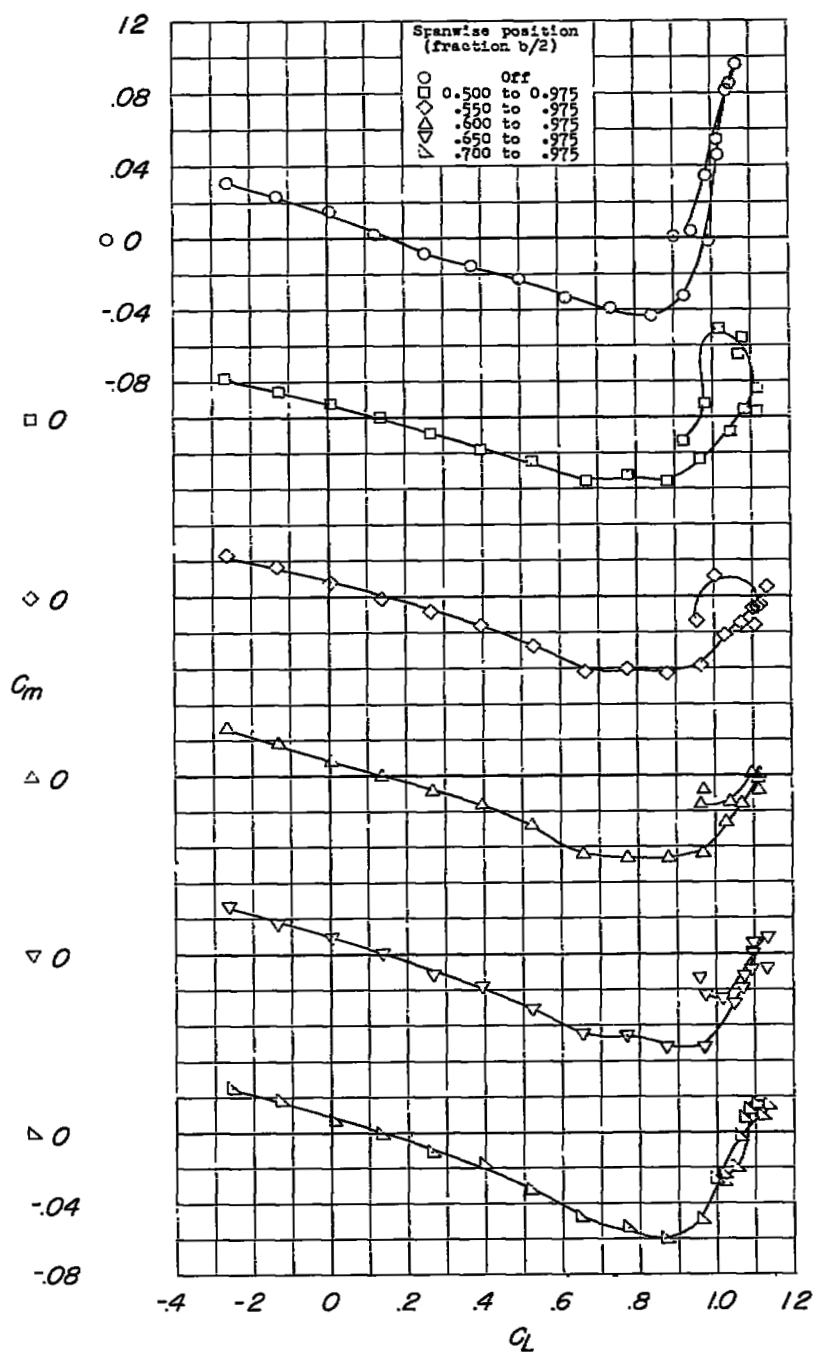
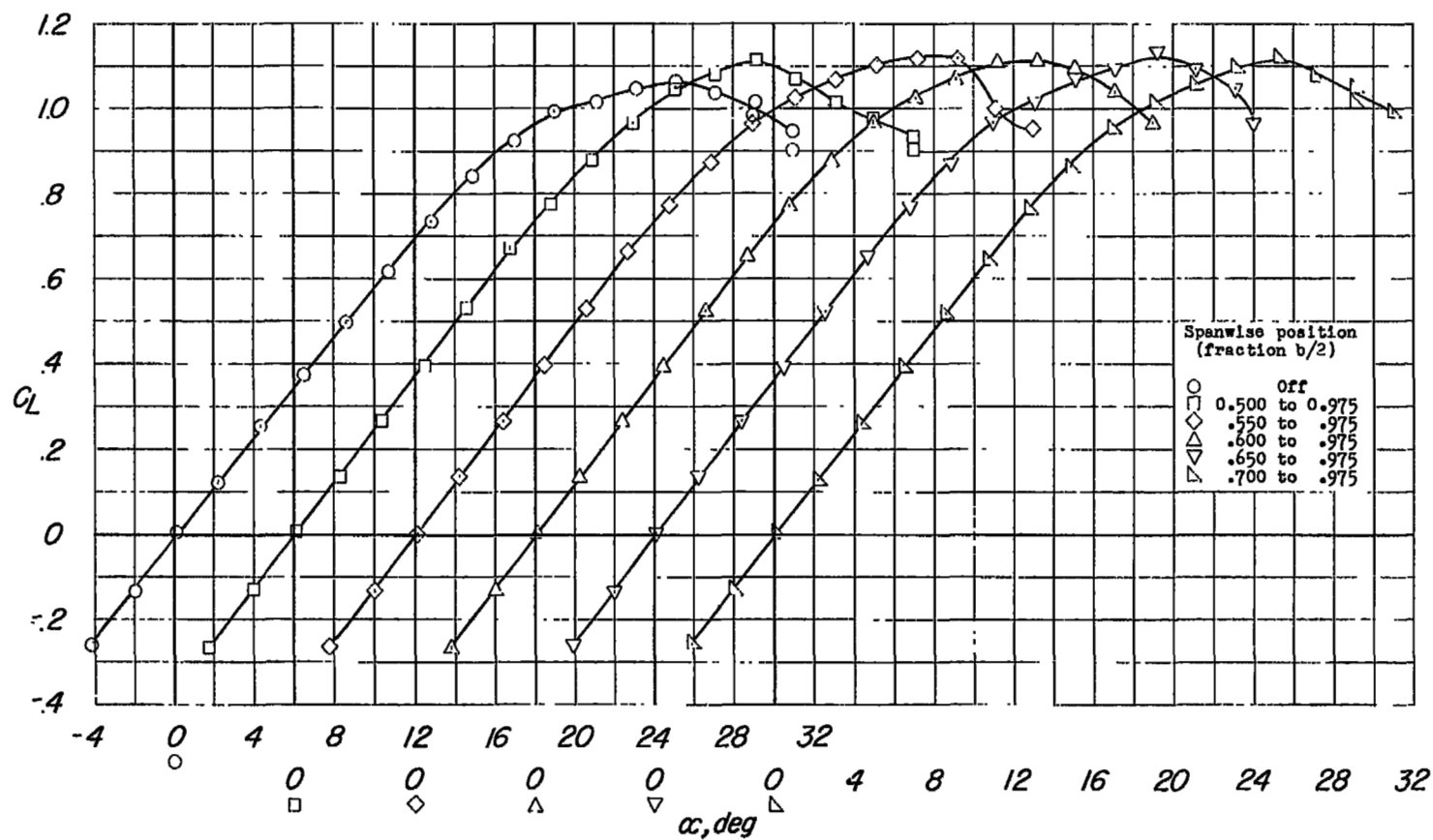
(b)  $C_m$  against  $C_L$ .

Figure 21.- Continued.



(c)  $C_L$  against  $\alpha$ .

Figure 21.- Concluded.

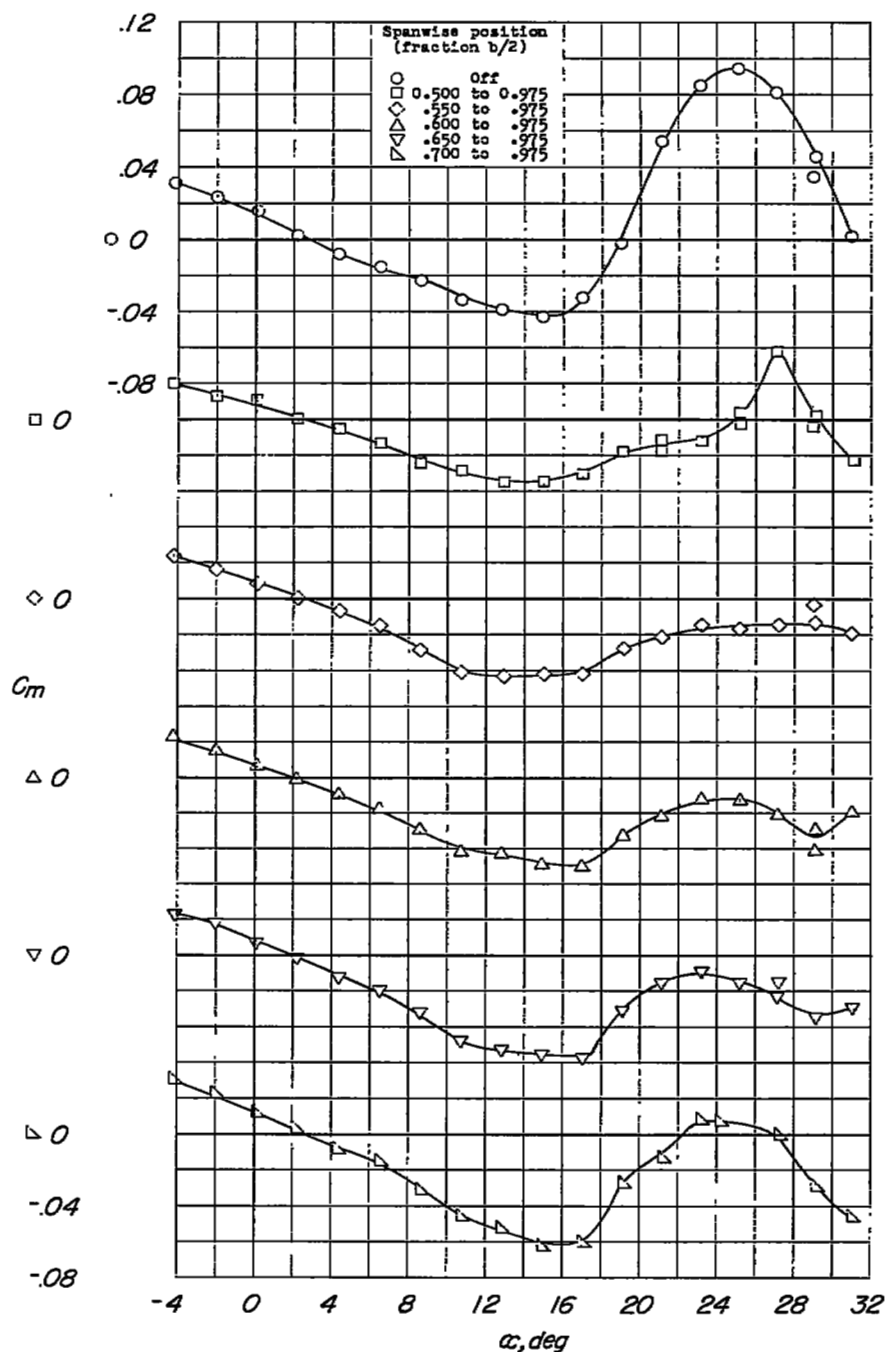
(a)  $C_m$  against  $\alpha$ .

Figure 22.- Lift and pitching-moment characteristics of wing with chord-extensions. Wing leading-edge radius, 0.0050c; chord-extension, 19.8 percent; chord-extension leading-edge radius, 0.00250c.

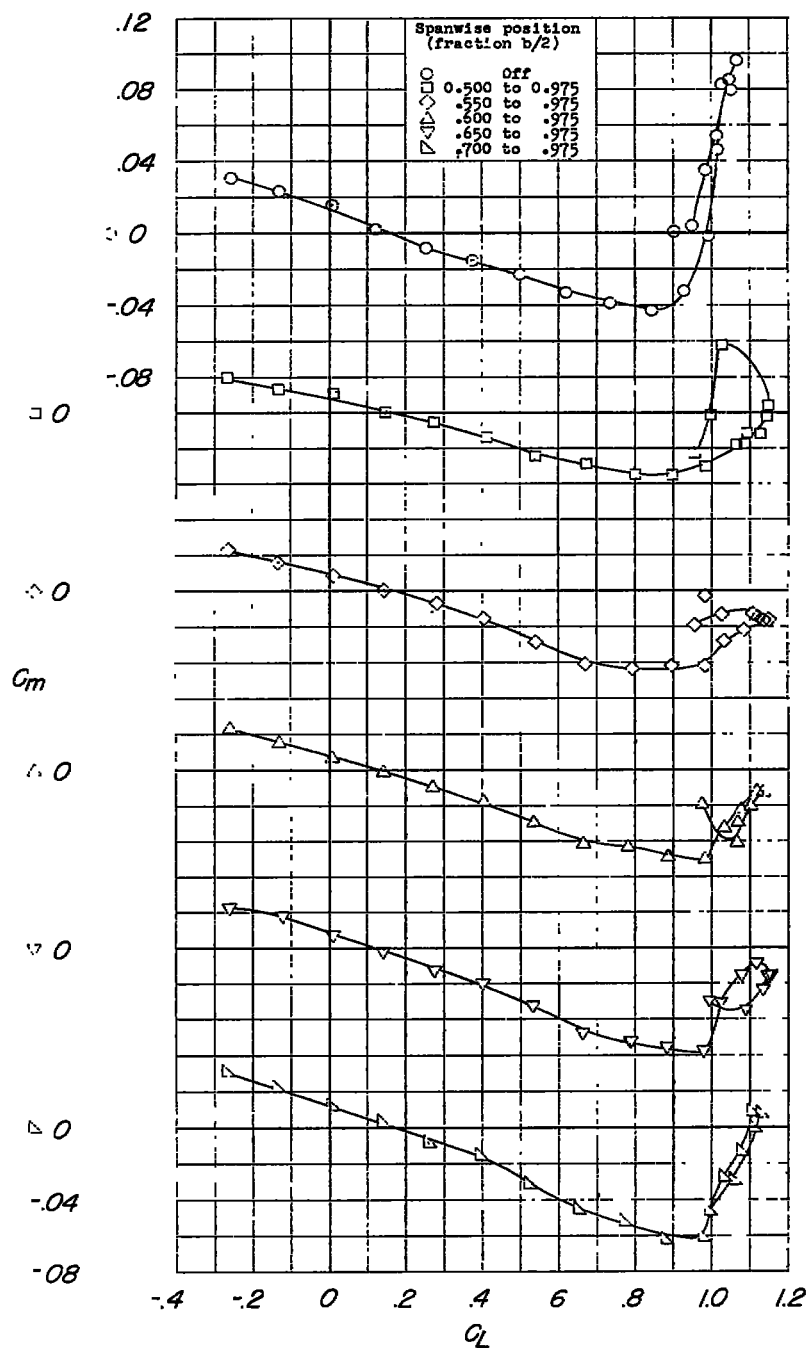
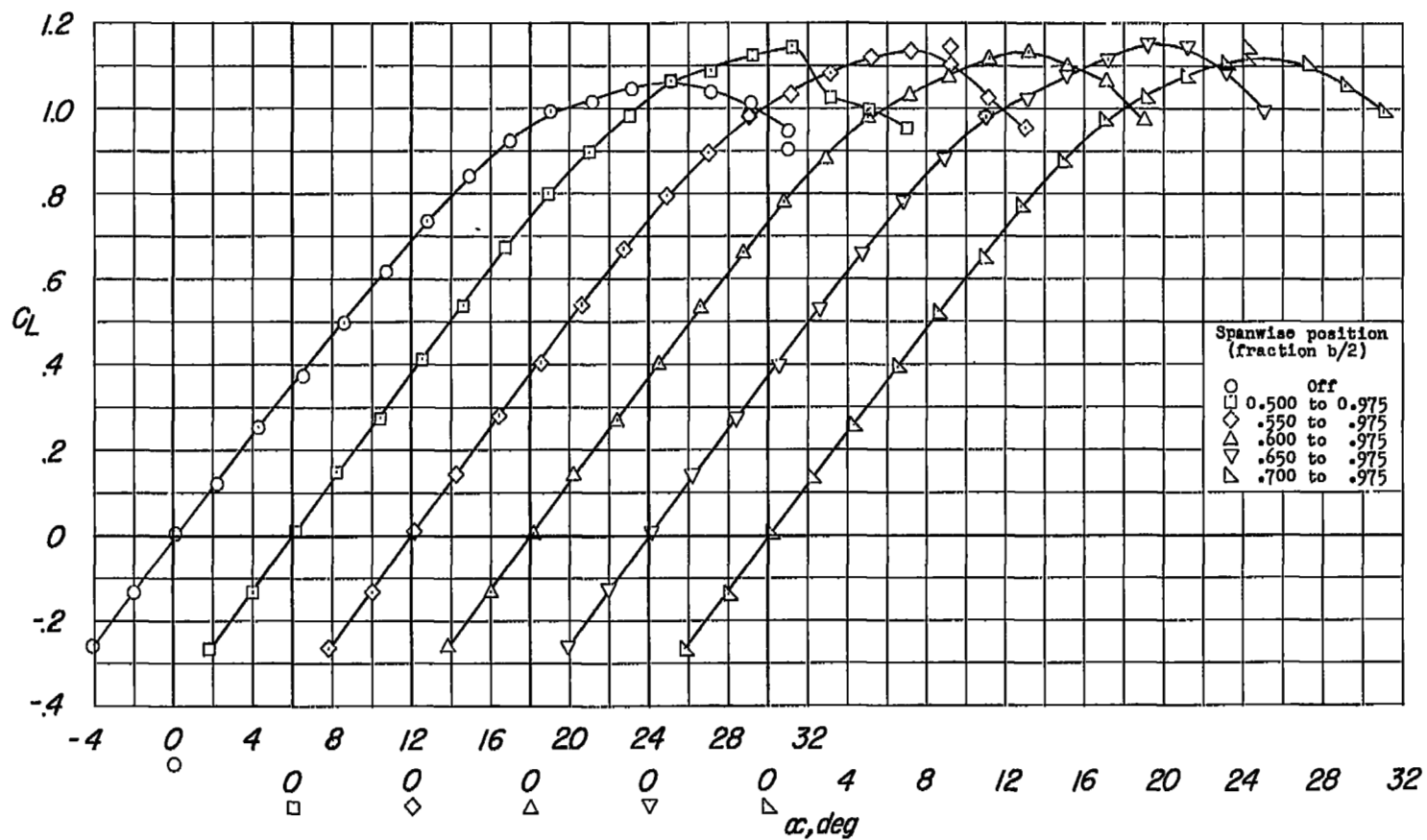
(b)  $C_m$  against  $C_L$ .

Figure 22.- Continued.



(c)  $C_L$  against  $\alpha$ .

Figure 22.- Concluded.

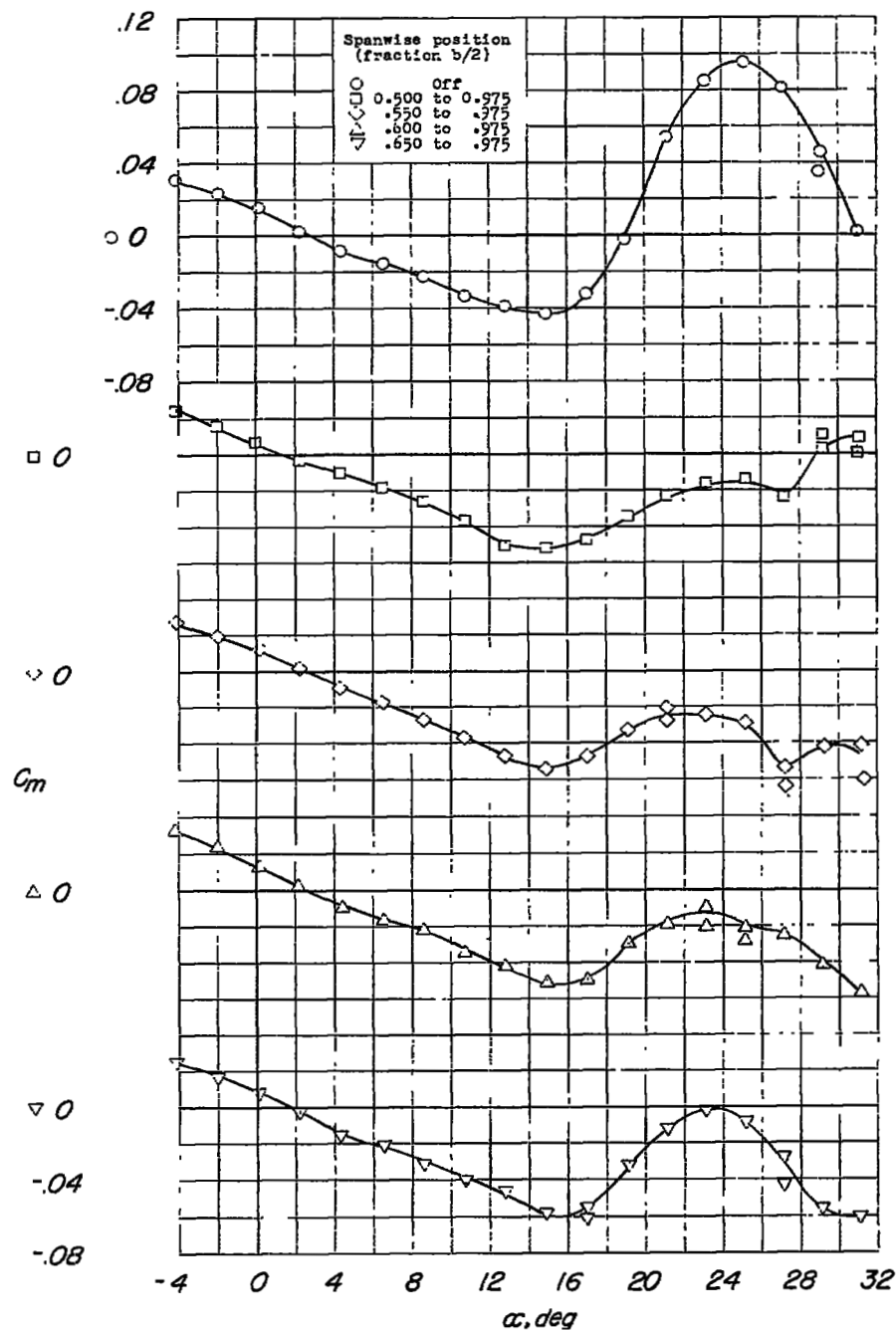
(a)  $C_m$  against  $\alpha$ .

Figure 23.- Lift and pitching-moment characteristics of wing with chord-extensions. Wing leading-edge radius, 0.0050c; chord-extension, 6.4 percent; chord-extension leading-edge radius, 0.00445c.

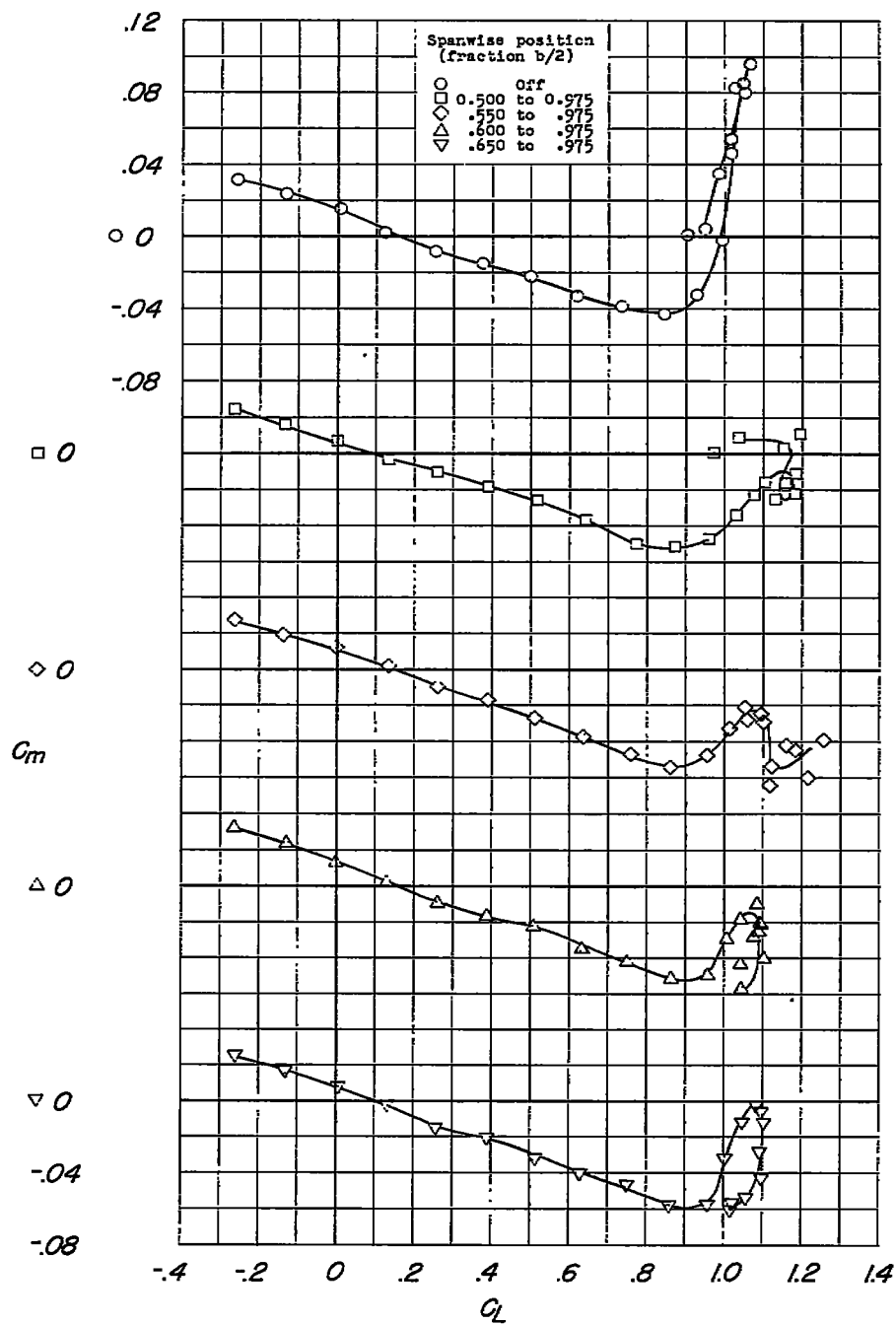
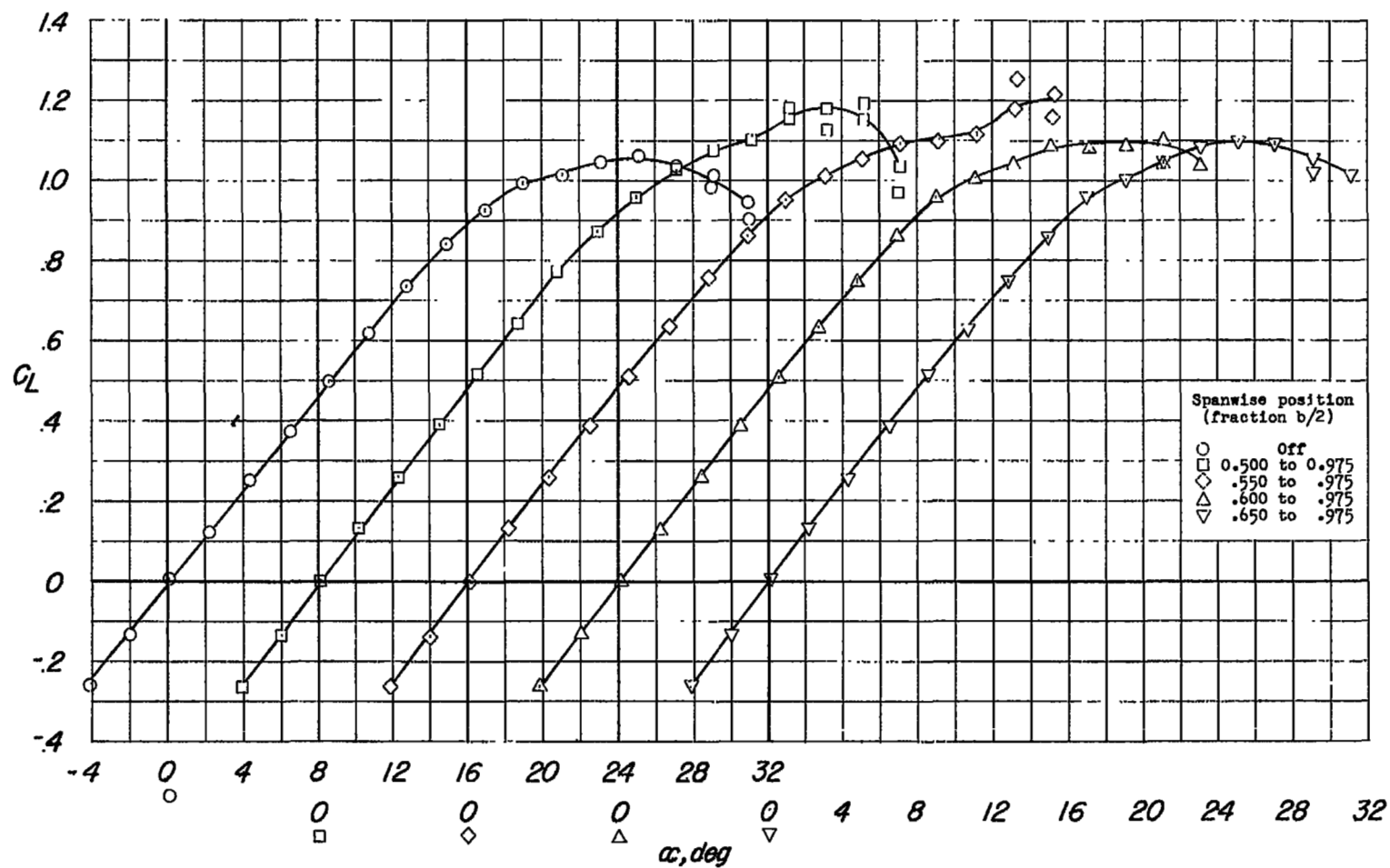
(b)  $C_m$  against  $C_L$ .

Figure 23.- Continued.



(c)  $C_L$  against  $\alpha$ .

Figure 23.- Concluded.

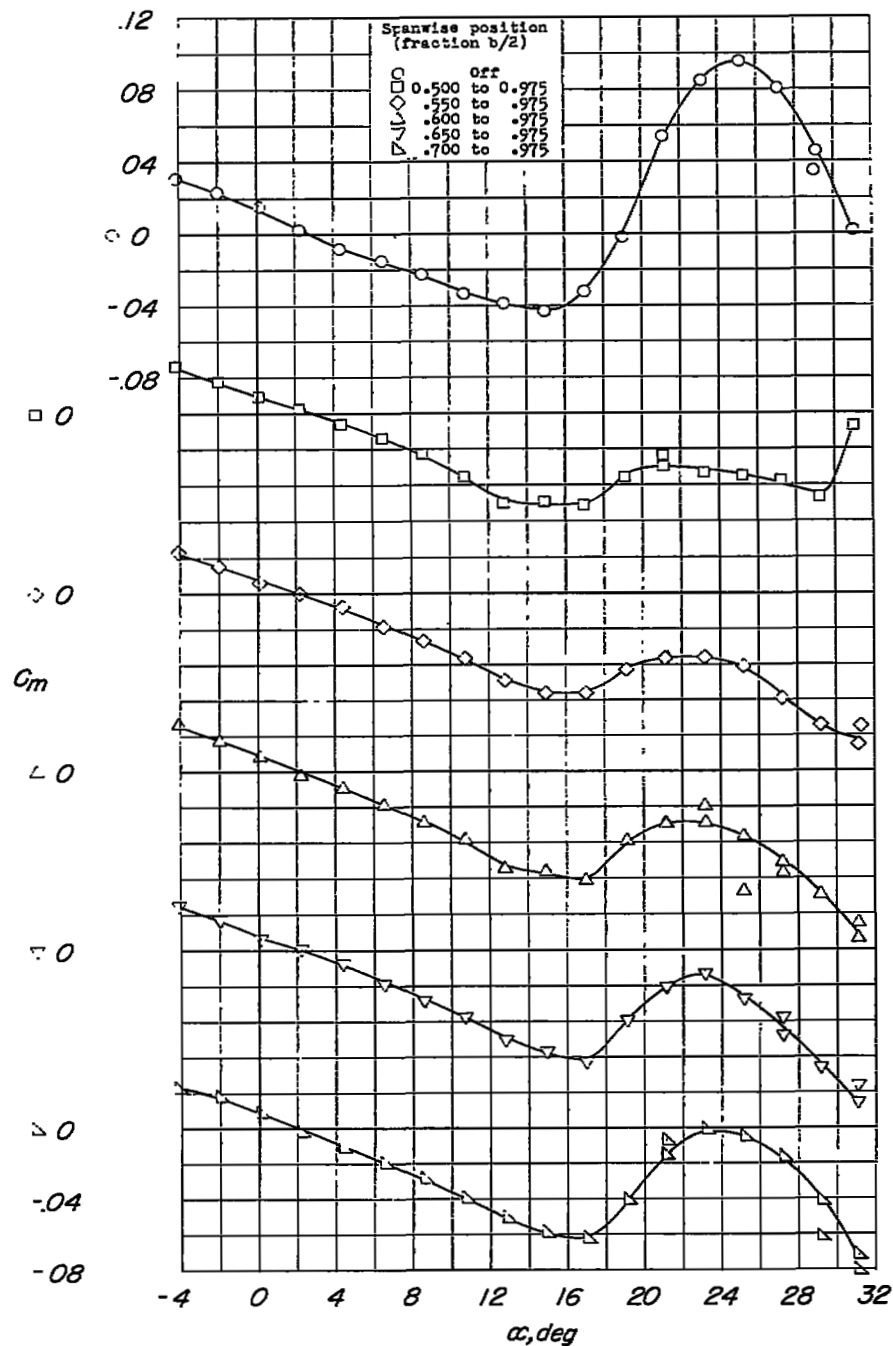
(a)  $C_m$  against  $\alpha$ .

Figure 24.- Lift and pitching-moment characteristics of wing with chord-extensions. Wing leading-edge radius, 0.0050c; chord-extension, 13 percent; chord-extension leading-edge radius, 0.00445c.

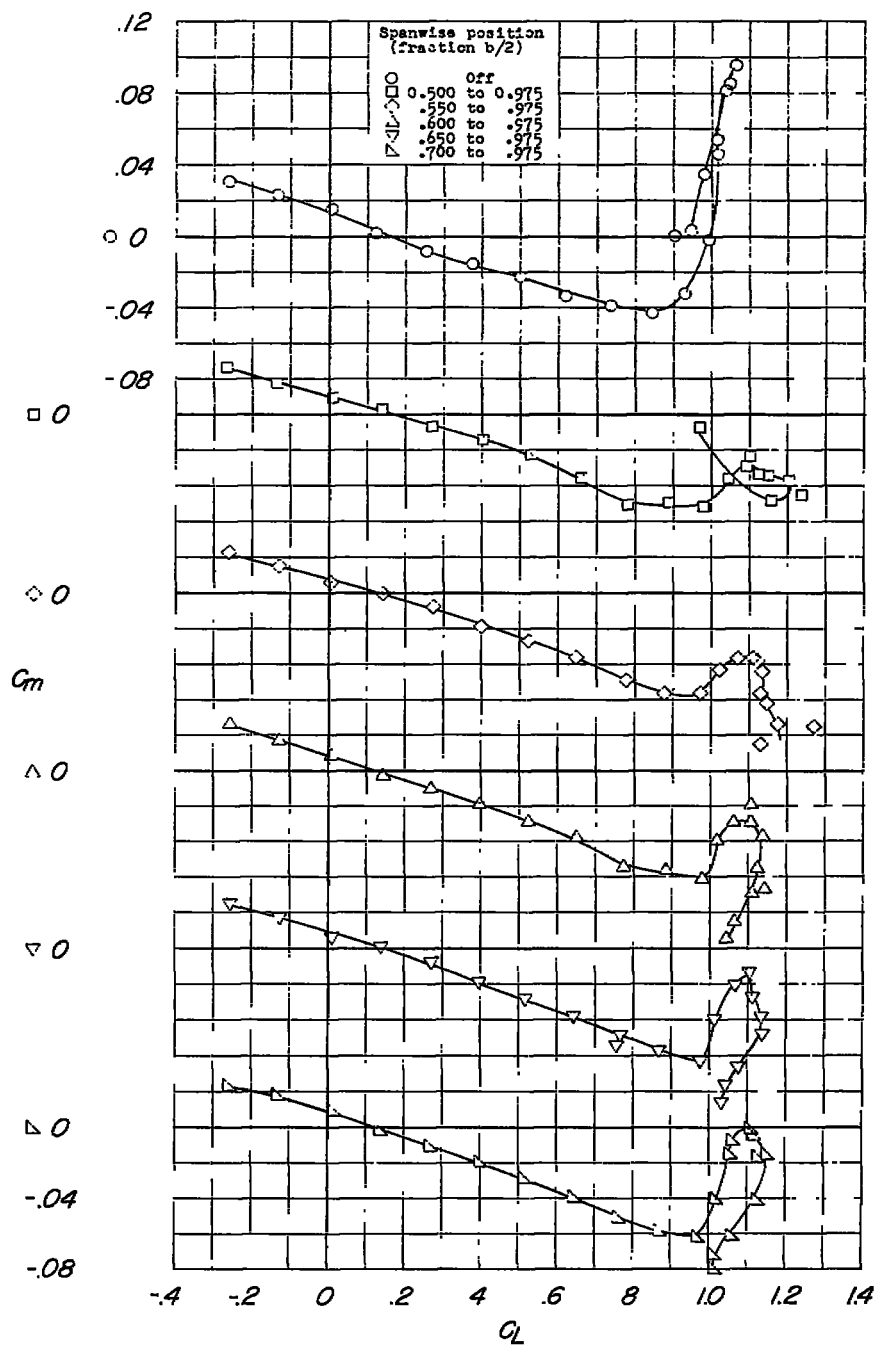
(b)  $C_m$  against  $C_L$ .

Figure 24.- Continued.

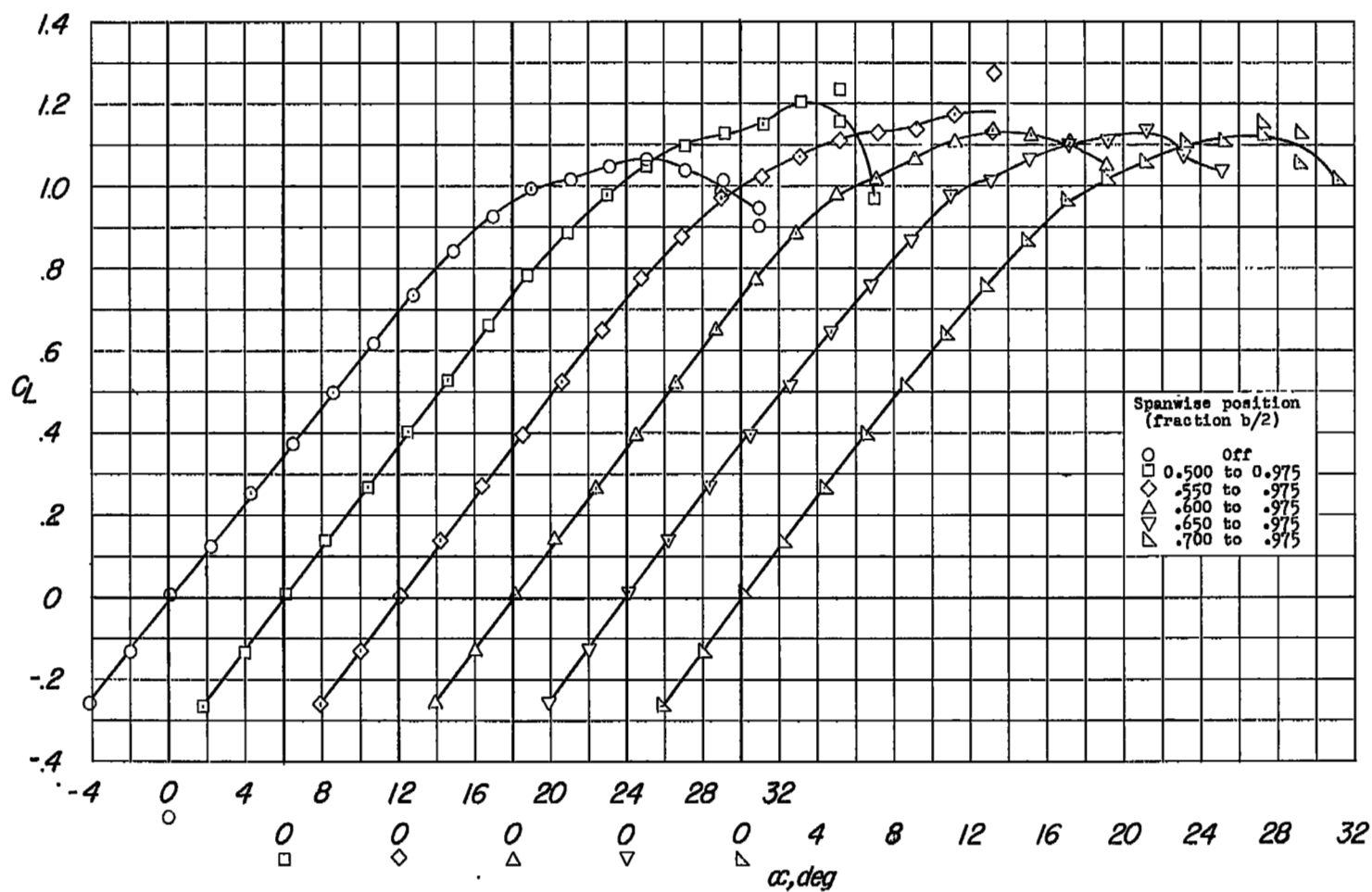
(c)  $C_L$  against  $\alpha$ .

Figure 24.- Concluded.

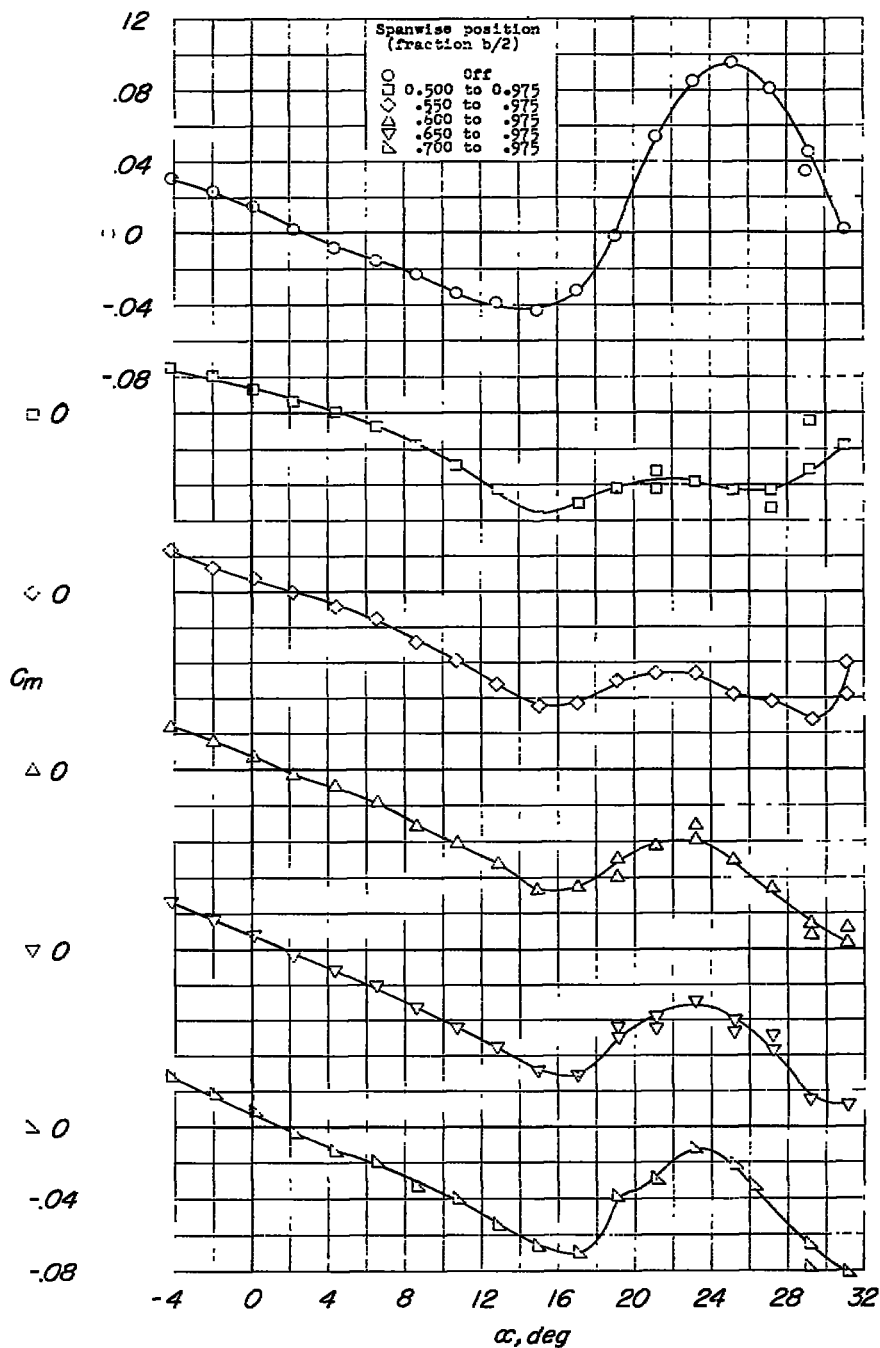
(a)  $C_m$  against  $\alpha$ .

Figure 25.- Lift and pitching-moment characteristics of wing with chord-extensions. Wing leading-edge radius, 0.0050c; chord-extension, 19.8 percent; chord-extension leading-edge radius, 0.00445c.

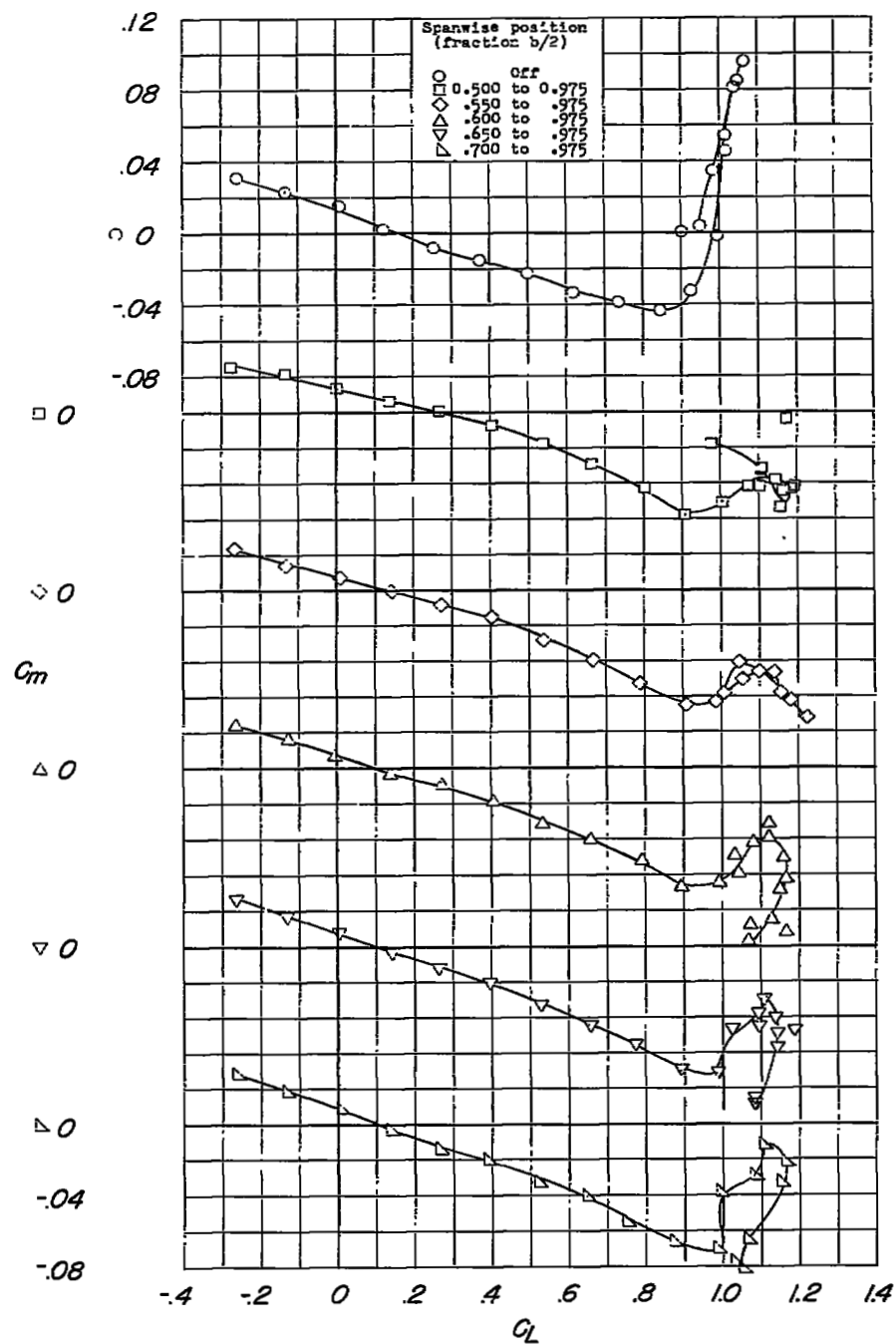
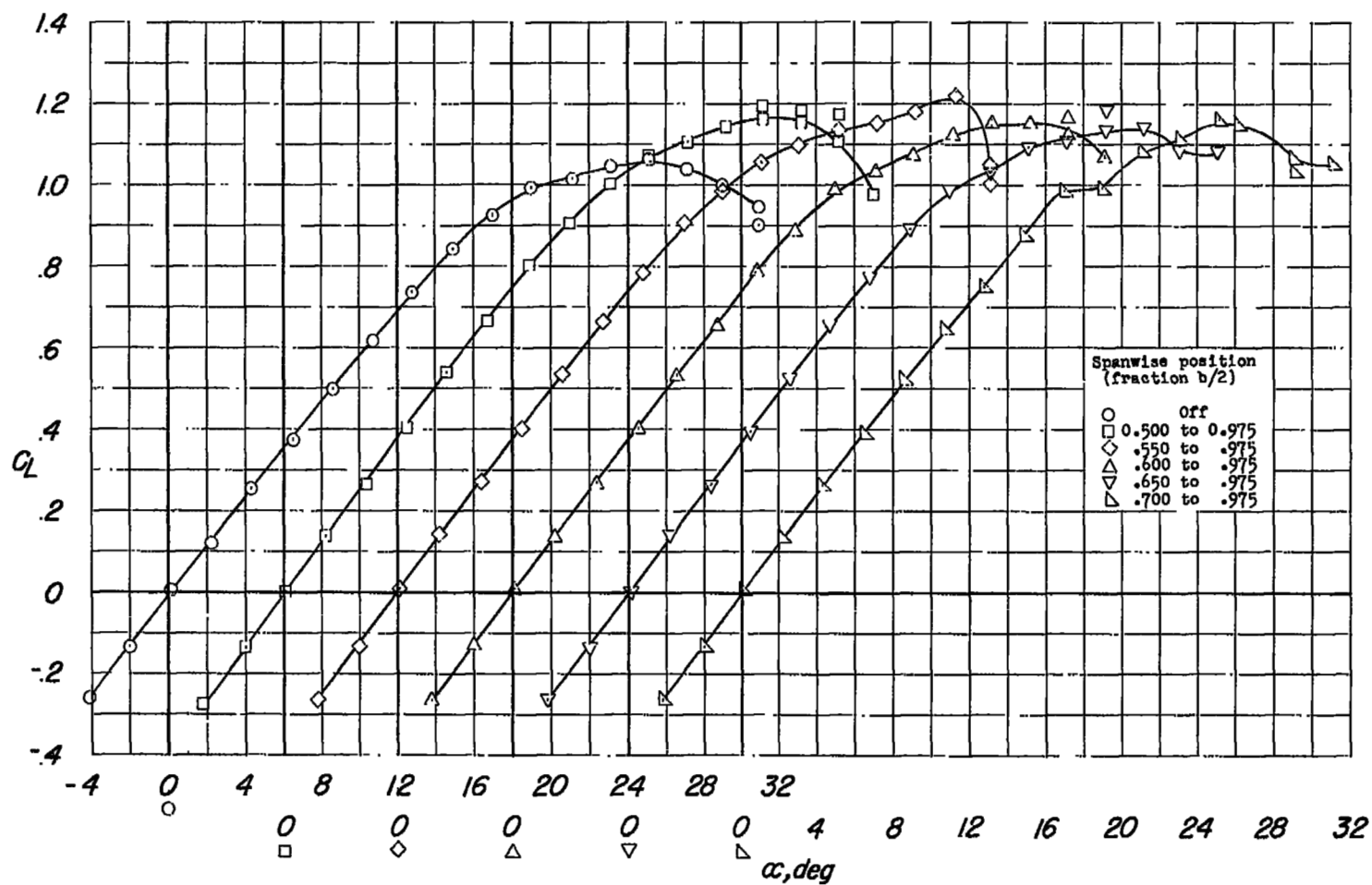
(b)  $C_m$  against  $C_L$ .

Figure 25.- Continued.



(c)  $C_L$  against  $\alpha$ .

Figure 25.- Concluded.

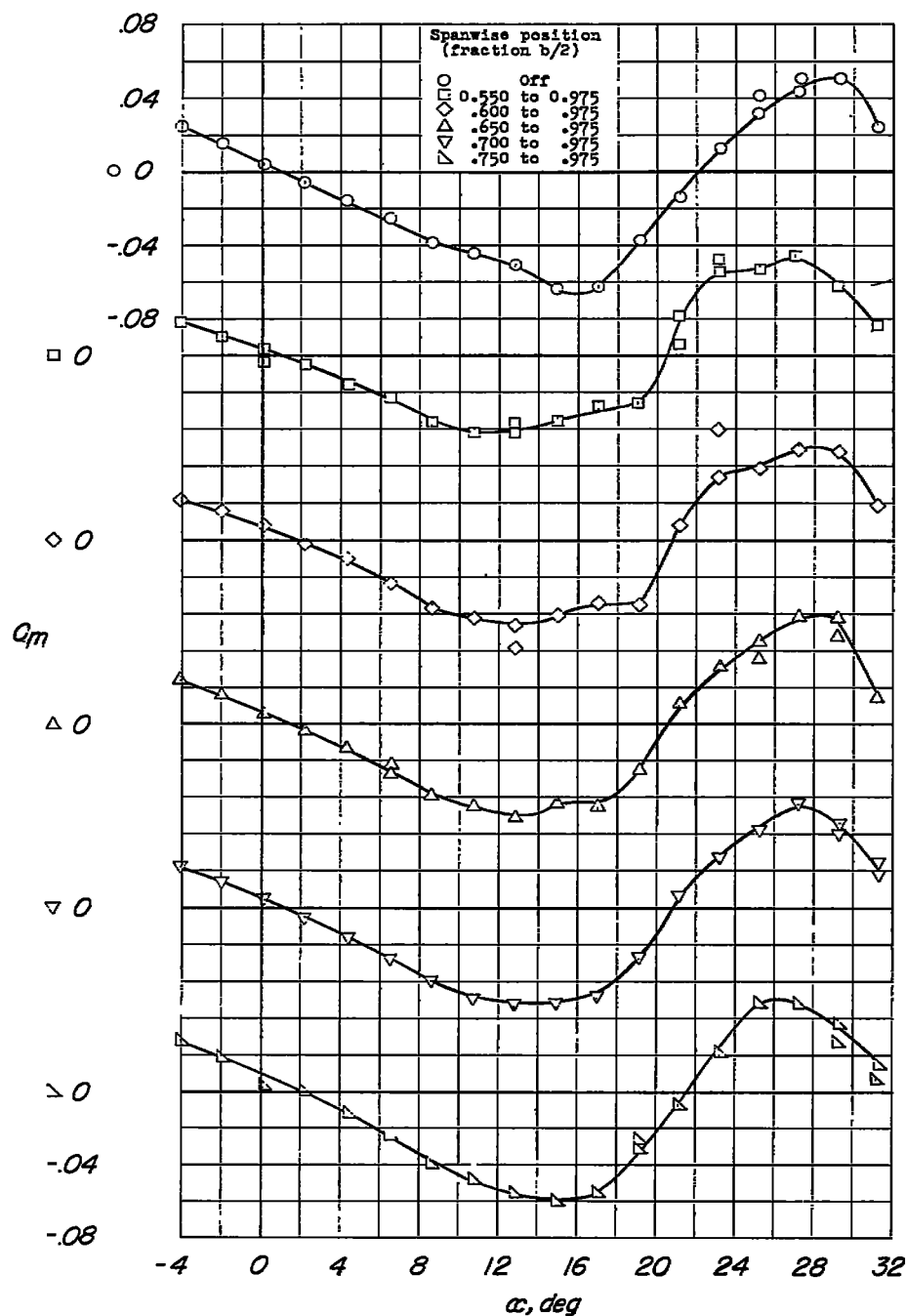
(a)  $C_m$  against  $\alpha$ .

Figure 26.- Lift and pitching-moment characteristics of wing with chord-extensions. Wing leading-edge radius, 0.0089c; chord-extension, 6.4 percent; chord-extension leading-edge radius, 0c.

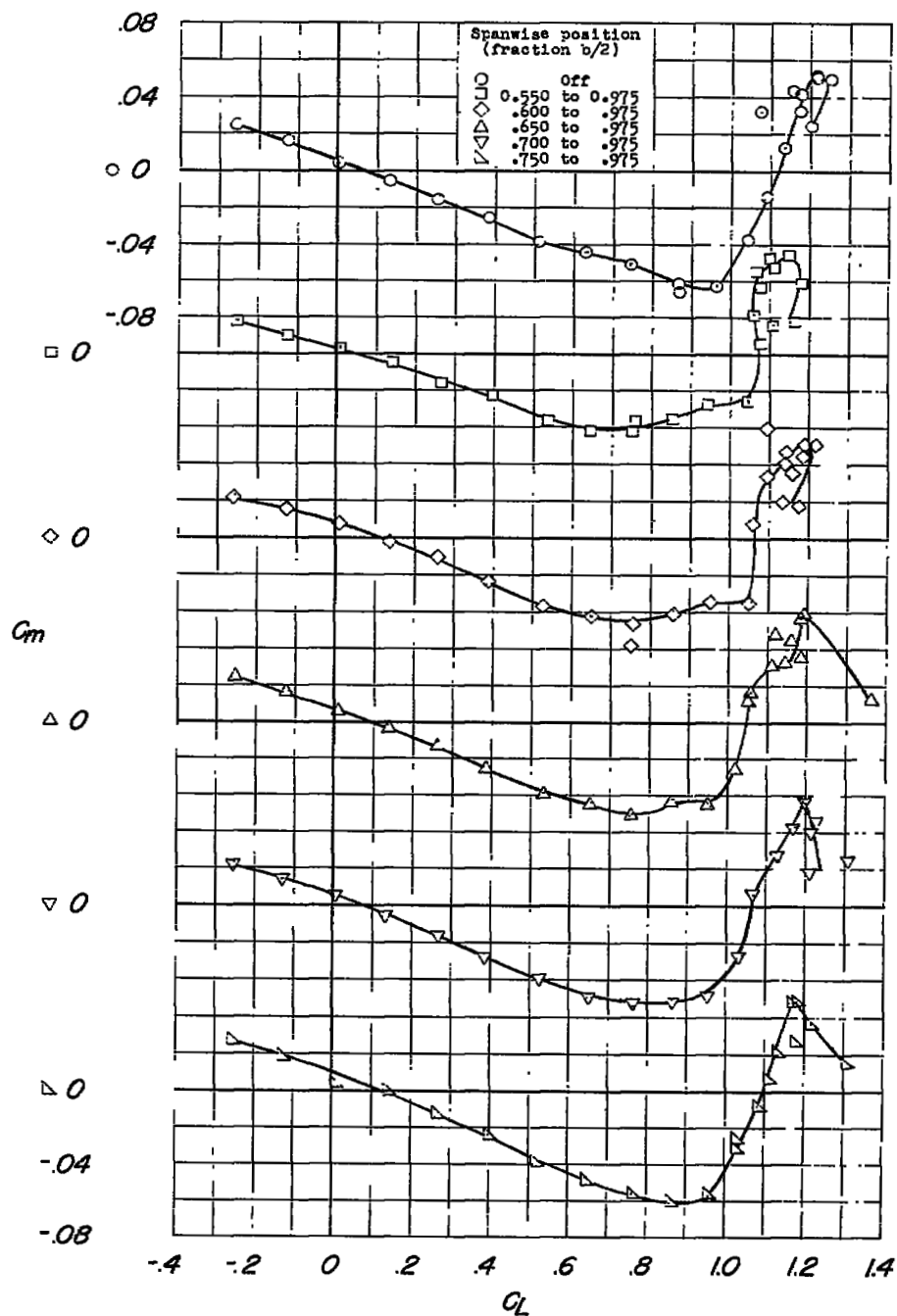
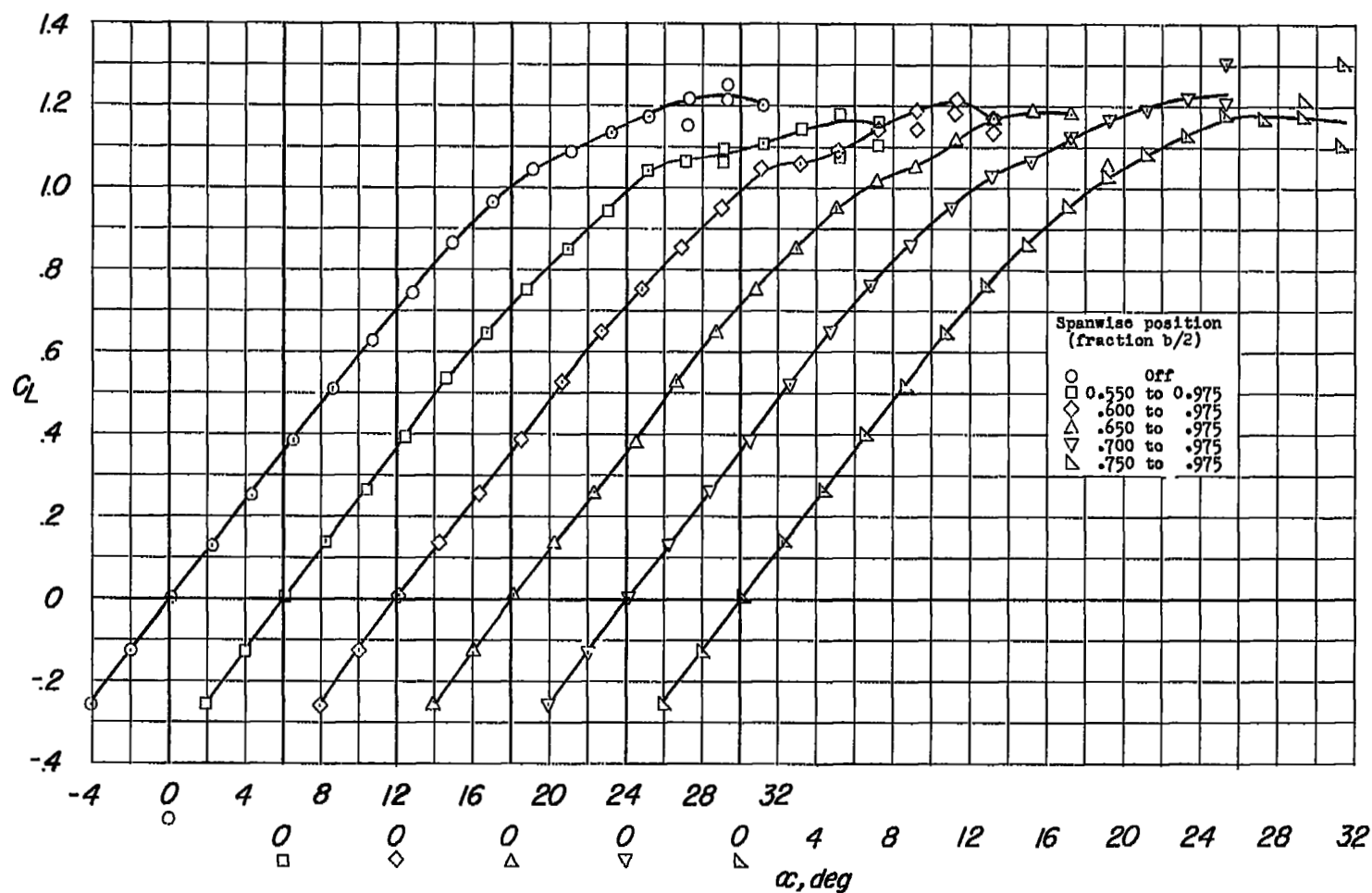
(b)  $C_m$  against  $C_L$ .

Figure 26.- Continued.



(c)  $C_L$  against  $\alpha$ .

Figure 26.- Concluded.

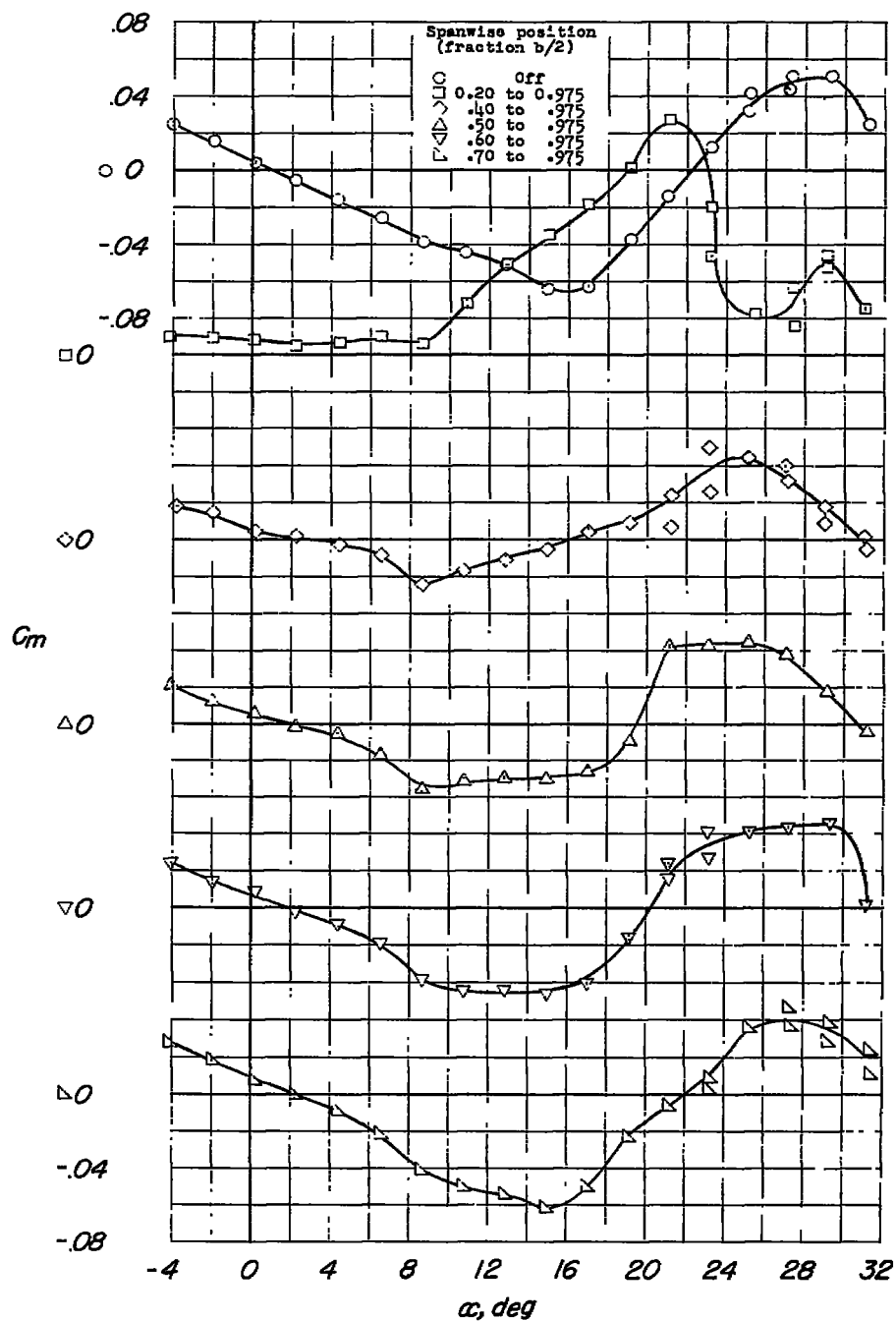
(a)  $C_m$  against  $\alpha$ .

Figure 27.- Lift and pitching-moment characteristics of wing with chord-extensions. Wing leading-edge radius, 0.0089c; chord-extension, 13.0 percent; chord-extension leading-edge radius, 0c.

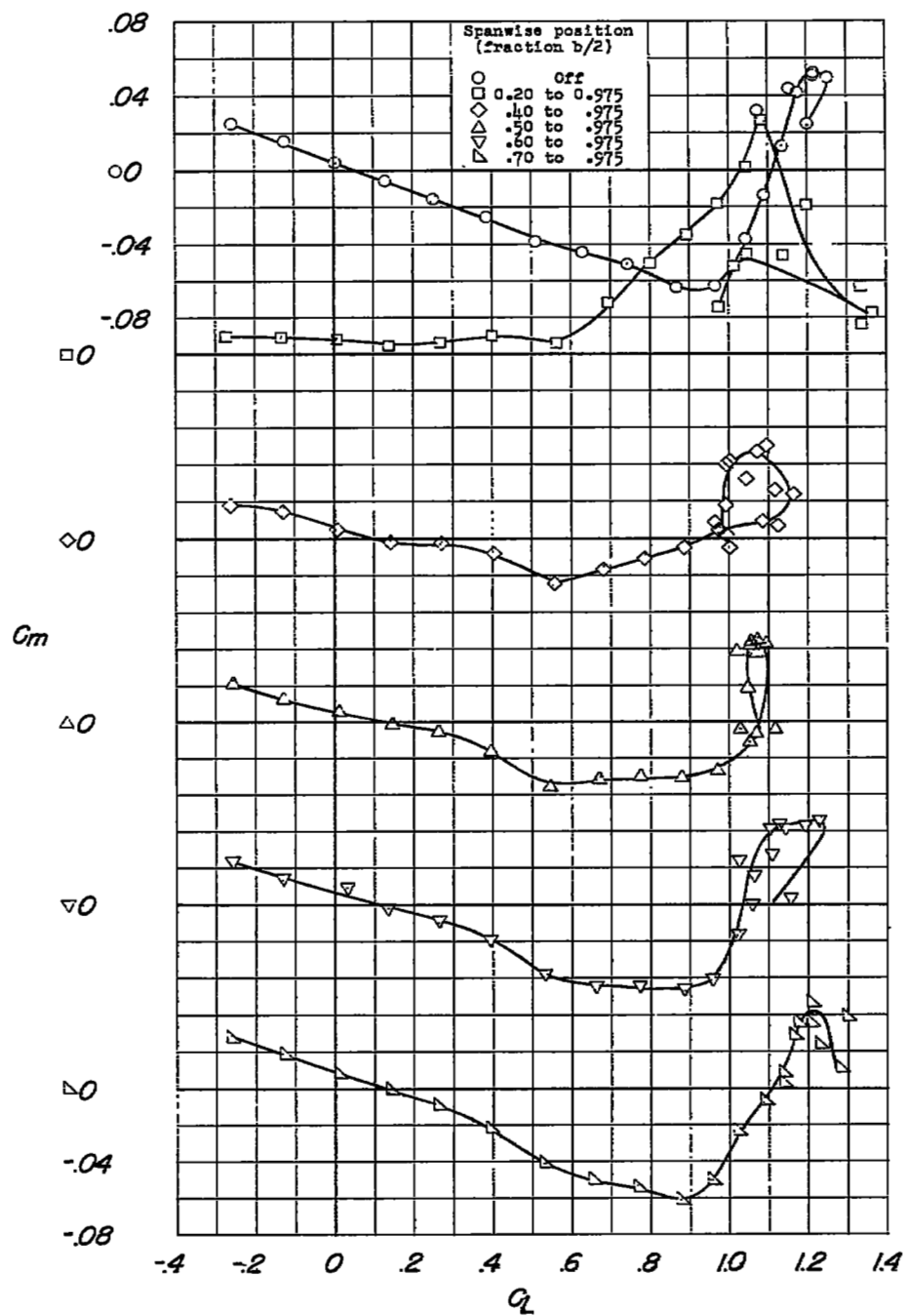
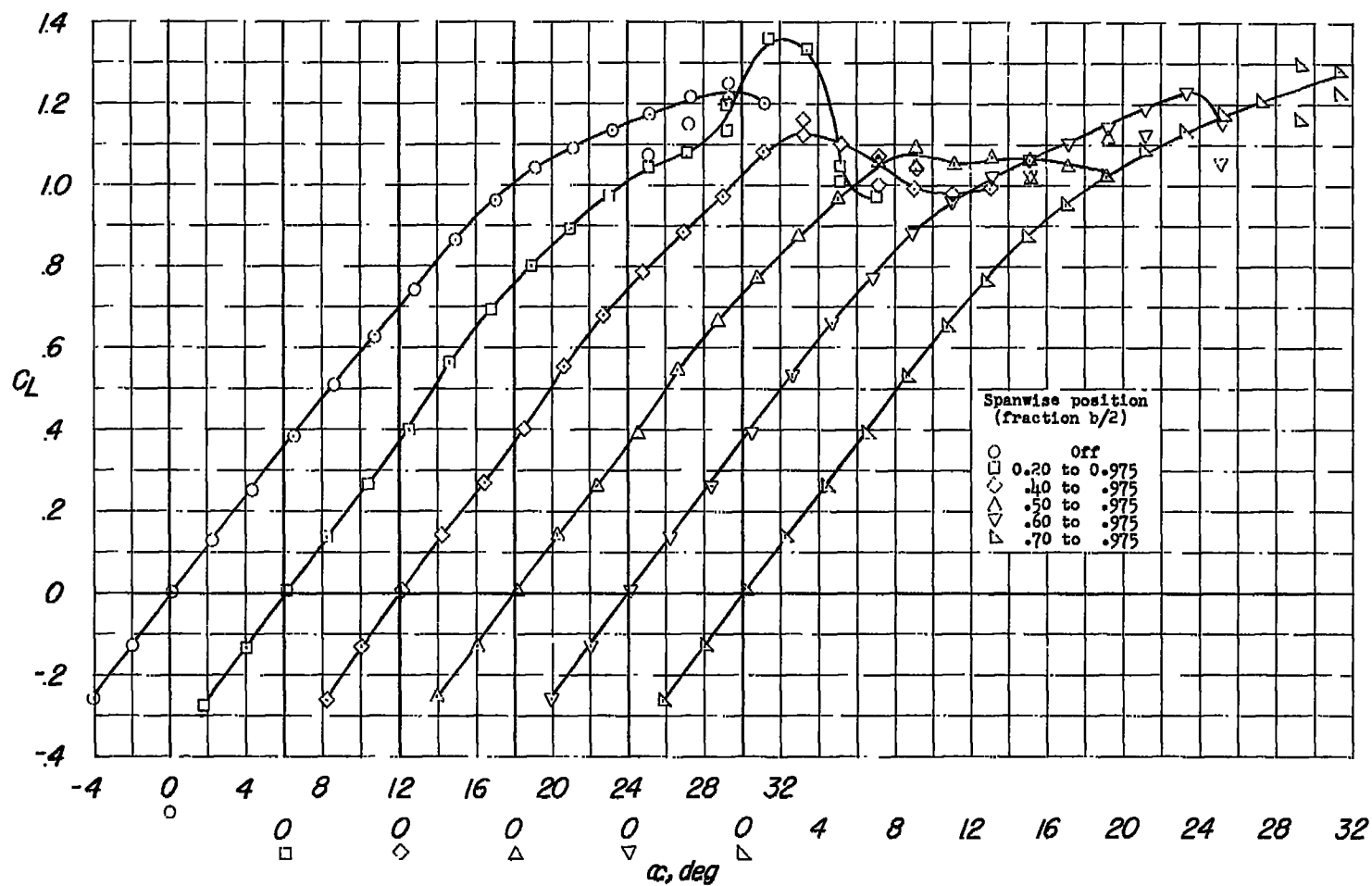
(b)  $C_m$  against  $C_L$ .

Figure 27.- Continued.



(c)  $C_L$  against  $\alpha$ .

Figure 27.- Concluded.

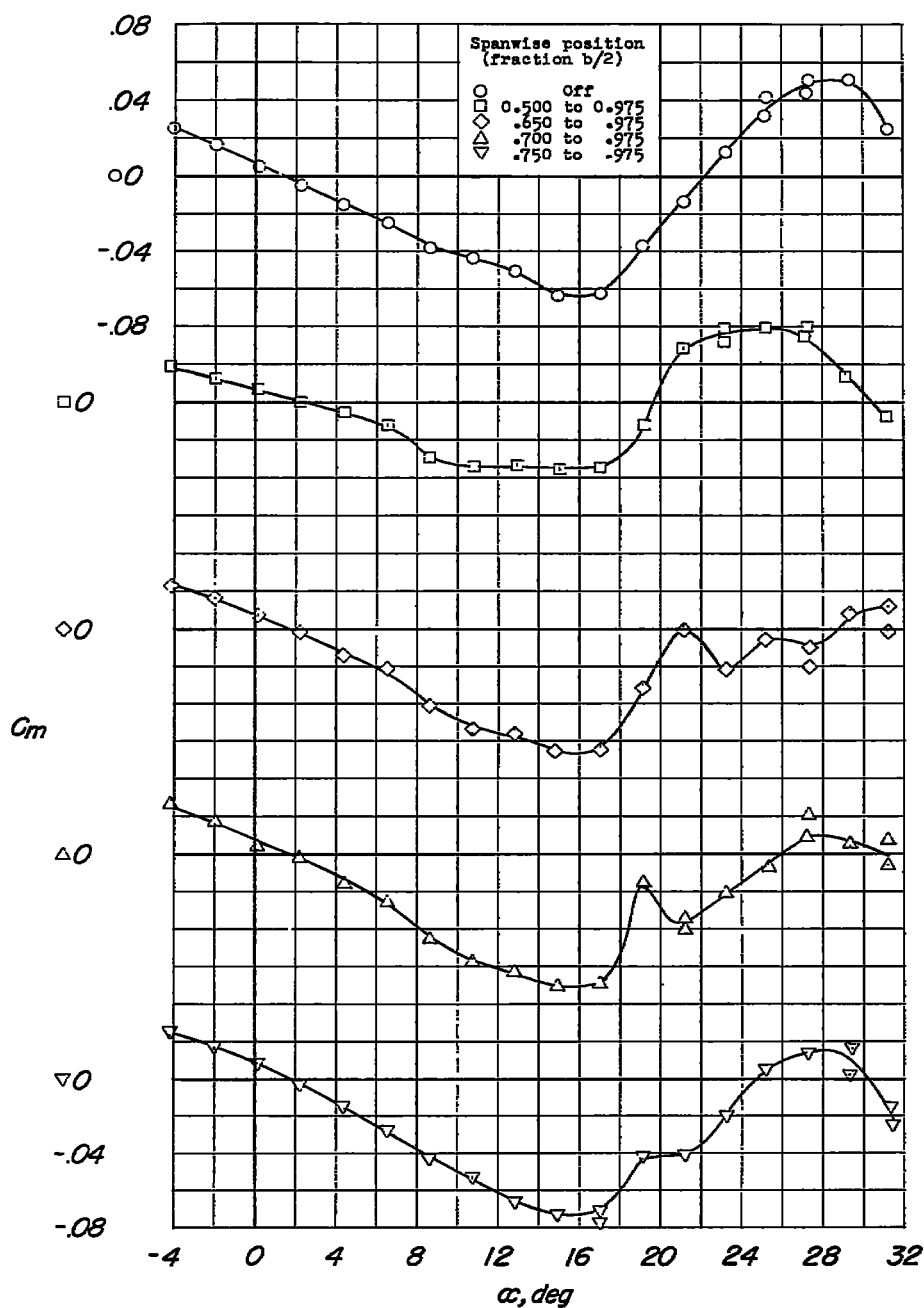
(a)  $C_m$  against  $\alpha$ .

Figure 28.- Lift and pitching-moment characteristics of wing with chord-extensions. Wing leading-edge radius, 0.0089c; chord-extension, 19.8 percent; chord-extension leading-edge radius, 0c.

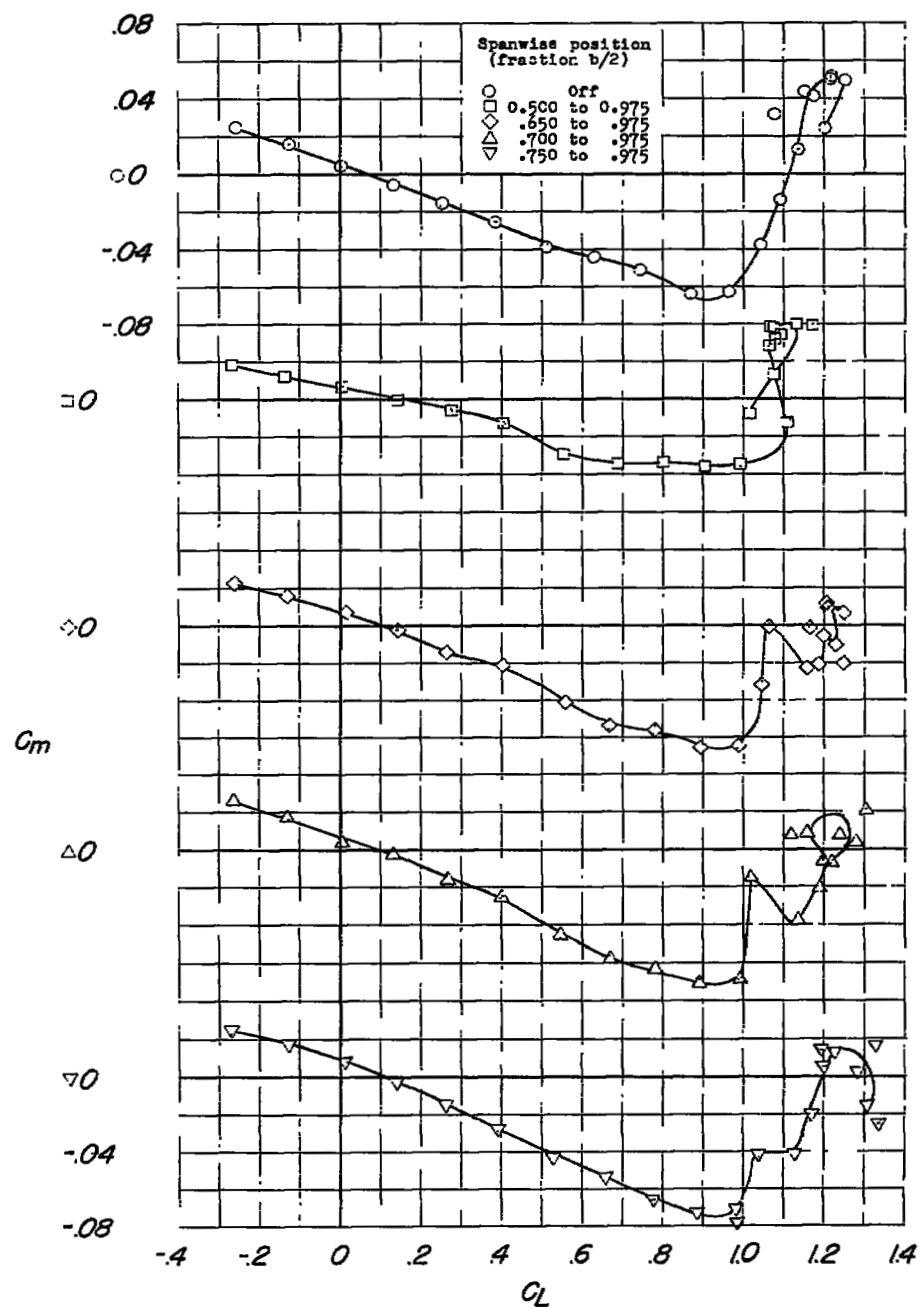
(b)  $C_m$  against  $C_L$ .

Figure 28.- Continued.

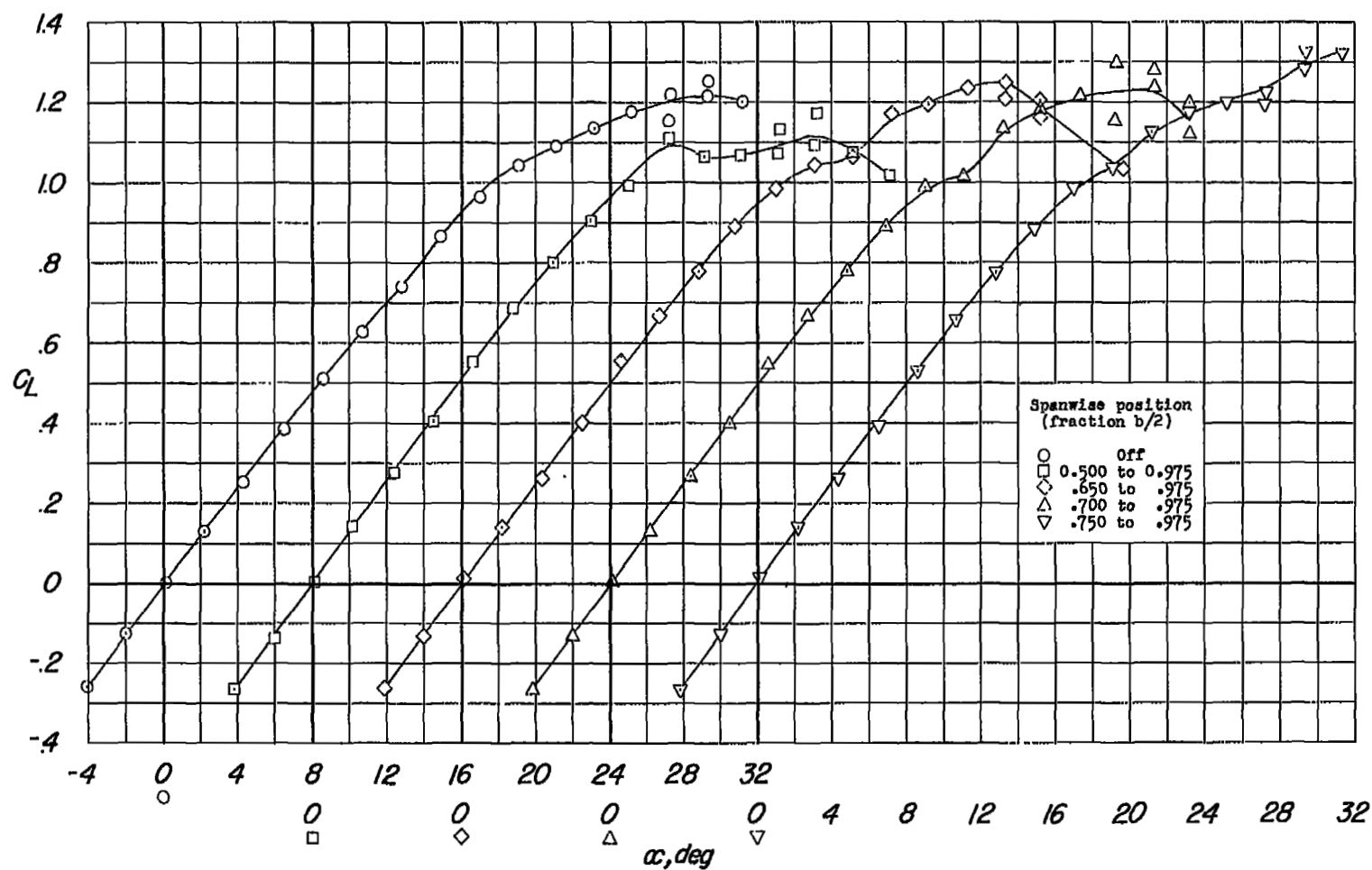
(c)  $C_L$  against  $\alpha$ .

Figure 28.- Concluded.

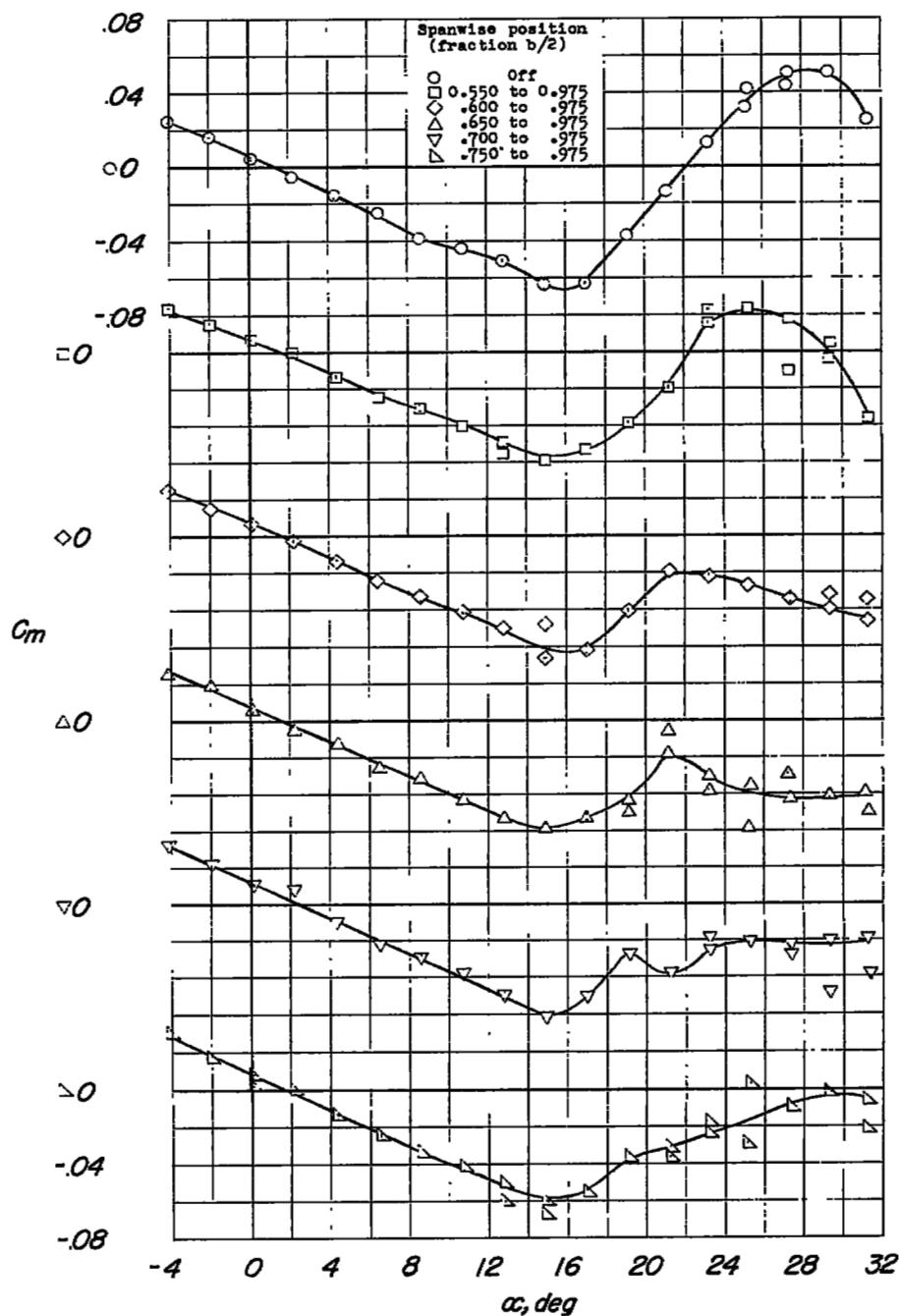
(a)  $C_m$  against  $\alpha$ .

Figure 29.- Lift and pitching-moment characteristics of wing with chord-extensions. Wing leading-edge radius, 0.0089c; chord-extension, 6.4 percent; chord-extension leading-edge radius, 0.00445c.

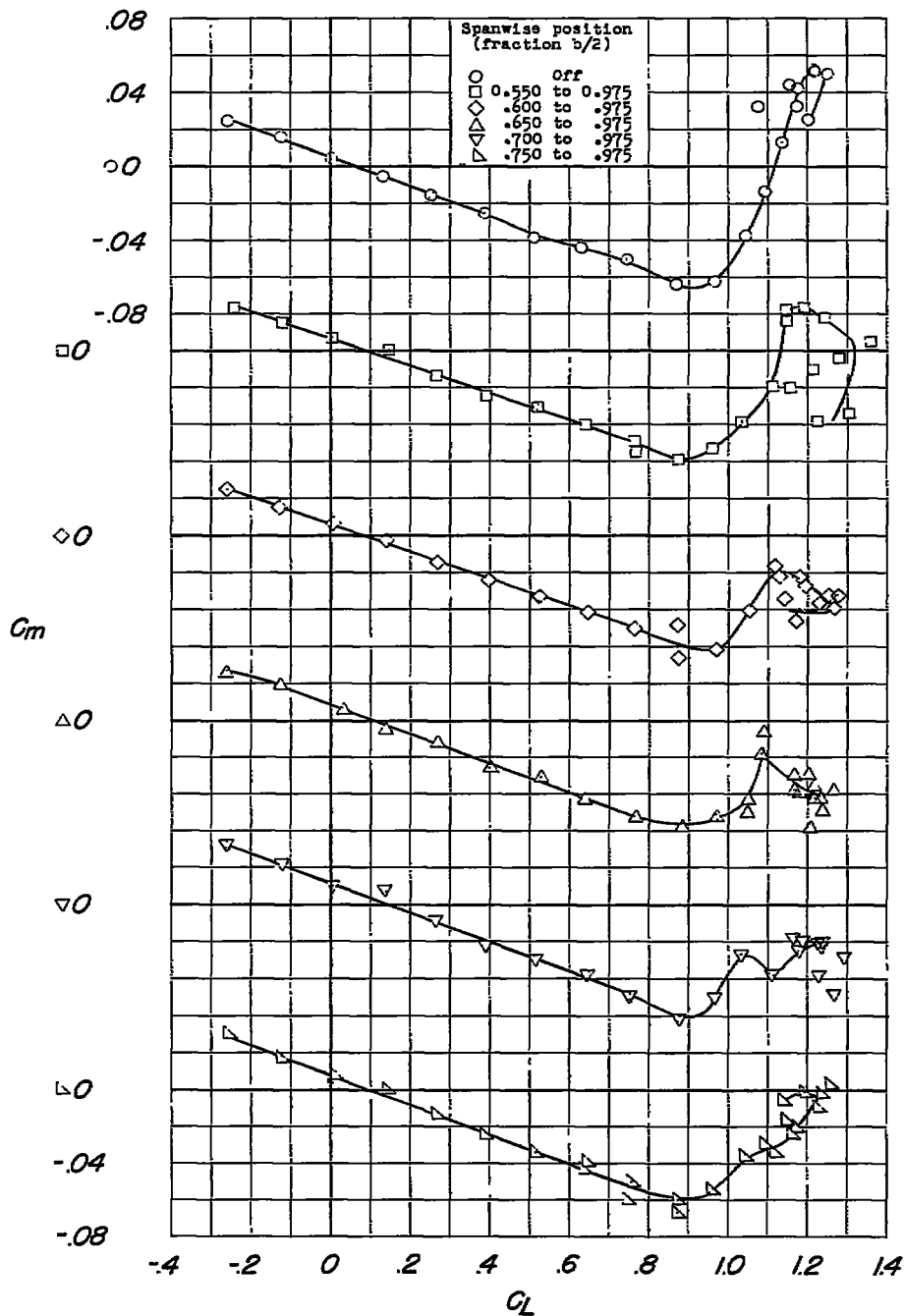
(b)  $C_m$  against  $C_L$ .

Figure 29.- Continued.

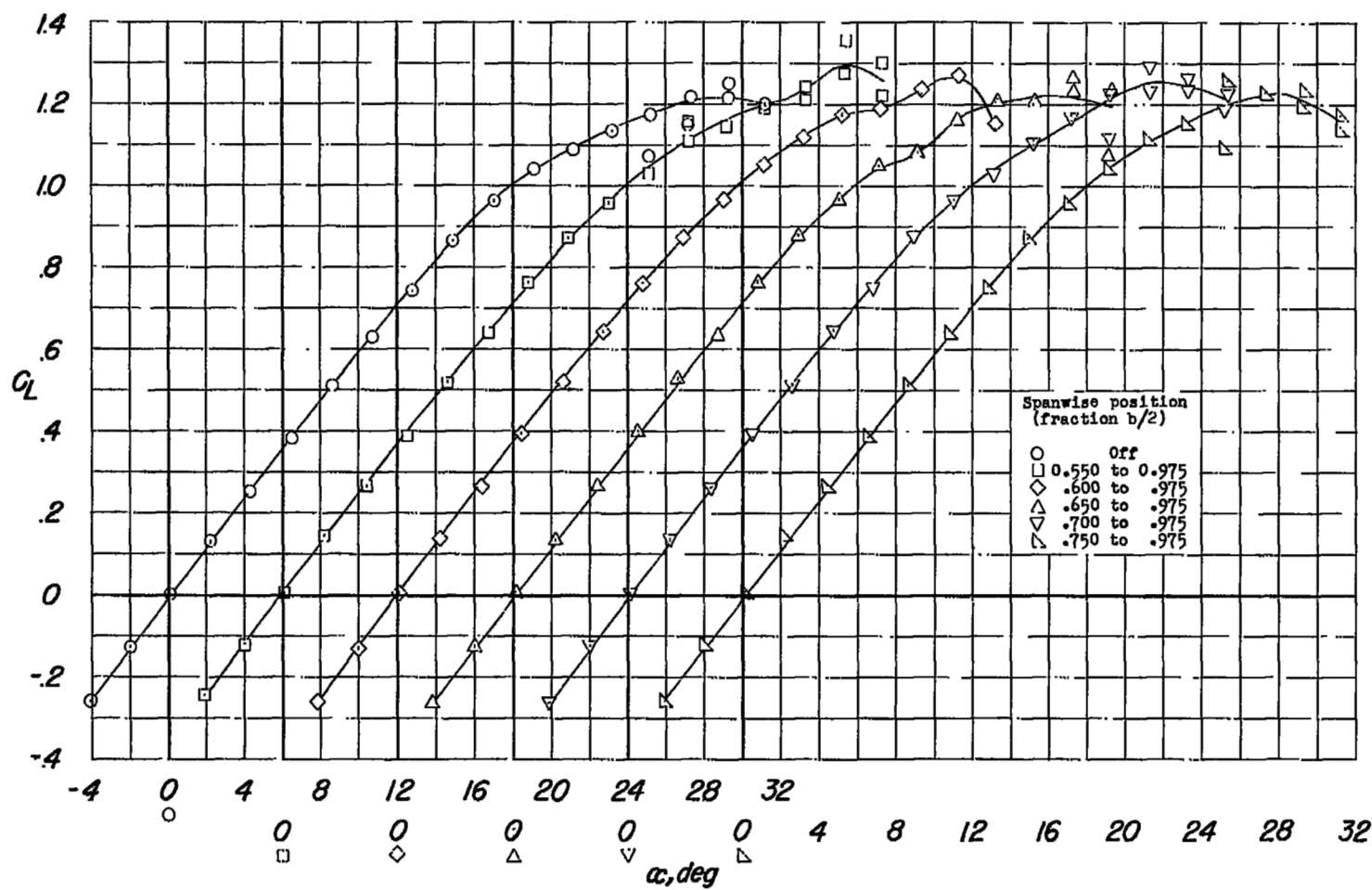
(c)  $C_L$  against  $\alpha$ .

Figure 29.- Concluded.

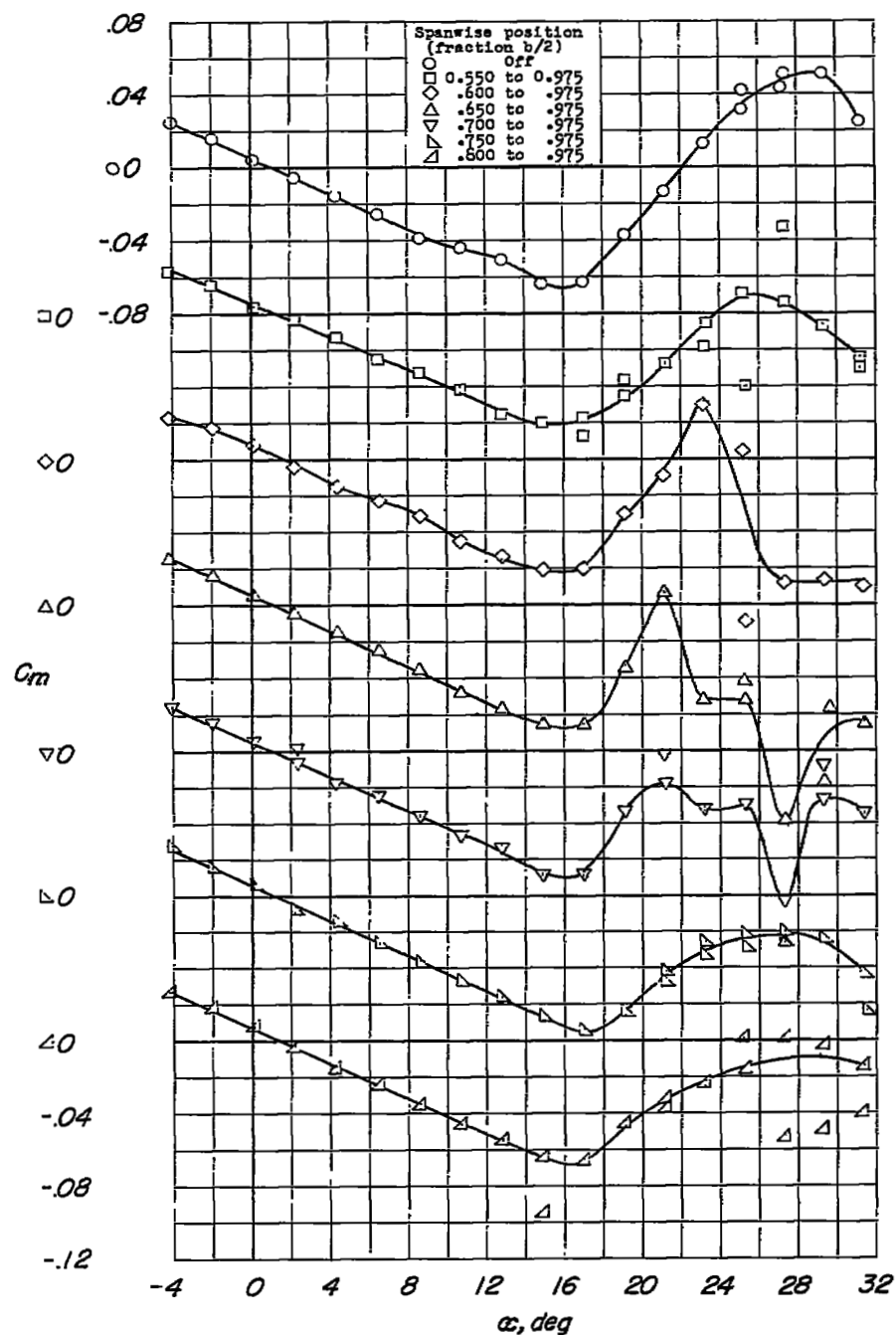
(a)  $C_m$  against  $\alpha$ .

Figure 30.- Lift and pitching-moment characteristics of wing with chord-extensions. Wing leading-edge radius, 0.0089c; chord-extension, 13.0 percent; chord-extension, leading-edge radius, 0.00445c.

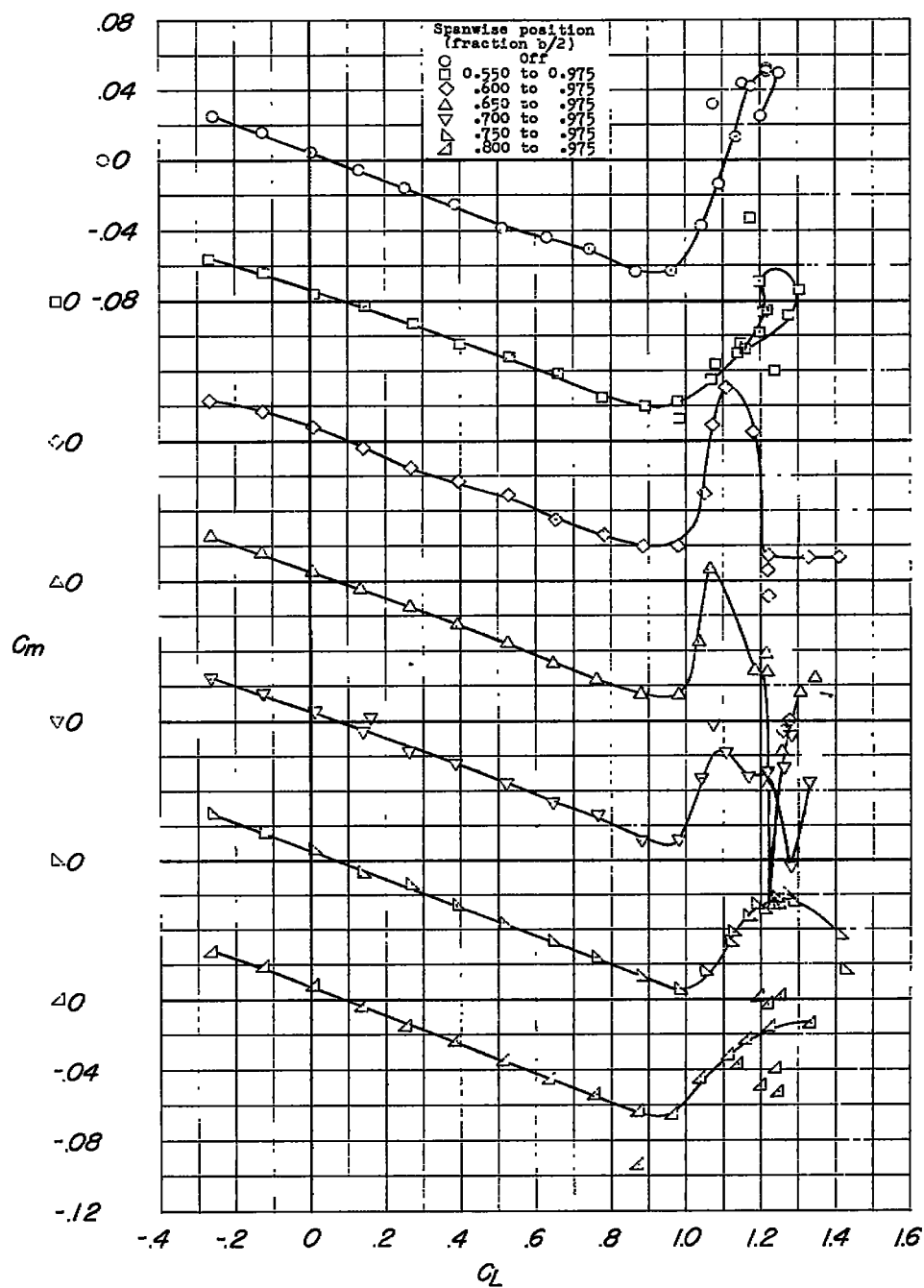
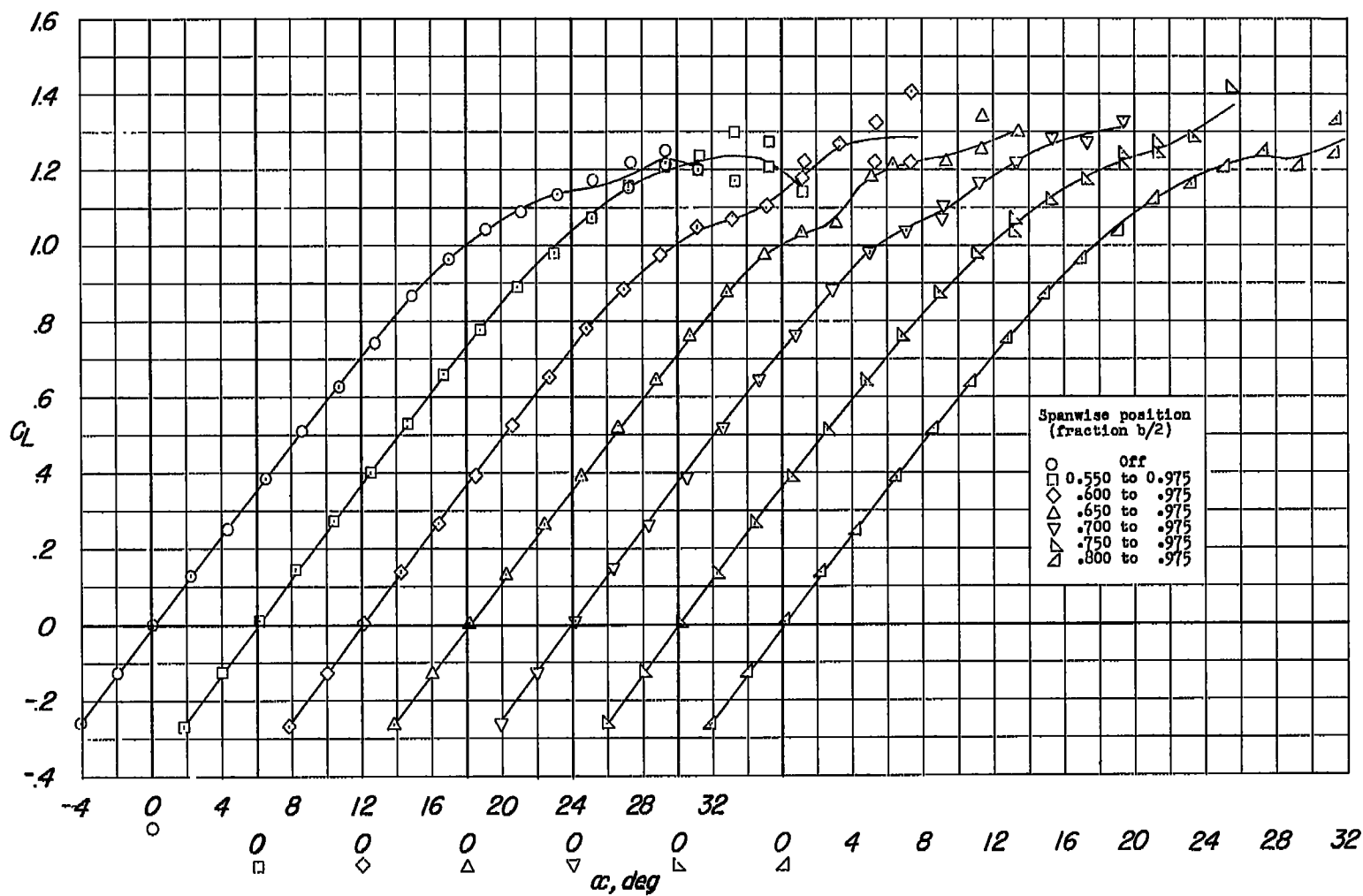
(b)  $C_m$  against  $C_L$ .

Figure 30.- Continued.



(c)  $C_L$  against  $\alpha$ .

Figure 30.- Concluded.

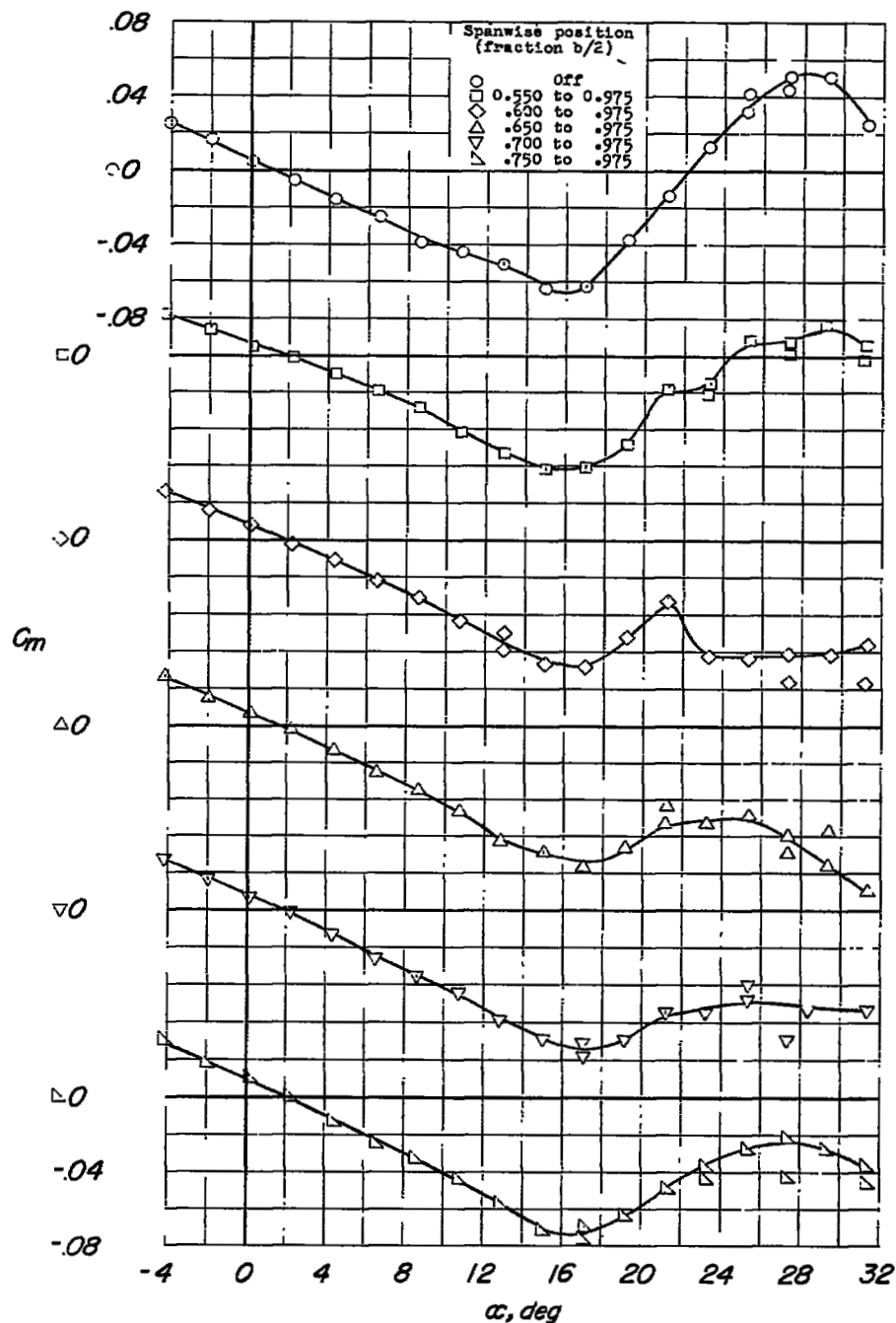
(a)  $C_m$  against  $\alpha$ .

Figure 31.- Lift and pitching-moment characteristics of wing with chord-extensions. Wing leading-edge radius, 0.0089c; chord-extension, 19.8 percent; chord-extension leading-edge radius, 0.00445c.

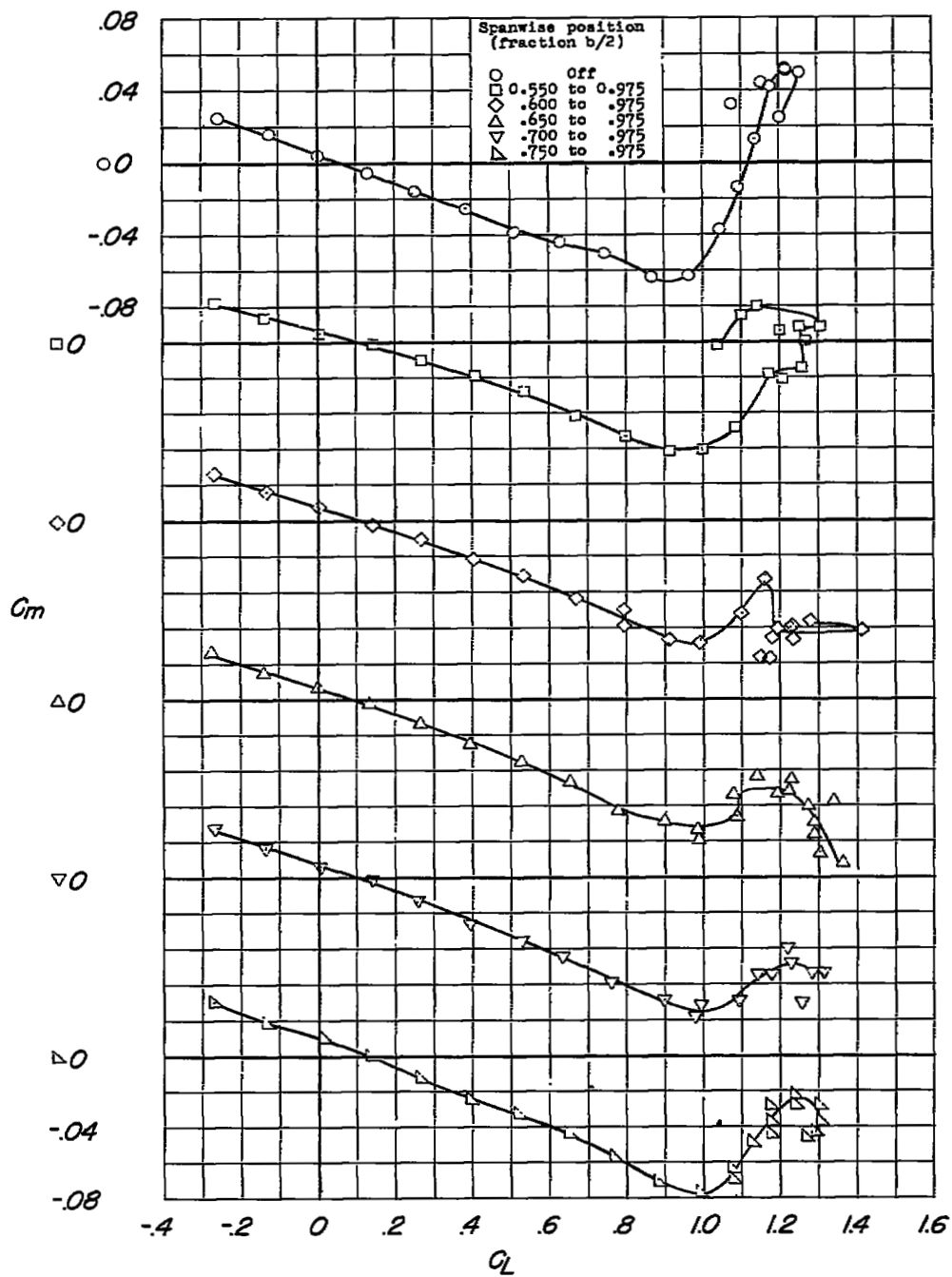
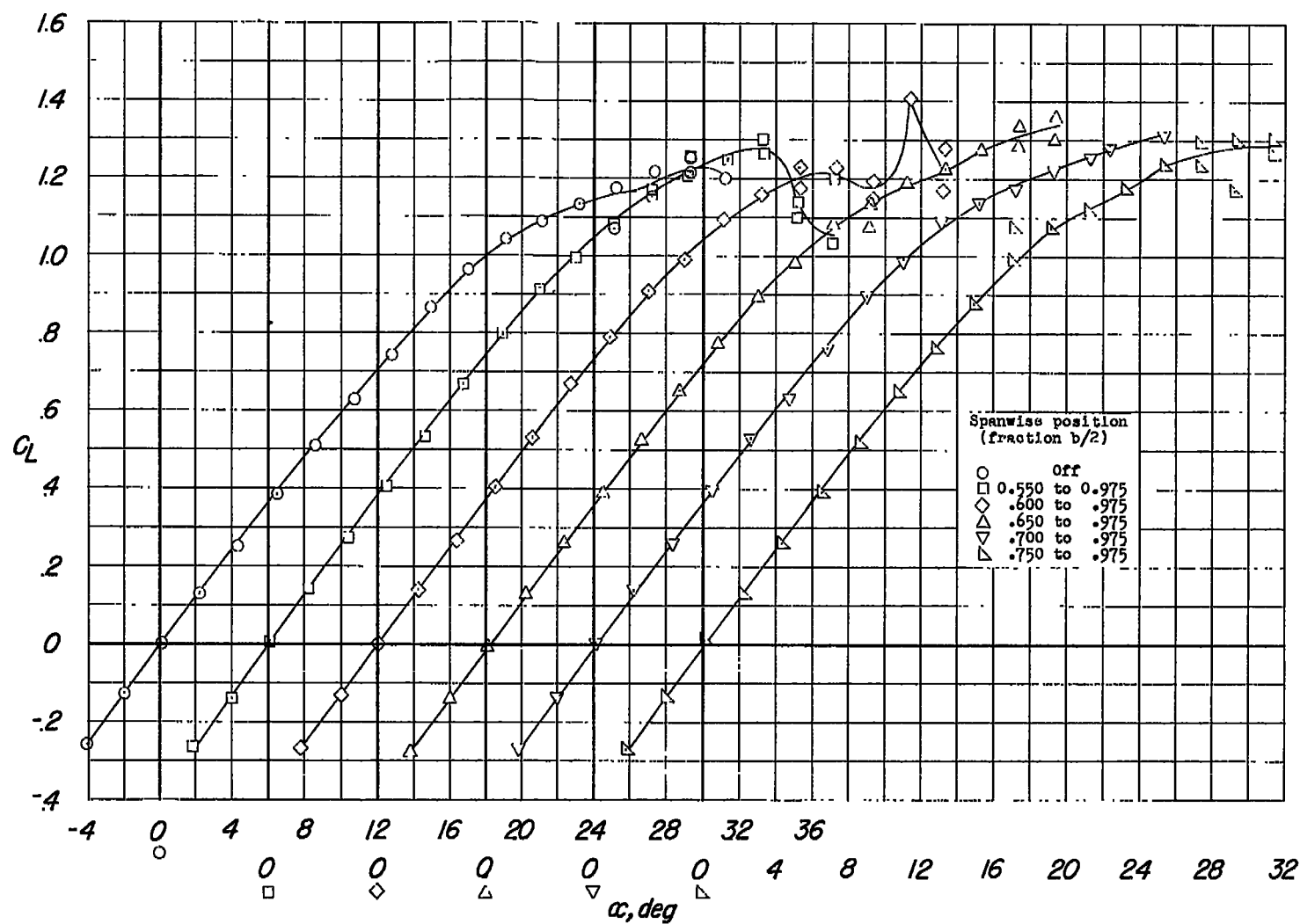
(b)  $C_m$  against  $C_L$ .

Figure 31.- Continued.



(c)  $C_L$  against  $\alpha$ .

Figure 31.- Concluded.

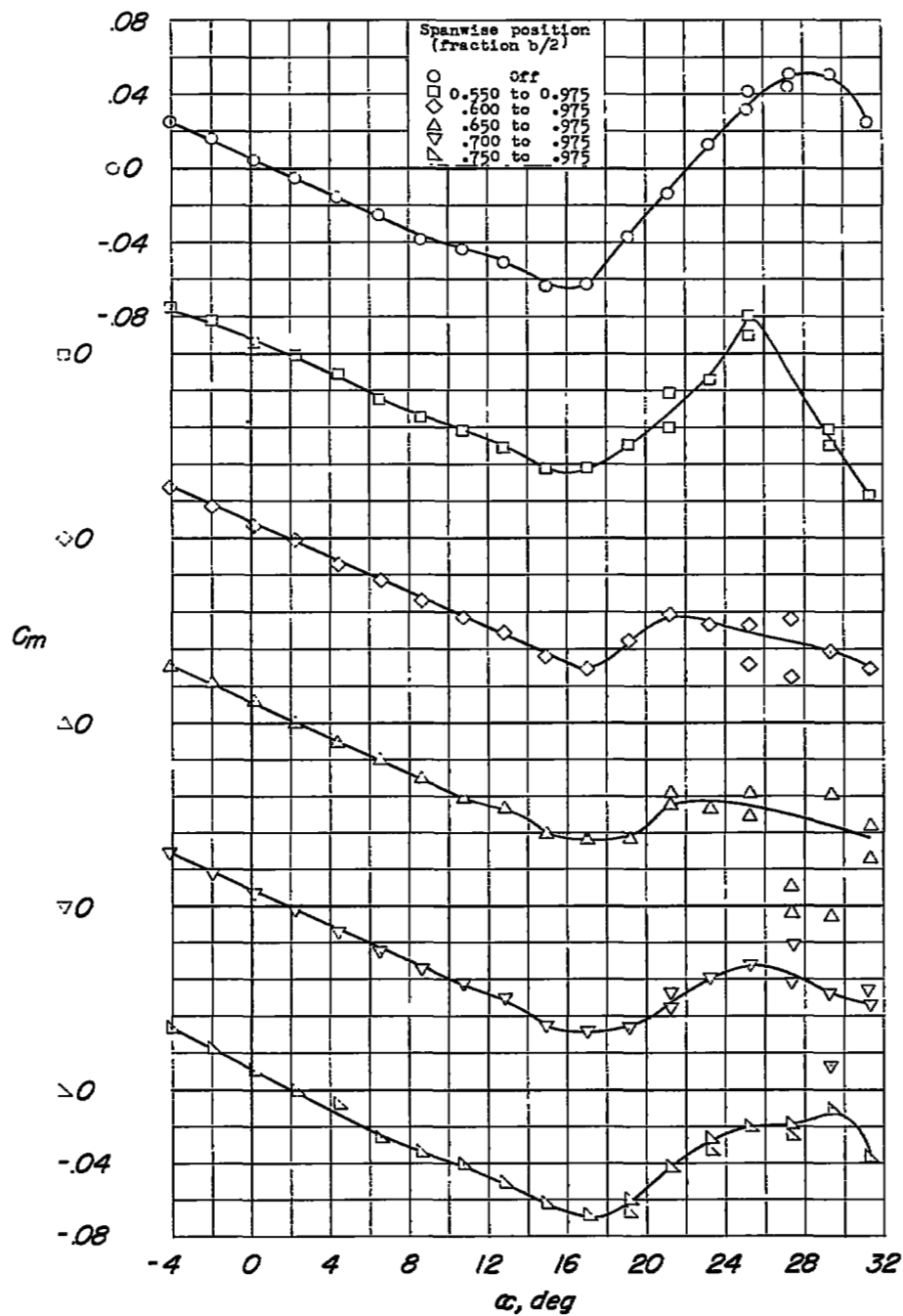
(a)  $C_m$  against  $\alpha$ .

Figure 32.- Lift and pitching-moment characteristics of wing with chord-extensions. Wing leading-edge radius, 0.0089c; chord-extension, 6.4 percent; chord-extension leading-edge radius, 0.00890c.

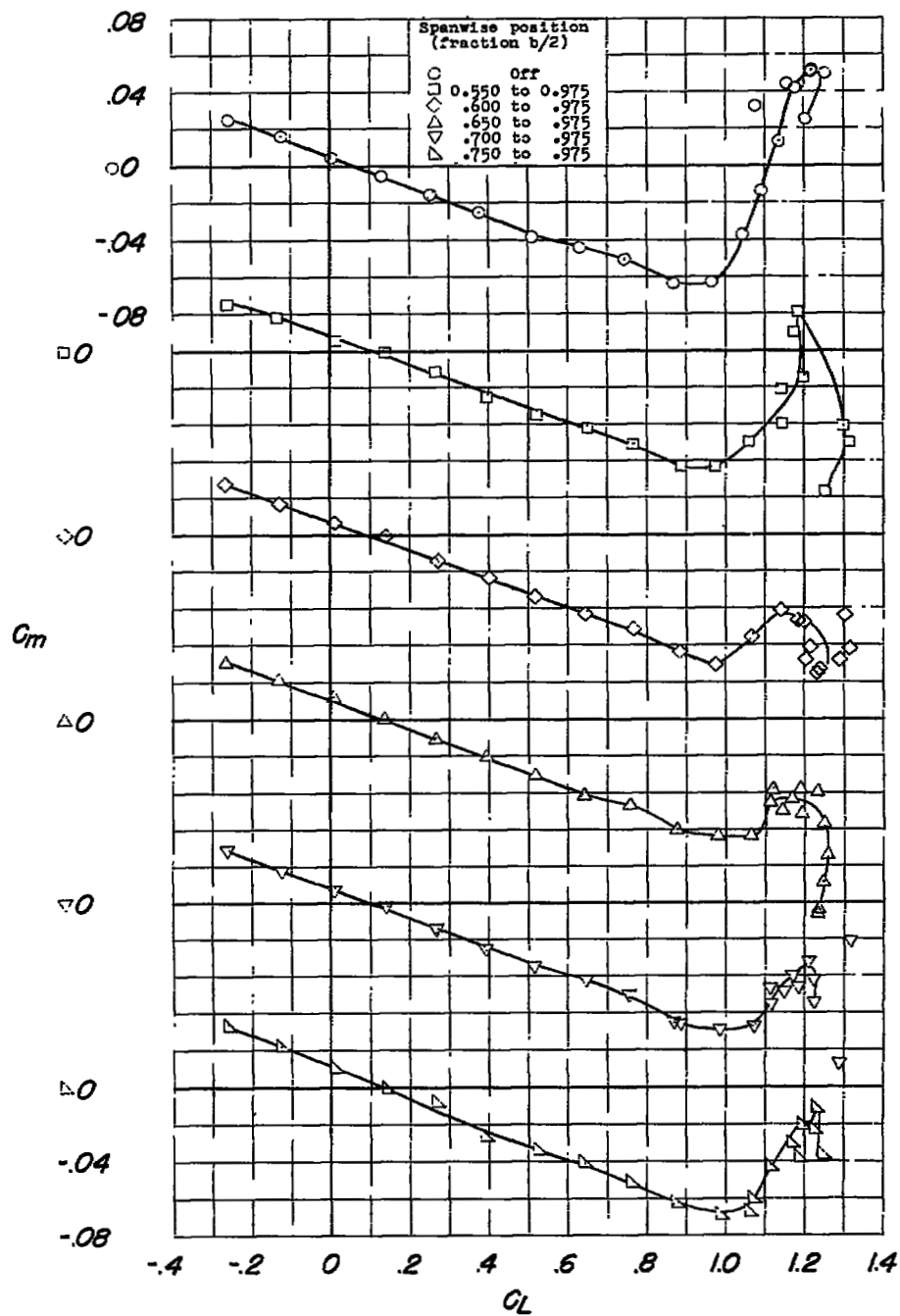
(b)  $C_m$  against  $C_L$ .

Figure 32.- Continued.

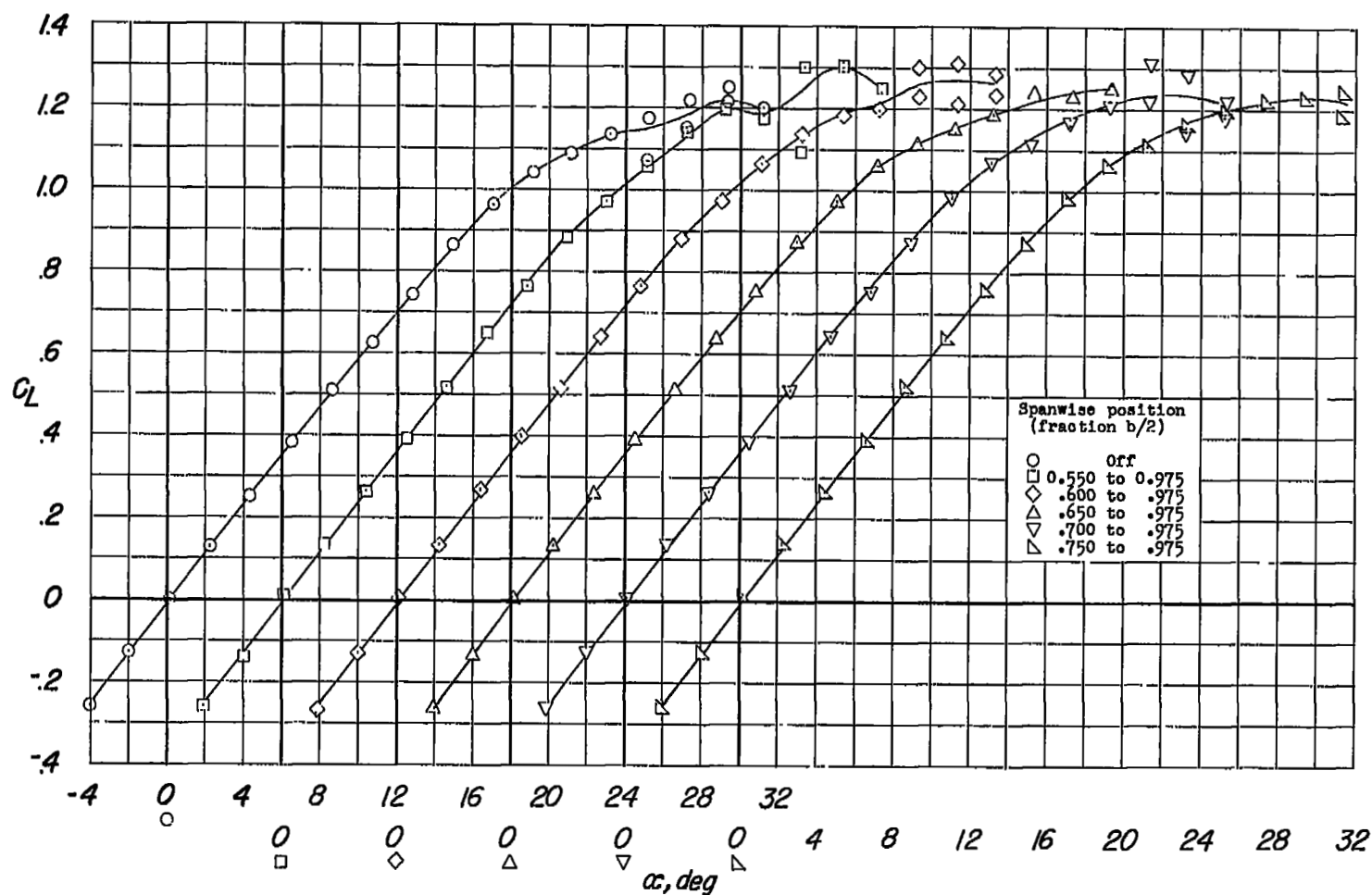
(c)  $C_L$  against  $\alpha$ .

Figure 32.- Concluded.

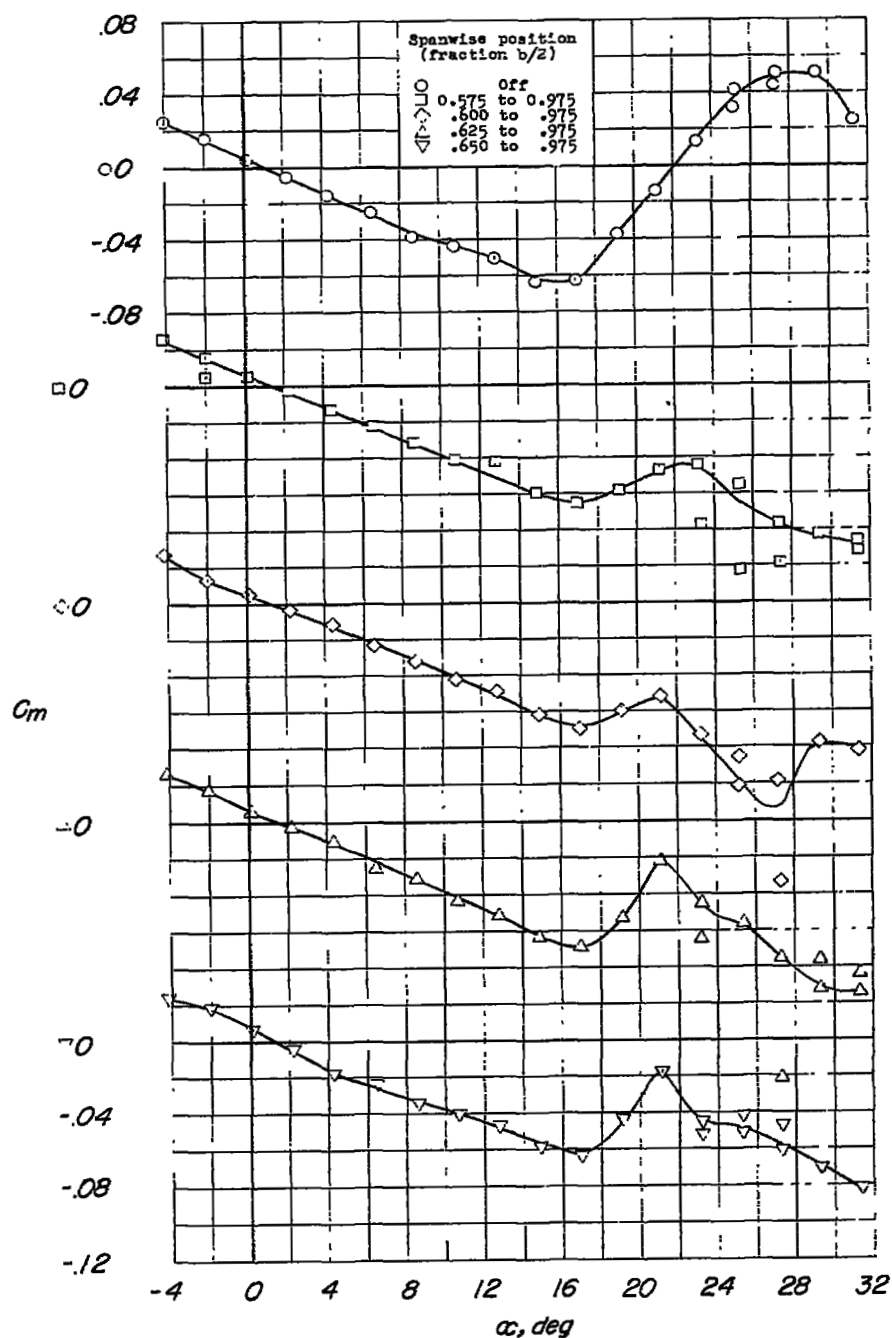
(a)  $C_m$  against  $\alpha$ .

Figure 33.- Lift and pitching-moment characteristics of wing with chord-extensions. Wing leading-edge radius, 0.0089c; chord-extension, 13.0 percent; chord-extension leading-edge radius, 0.00890c.

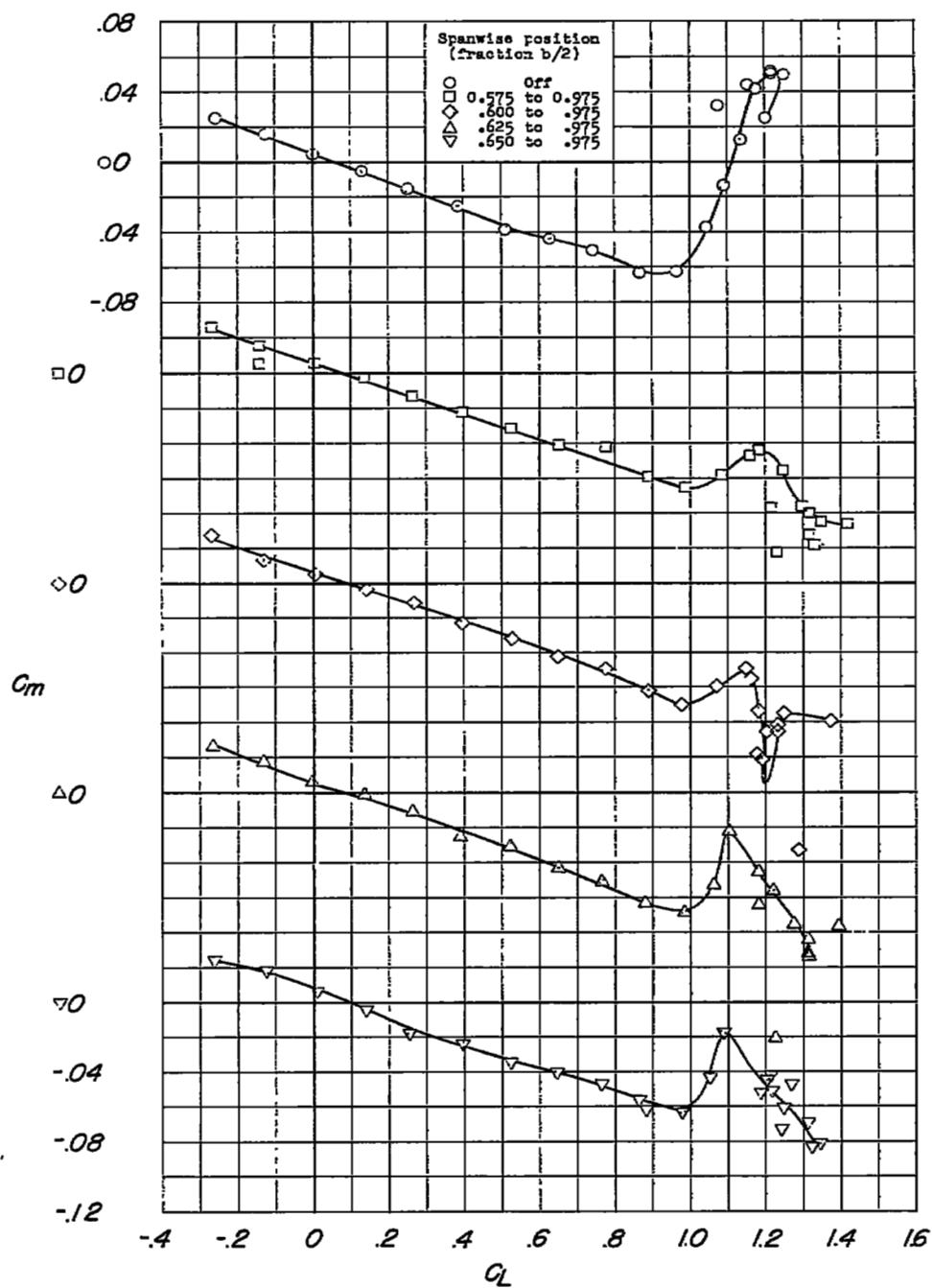
(b)  $C_m$  against  $C_L$ .

Figure 33.- Continued.

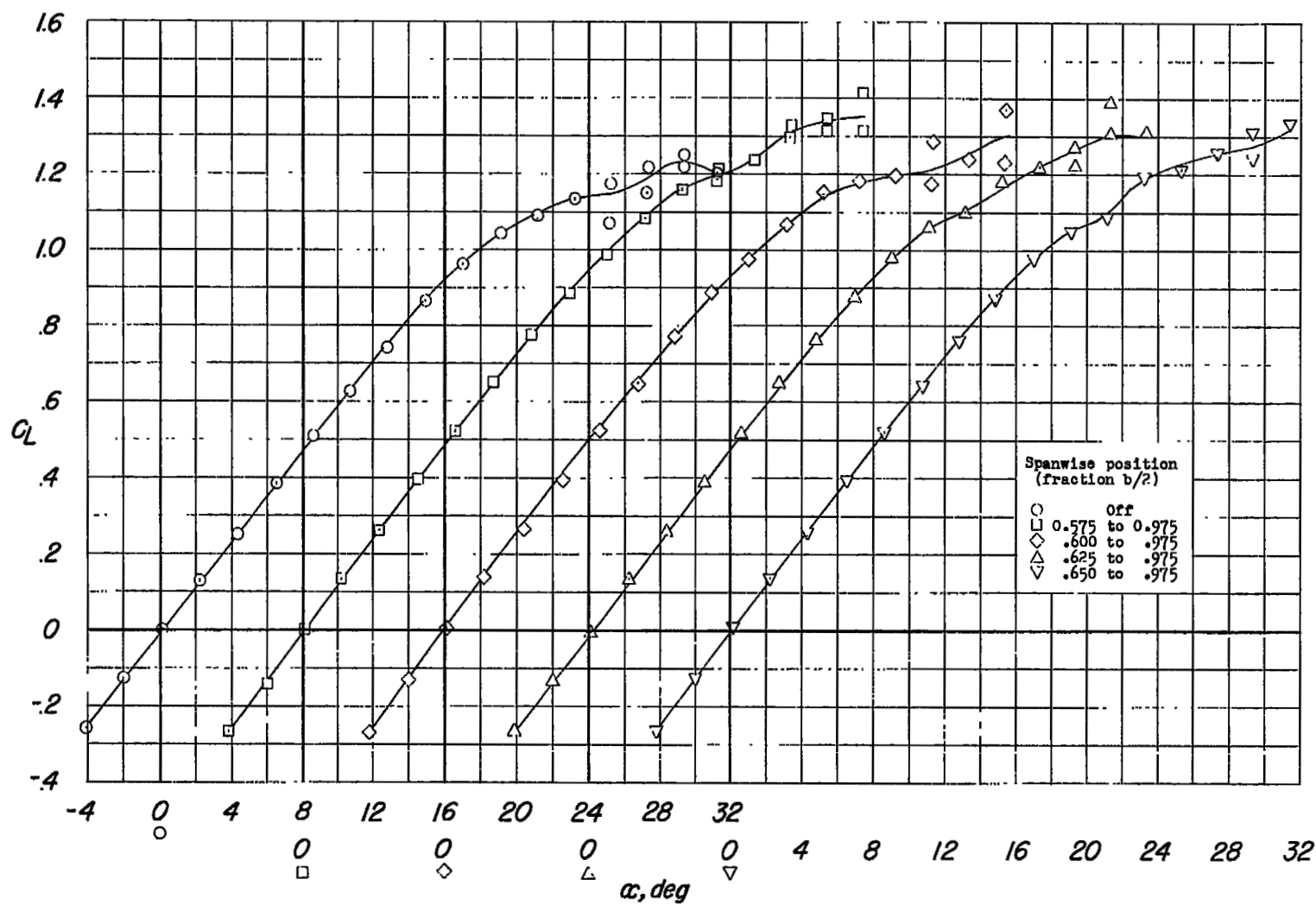
(c)  $C_L$  against  $\alpha$ .

Figure 33.- Concluded.

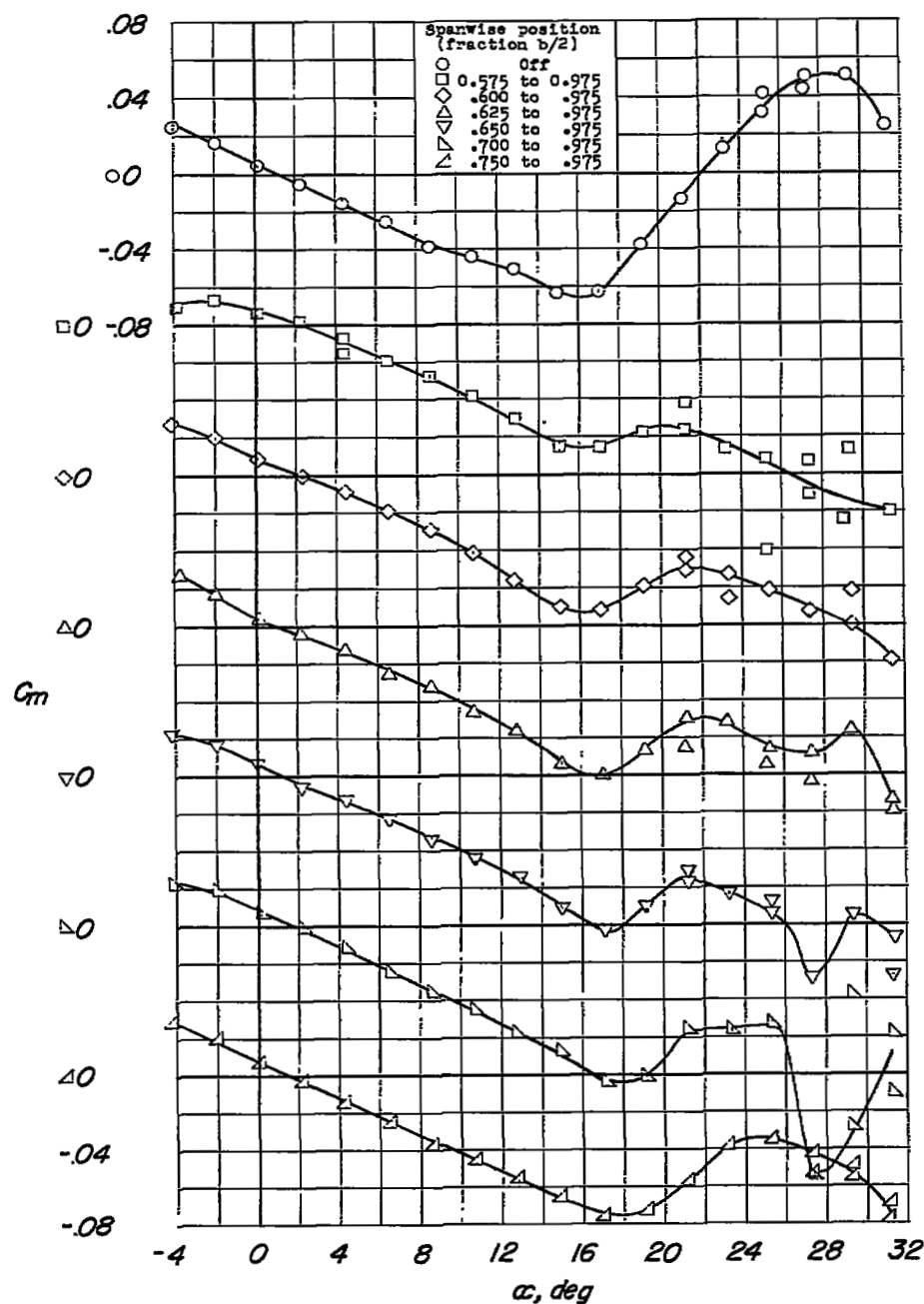
(a)  $C_m$  against  $\alpha$ .

Figure 34.- Lift and pitching-moment characteristics of wing with chord-extensions. Wing leading-edge radius, 0.0089c; chord-extension, 19.8 percent; chord-extension leading-edge radius, 0.00890c.

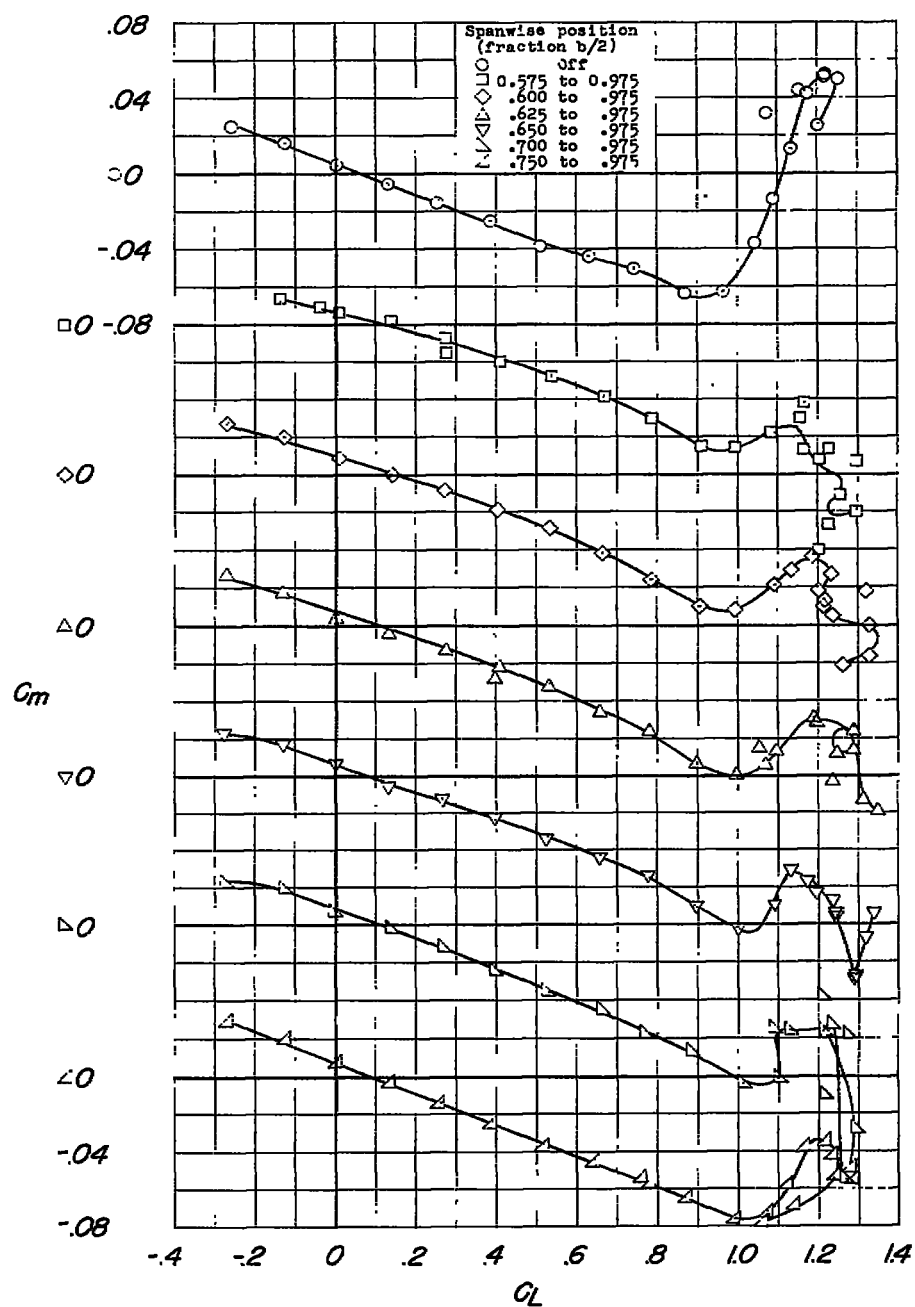
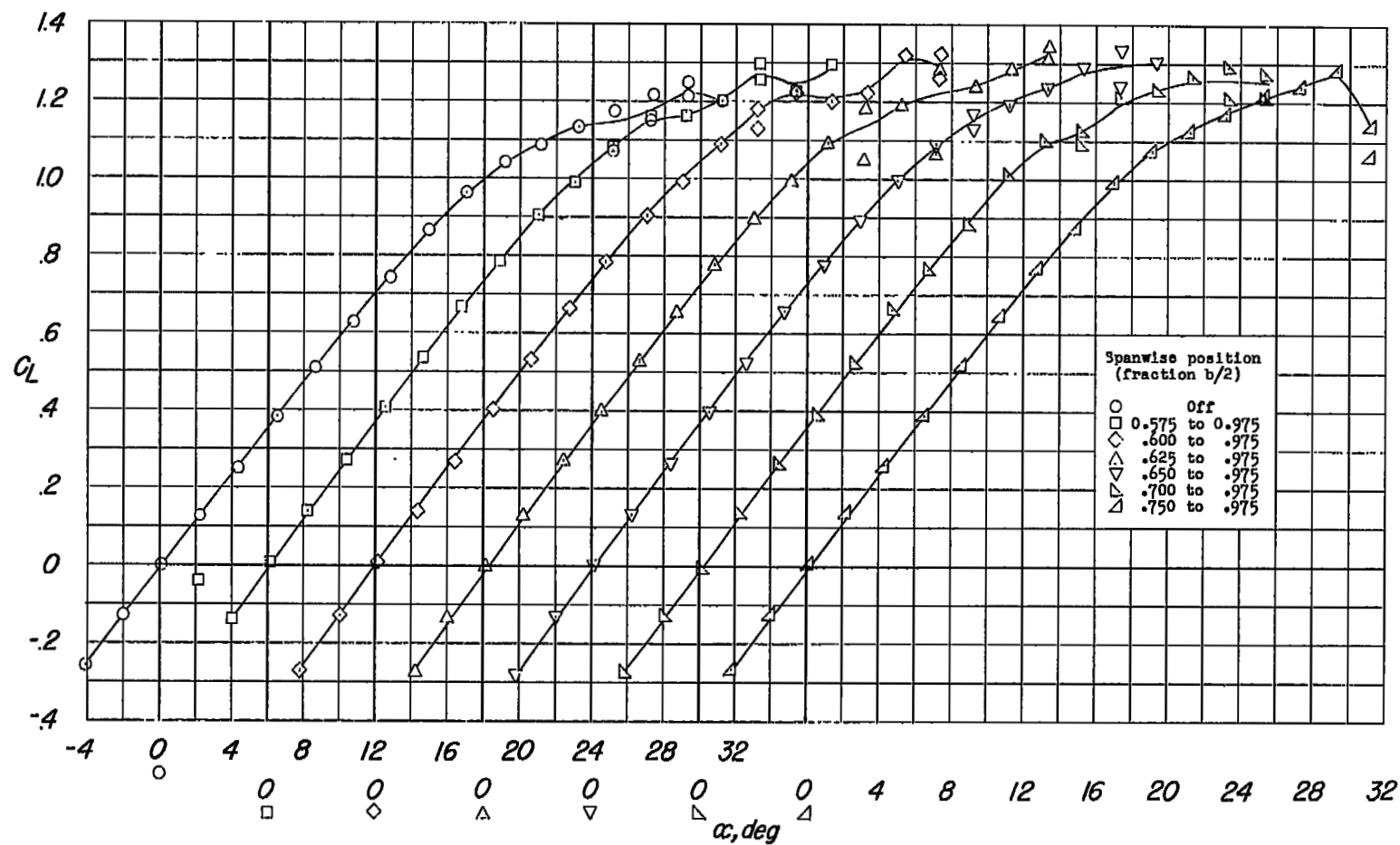
(b)  $C_m$  against  $C_L$ .

Figure 34.- Continued.



(c)  $C_L$  against  $\alpha$ .

Figure 34.- Concluded.

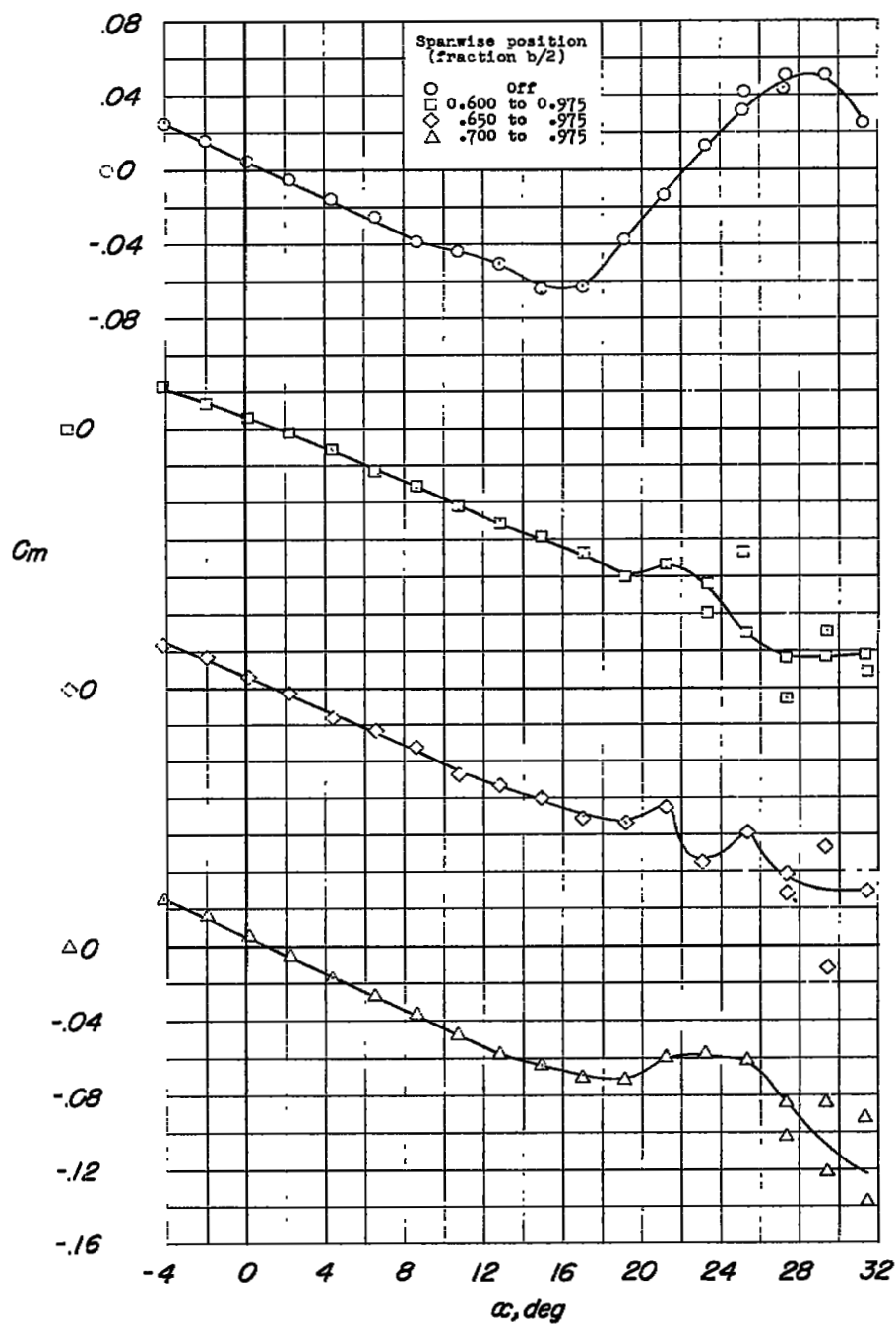
(a)  $C_m$  against  $\alpha$ .

Figure 35.- Lift and pitching-moment characteristics of wing with chord-extensions. Wing leading-edge radius, 0.0089c; chord-extension, 18.0 percent; drooped chord-extension leading-edge radius, 0.00890c.

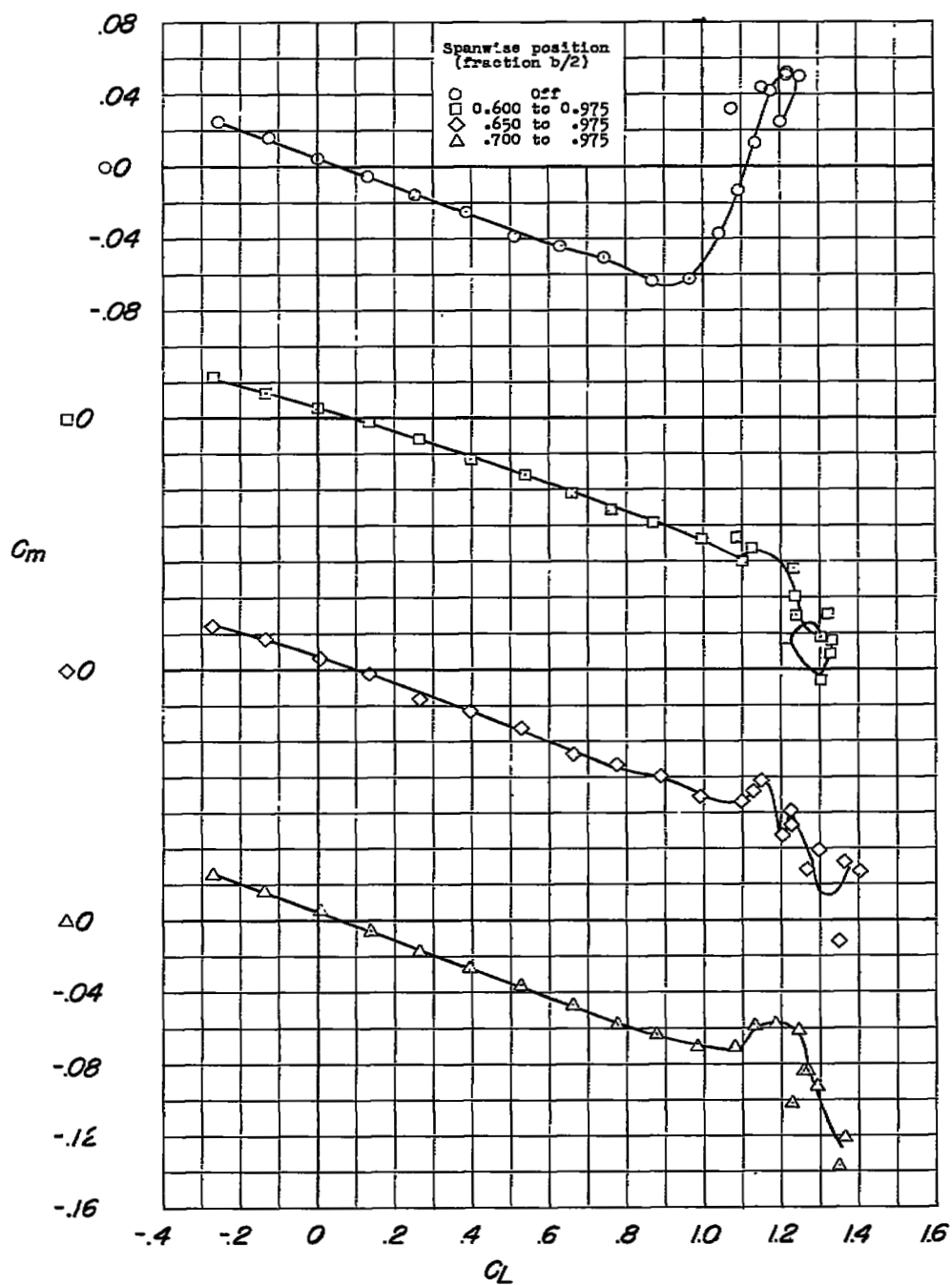
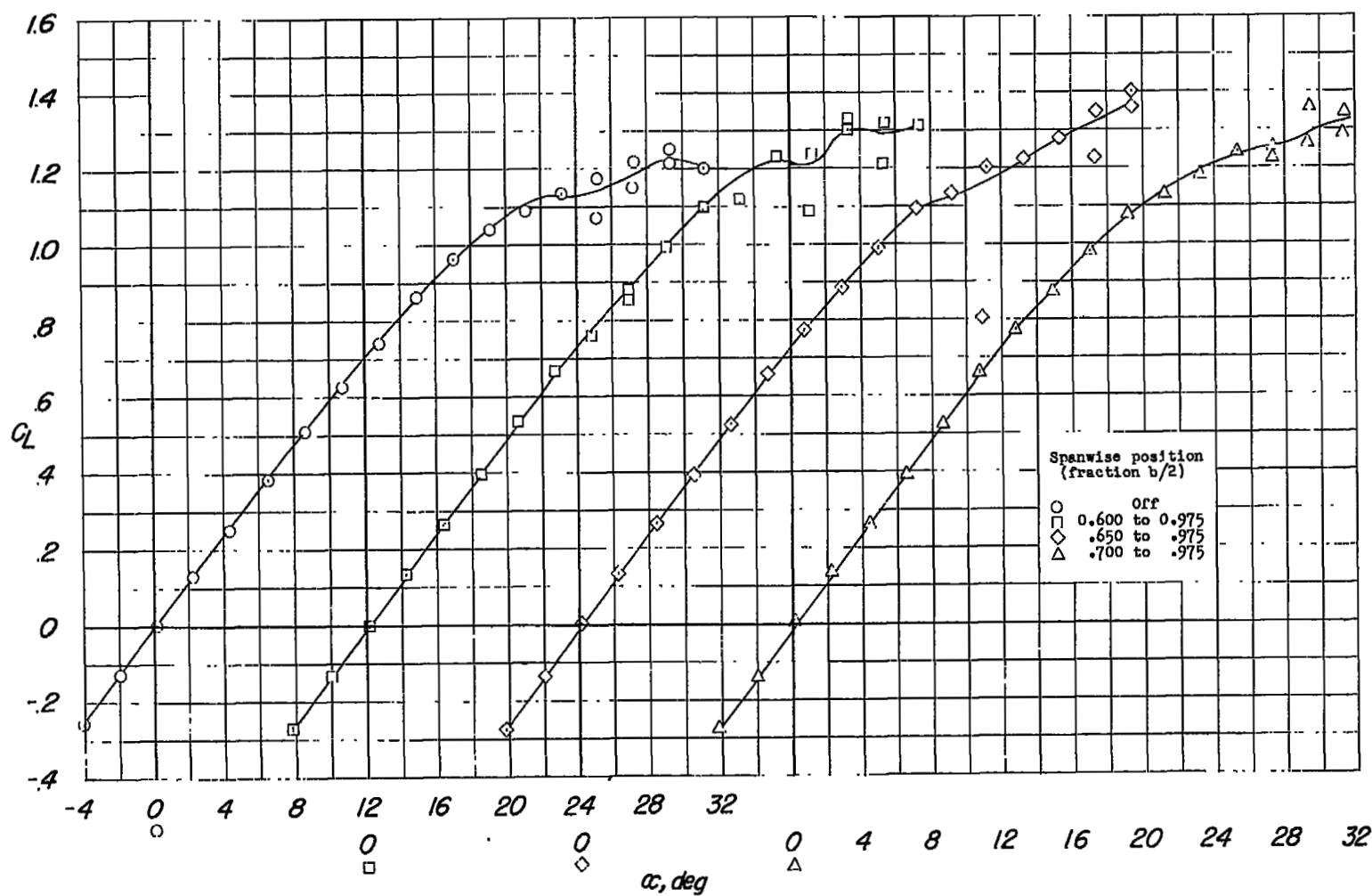
(b)  $C_m$  against  $C_L$ .

Figure 35.- Continued.



(c)  $C_L$  against  $\alpha$ .

Figure 35.- Concluded.

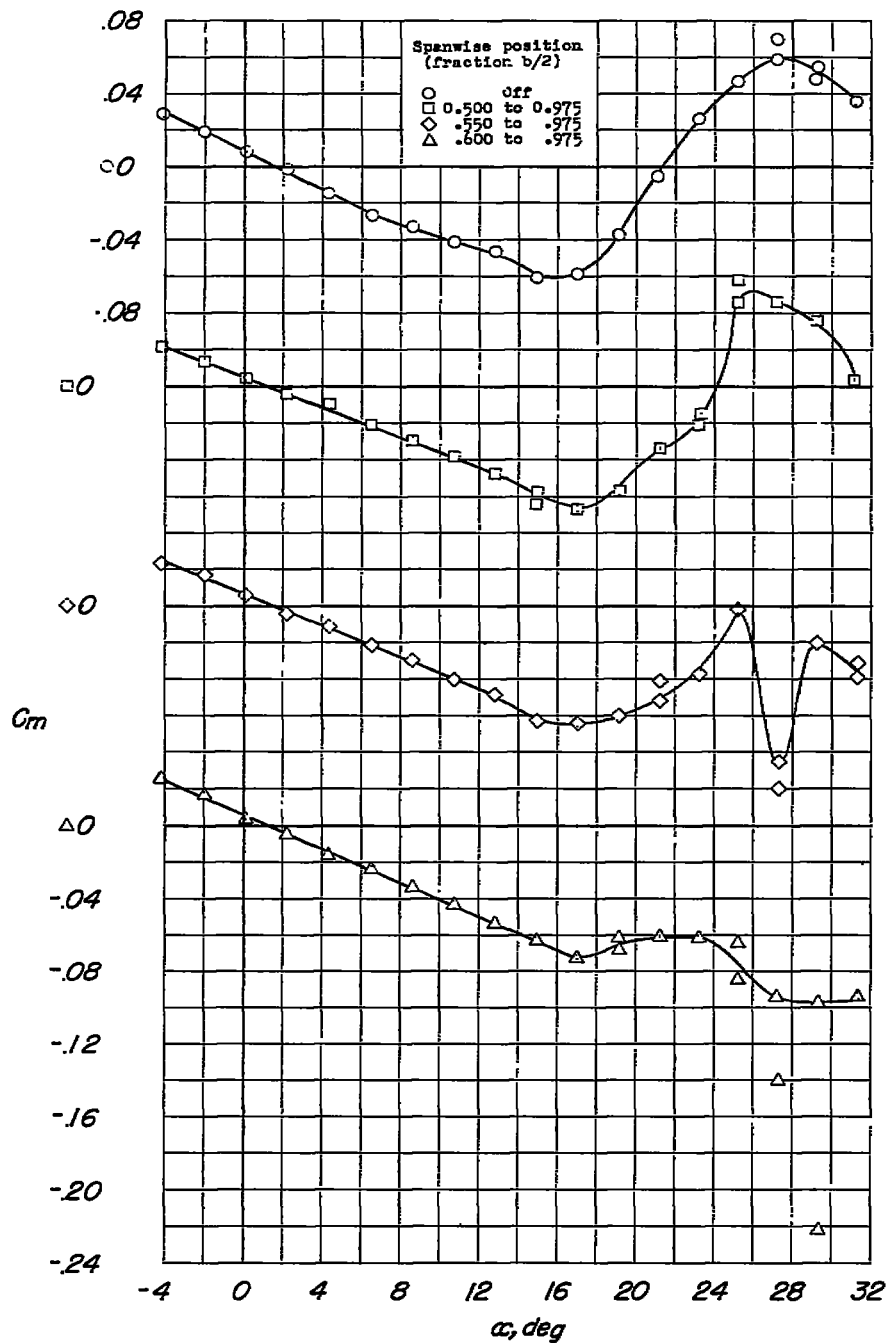
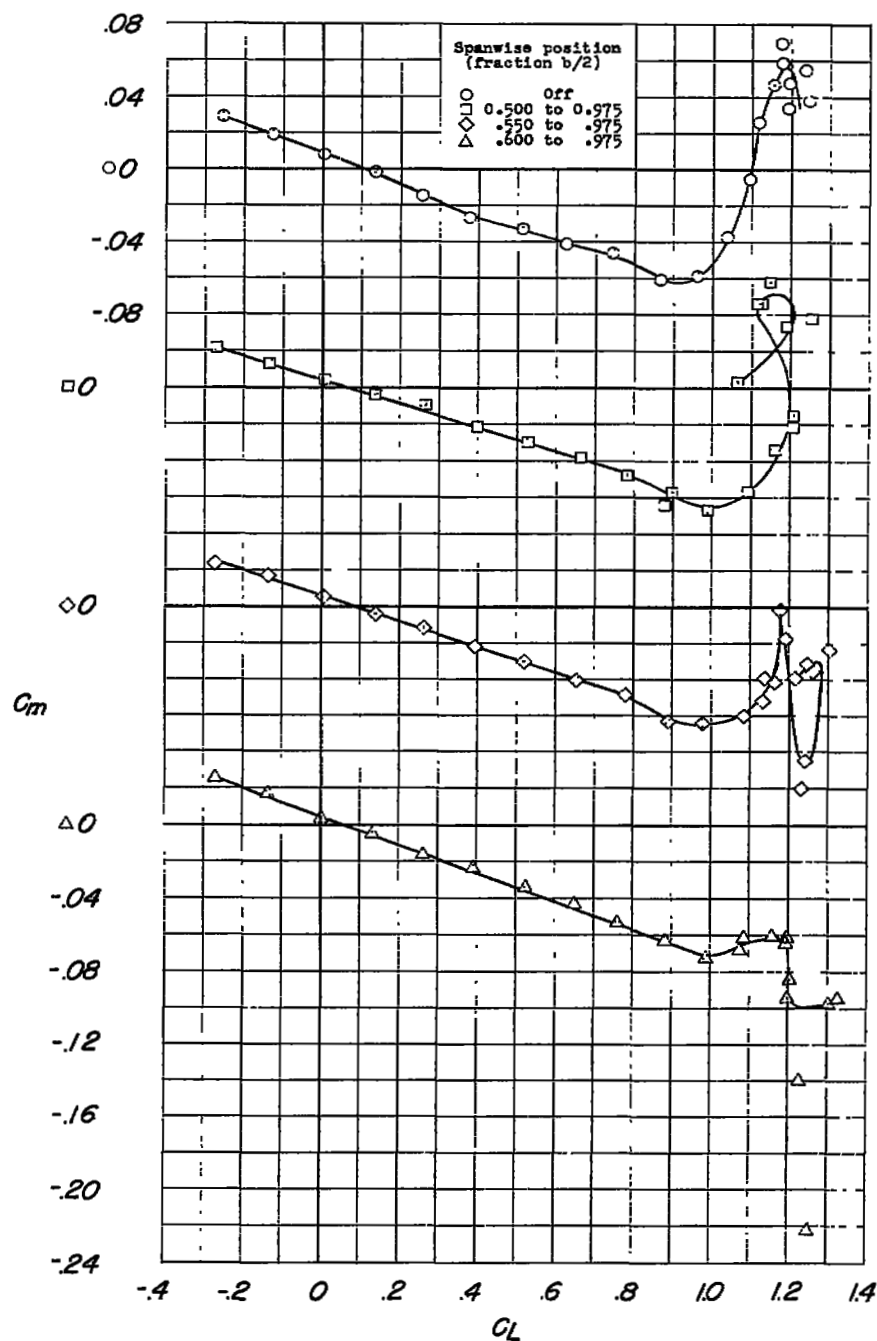
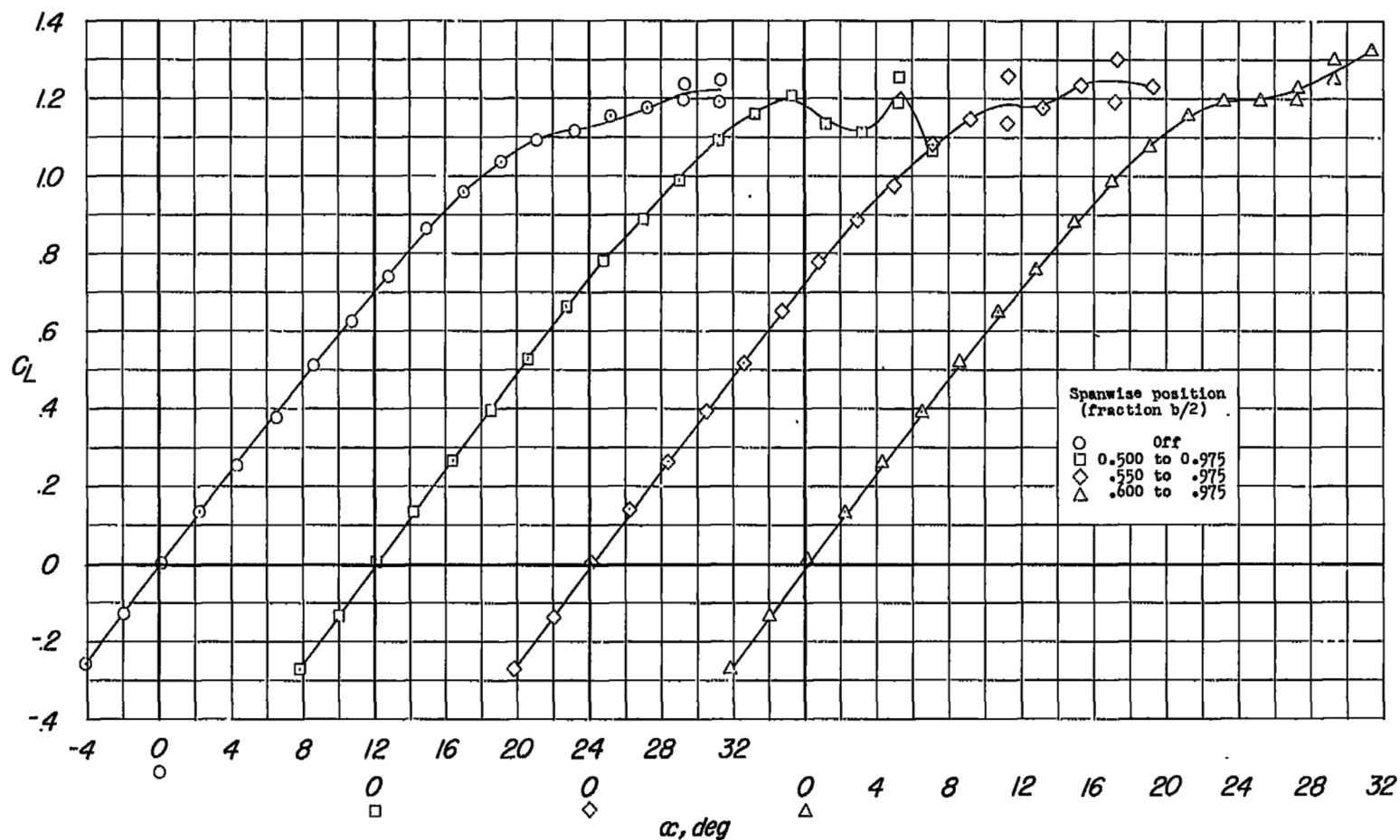
(a)  $C_m$  against  $\alpha$ .

Figure 36.- Lift and pitching-moment characteristics of wing with chord-extensions. Wing leading-edge radius, 0.0089c; chord-extension, 13.0 percent; chord-extension leading-edge radius, 0.00890c; Reynolds number,  $4.87 \times 10^6$ .



(b)  $C_m$  against  $C_L$ .

Figure 36.- Continued.



(c)  $C_L$  against  $\alpha$ .

Figure 36.- Concluded.

NASA Technical Library



3 1176 01438 0548

